④

ANNUAL REPORT

Growth, Characterization and Device Development in Monocrystalline Diamond Films

**DTIC
ELECTE
FEB 2 0 1990
S
D**

College of Engineering
North Carolina State University
Raleigh, North Carolina

90 02 16 107

REPORT DOCUMENTATION PAGE

Public reporting burden for this collection of information is estimated to average 1 hour per response, including the time for reviewing instructions, searching existing data sources, gathering and maintaining the data needed, and completing and reviewing the collection of information. Send comments regarding this burden estimate or any other aspect of this collection of information, including suggestions for reducing this burden, to Washington Headquarters Services, Directorate for Information Operations and Reports, 1215 Jefferson Davis Highway, Suite 1204, Arlington, VA 22202-4302, and to the Office of Management and Budget, Paperwork Reduction Project (0704-0188), Washington, DC 20503

1. AGENCY USE ONLY (Leave blank)	2. REPORT DATE February, 1990	3. REPORT TYPE AND DATES COVERED Annual 6/1/88-5/31/89

4. TITLE AND SUBTITLE

Growth, Characterization and Device Development in Monocrystalline Diamond Films

5. FUNDING NUMBERS

6322 OC
IST
SRR
003

6. AUTHOR(S)

R. F. Davis, J. T. Glass, K. J. Bachmann,
R. J. Trew, and R. J. Nemanich

7. PERFORMING ORGANIZATION NAME(S) AND ADDRESS(ES)

NORTH CAROLINA STATE UNIVERSITY
c/o Materials Science and Engineering
Box 7907
Raleigh, NC   27695-7907

8. PERFORMING ORGANIZATION REPORT NUMBER

N00014-86-K-0666

9. SPONSORING/MONITORING AGENCY NAME(S) AND ADDRESS(ES)

Sponsoring Agency: SDIO, Ist, Washington, DC
Monitoring Agency: Office of Naval Research,
   Code 1114, Arlington, VA   22217

10. SPONSORING/MONITORING AGENCY REPORT NUMBER

11. SUPPLEMENTARY NOTES

12a. DISTRIBUTION/AVAILABILITY STATEMENT

Approved for public release; distribution unlimited

12b. DISTRIBUTION CODE

13. ABSTRACT (Maximum 200 words)

Two chemical vapor deposition (CVD) systems (hot filament and microwave plasma) and a multitechnique analysis system have been designed, constructed and characterized. The effects of surface steps, substrate material and substrate/filament bias have been examined. Diamond films from outside sources have been analyzed by a variety of techniques. Most notably, numerous defects, especially (111) twins, have been identified by TEM and are similar to those found in natural diamond. Certain diamond particles were in a twinned epitaxial relationship with the (Si) substrate. It has also been found that a thin SiC layer forms immediately (i.e. <5 min) upon exposure to the CH_4+H_2 plasma, followed by the slow formation of the diamond crystallites.

Large-Signal, nonlinear device models for both microwave diamond power MESFETs and mm-wave diamond IMPATT diodes have been developed. Diamond power MESFETs operating in X-band are found to be capable of producing approximately 25 W/unit gate width of RF power with a power-added efficiency of greater than 40%. A diamond IMPATT oscillator should produce about 2 W RF power with an efficiency of 10% at 100 GHz.

14. SUBJECT TERMS

15. NUMBER OF PAGES
140

16. PRICE CODE

17. SECURITY CLASSIFICATION OF REPORT	18. SECURITY CLASSIFICATION OF THIS PAGE	19. SECURITY CLASSIFICATION OF ABSTRACT	20. LIMITATION OF ABSTRACT
Unclassified	Unclassified	Unclassified	

Table of Contents

Accesion For

NTIS CRA&I		
DTIC TAB		☐
Unannounced		☐
Justification		

By _____

Distribution/

_____

A-1

I. Introduction

Diamond is an excellent candidate material for various electronic microwave devices as well as devices for use in high temperature and/or high flux radiation environments and for high current density or high power applications. This very diverse applicability is due to its superior thermal conductivity, saturated drift velocities, resistance to chemical attack and thermal stability. However, to realize this potential of diamond, high quality monocrystalline films must be grown and thoroughly characterized. The latter research is necessary as an iterative procedure for the improvement of the growth process and to guide future device design and fabrication. To achieve these goals, the NCSU diamond program couples investigators from four departments to obtain a unique combination of expertise and experience.

More specifically, the principal objectives of this collaborative research are to (1) grow monocrystalline diamond films on suitable substrates such as Ni and SiC using both past and newly generated knowledge regarding gas species generation, deposition and reaction, and energy and momentum transfer at the growing surface, (2) characterize these films in terms of bonding, structural and electrical character, (3) model and fabricate device structures from these films and (4) work in a collaborative manner with personnel in other SDIO/ONR programs in their diamond research.

This report is comprised of several papers which have been published or submitted for publication during the past year. These manuscripts discuss the most important progress during this period. A summary of each of these is given below:

Characterization of diamond thin films: diamond phase identification, surface morphology, and defect structures

Several conclusions have been drawn from the present research: (i) Films grown from a methane/hydrogen gas mixture by microwave plasma enhanced CVD were determined to be comprised almost entirely of diamond in terms of composition, structure, and bonding. (ii) The surface morphology of the diamond films has been observed to be a function of position on the sample surface and methane concentration in the feedgas. That is, well-faceted diamond crystals were observed near the center of the sample whereas an apparently non-faceted cauliflower texture was found very close to the sample edges, presumably due to temperature variations. Regarding the methane concentration dependence, for 0.3% CH_4 in H_2, threefold {111} facets were dominant, while at 1.0% and 2.0% CH_4 in H_2 fourfold {100} facets were dominant. (iii) A high defect density within individual diamond crystals was observed. The defects observed include {111} type twins, {111} stacking faults, dislocations, and grain boundaries. (iv) XTEM of a diamond film grown at 0.3% CH_4 has revealed a 50 Å epitaxial layer of β–SiC at the diamond-silicon interface. However, no evidence for any buffer layer of β–SiC was observed on a diamond film grown at 2.0% CH_4. (v) Local regions of "twinned epitaxy" have been observed in the films, indicating that the substrate orientation does appear to play a role in the growth of some of the diamond grains.

Surface analysis of diamond nucleation on silicon and electron microscopy of the diamond/silicon interface

Diamond films grown by microwave plasma CVD have been examined by AES, XPS and TEM. The surface analysis of a series of samples grown for various times indicated that a detectable SiC layer forms within the first five minutes of growth. Diamond then slowly begins to become detectable until, after two hours of growth, the SiC is no longer observed. In cross sectional electron microscopy, the presence of an epitaxial SiC layer was observed for samples grown with a low CH_4 concentration. However, contrary to the surface analysis results, such a layer was not observed in the samples grown with higher CH_4 concentrations. This is believed to be due to the very thin nature of the SiC layer in this case, probably caused by the diamond film "capping" the substrate more quickly and thus preventing further carburization.

Electron microscopy of vapor phase deposited diamond

High resolution electron microscopy (HREM) has been utilized to lattice image individual defects in polycrystalline diamond films. Numerous twins and stacking faults were observed, including their intersections. Five fold multiply twinned particles have been observed and it was found that the 7.5° misfit present in such particles has been accommodated at the twin boundaries rather than by elastic deformation. This creates a twin boundary coincident with a low angle grain boundary which has been termed a "tilted twin boundary." The density of defects in these particles is generally high; however, a dramatic reduction in the defect density near the twin boundaries was observed. This defect reduction is significant because if its origin can be determined, this information may be useful in producing higher quality diamond films.

Precursor structures in the formation of diamond films

The carbon bonding configurations of films prepared by plasma excited deposition of methane diluted with hydrogen are examined by Raman spectroscopy. In the limits of methane concentrations less than 1% of the films show predominant diamond character while for methane concentrations greater than 3%, Raman spectra are similar to those of microcrystalline or disordered graphite. At concentration of 2%, near the onset of diamond formation, a new feature is detected which exhibits a frequency similar to that expected for amorphous or microcrystalline diamond.

Bias controlled chemical vapor deposition of diamond thin film

The growth of diamond films on (001) Si substrates by bias controlled chemical vapor deposition is described. The film quality as judged by Raman spectroscopy and scanning electron microscopy depends strongly on the biasing conditions. Under low current reverse bias conditions, highly facetted cubooctahedral diamond growth

exhibiting a single sharp Raman line at 1332 cm^{-1} was obtained, while biasing in high current conditions which created a plasma resulted in multiply twinned, microcrystalline growth incorporating sp^2 bonded carbon into the diamond film.

Electrical Properties of B Doped CVD Grown Polycrystalline Diamond Films

B doped diamond films were synthesized by microwave plasma CVD, and the crystal quality and the electrical properties were investigated. From SEM, clear facets were observed and X-ray diffraction data showed that only the diamond phase was present. Raman spectroscopy verified the presence of diamond and indicated that the crystal quality increased when B is incorporated in the films up to 400 ppm. SIMS analysis showed that on the order of 10^{20}/cm^3 (564 ppm) of B was incorporated in the diamond films with a gas phase B/C ratio of 400 ppm. Electrode patterns of Pt were fabricated on the films and electrical properties were investigated. Undoped diamond films showed rectifying contacts with small leakage currents and B doped diamond films with a B concentration of 400 ppm showed ohmic behavior. The B in these films had small activation energies, which indicates that impurity band conduction plays an important role.

Diamond Electronic Devices for Microwave and MM/wave applications

Diamond IMPATTS show power conversion efficiency similar to that of conventional semiconductors (Si and GaAs) from 35 through 94 GHZ.

Due to the higher breakdown voltages and thermal conductivity, diamond IMPATTs are able to produce greater power than other semiconductors at the same frequency.

Large-signal computer simulations show that diamond IMPATTs can operate at 35 GHZ with 8.26 W, at 60 GHz producing 3.40 W, at 94 GHz producing 1.51 W, and at 220 GHz producing 54 mW of power.

The optimized design of uniform doped p-channel X-band diamond power MESFET has been investigated.

A p-channel diamond MESFET offers the potential to produce devices with RF output power greater than 10 W/mm gate width (or 18 W/unit gate width) with greater than 40% power-added efficiency at 10 GHz.

The high thermal conductivity of diamond allows high RF output power before thermal effects occur.

The high breakdown voltage of diamond allows large input RF voltages to be applied before saturation occurs.

The large-signal performance of a p-channel diamond power MESFET has been compared to an n-channel GaAs MESFET at 10 GHz.

Various designs of p-channel diamond devices have been investigated for a range of frequency 10 GHz - 100 GHz.

N-channel diamond MESFETs have improved RF performance compared to comparable p-channel MESFETs. A comparison at 60 GHz has been presented.

Collaboration with Other SDIO programs

For the most effective use of SDIO/IST funds cooperation and collaboration of SDIO contractors is very desirable. NCSU has a significant history of past collaboration with other diamond programs and will continue this spirit in the future.

Characterization of diamond thin films: Diamond phase identification, surface morphology, and defect structures

B. E. Williams and J. T. Glass

Department of Materials Science and Engineering, North Carolina State University, Raleigh, North Carolina 27695-7907

Thin carbon films grown from a low pressure methane-hydrogen gas mixture by microwave plasma enhanced CVD have been examined by Auger electron spectroscopy, secondary ion mass spectrometry, electron and x-ray diffraction, electron energy loss spectroscopy, and electron microscopy. They were determined to be similar to natural diamond in terms of composition, structure, and bonding. The surface morphology of the diamond films was a function of position on the sample surface and the methane concentration in the feedgas. Well-faceted diamond crystals were observed near the center of the sample whereas a less faceted, cauliflower texture was observed near the edge of the sample, presumably due to variations in temperature across the surface of the sample. Regarding methane concentration effects, threefold $\{111\}$ faceted diamond crystals were predominant on a film grown at 0.3% CH_4 in H_2 while fourfold $\{100\}$ facets were observed on films grown in 1.0% and 2.0% CH_4 in H_2. Transmission electron microscopy of the diamond films has shown that the majority of diamond crystals have a very high defect density comprised of $\{111\}$ twins, $\{111\}$ stacking faults, and dislocations. In addition, cross-sectional TEM has revealed a 50 Å epitaxial layer of β–SiC at the diamond-silicon interface of a film grown with 0.3% CH_4 in H_2 while no such layer was observed on a diamond film grown in 2.0% CH_4 in H_2.

I. INTRODUCTION

Diamond is an excellent candidate material for use in both electronic and wear resistant coating applications due to its exceptional hardness, strength, thermal conductivity, electron saturated drift velocity, hole and electron mobilities, chemical and thermal stability, radiation hardness, and optical transmission.[1-3] Electronic devices of particular interest include high power/high frequency devices and devices to be utilized in high temperature, chemically harsh, and/or high radiation flux environments. Recent developments in the growth of diamond films from low pressure (i.e., less than one atmosphere) gases have made the fabrication of such devices a real possibility, particularly since it has been shown that epitaxial diamond films can be grown on diamond substrates.[4-9] However, for diamond to reach its true potential, high quality monocrystalline films must be grown on economically viable, non-diamond substrates. Judging from various previous investigations, this is a formidable task since numerous experiments have yielded only highly defective, polycrystalline films to date. Therefore, to achieve high quality, monocrystalline films, we must gain a greater understanding of the nucleation and growth of diamond by thoroughly characterizing the films achieved to date. The information obtained from this characterization can then be fed back to the growth of these films to improve film quality and properties.

Diamond films have now been grown on various substrates (i.e., Si, SiO_2, Al_2O_3, β–SiC, α–SiC, Cu, Mo, W, WC, and Ni) by several different methods including hot filament enhanced chemical vapor deposition (CVD),[10-12] RF plasma enhanced CVD,[13] and microwave plasma enhanced CVD.[14-21] Scanning electron microscopy (SEM) has been utilized most extensively in order to examine surface morphology.[10-21] Raman spectroscopy has also been used in numerous investigations[12,14,15,19,20,22,23] to determine if diamond bonding was present. Reflection high energy electron diffraction and x-ray diffraction (XRD) have been used principally for comparing the lattice spacings of the diamond films with those reported for natural diamond.[10,12-14,17-21] More recently, transmission electron microscopy (TEM) has also been used in an initial study of defect structures in the film and the nucleation of diamond particles.[11,24,25]

For the research presented here, several different techniques have been utilized to thoroughly characterize diamond films grown by microwave plasma enhanced CVD in terms of the following: (i) elemental composition, structure, and bonding, (ii) surface morphology, and (iii) defect structures. Secondary ion mass spectrometry (SIMS) and Auger electron spectroscopy (AES) were used to determine the elemental composition of the film. Transmission electron diffraction and XRD allowed the determination of crystal structure and lattice spacing. AES was also used to examine the type of bonding (sp^2 vs sp^3) present at the surface of the film. Also, localized bonding in the bulk film was observed in the TEM via electron energy loss spectroscopy (EELS). SEM was utilized to examine the surface morphology of the diamond films. TEM was also utilized to observe the defect microstructure within single crystals in the films, to look for evidence of epitaxial

growth, and to examine the interface between the film and the substrate.

II. EXPERIMENTAL

A schematic diagram of the microwave plasma enhanced CVD system used to grow the diamond films in this research is shown in Fig. 1.[26] The microwaves from a 2.45 GHz power supply were guided via a rectangular waveguide through an isolator and a three-stub tuner to a 44 mm inner diameter quartz tube reaction chamber. The substrate was placed in the quartz tube which was in the path of the rectangular waveguide. The substrate temperature depended strongly on the microwave power and the gas pressure since microwave induction heating and plasma-substrate interactions were responsible for substrate heating (no independent substrate heater was utilized).

The diamond films analyzed in this research were grown on 2 cm by 1 cm n-type Si(111) substrates immersed in the CH_4/H_2 plasma created by the 2.45 GHz microwave source. The substrate temperature as measured by an optical pyrometer was maintained at approximately 800 °C by controlling the microwave power (which was typically 300–350 watts). No corrections were made for emissivity changes or for the quartz window; therefore, this temperature is an approximation. The total pressure in the chamber was maintained at 30 Torr, and only the CH_4/H_2 ratio in the feedgas was varied for the films studied in this work (between 0.3 and 2.0% CH_4 in H_2).

Prior to growth, the commercially polished silicon substrates were scratched with 0.25 μm diamond paste for one hour in order to increase the nucleation density of the diamond particles which make up the film. The substrates

FIG. 1. Schematic diagram of microwave plasma CVD system used for the deposition of diamond films.

were then ultrasonically cleaned in acetone, ethanol, and distilled water. Following growth, AES, SIMS, XRD, and SEM were performed without cleaning or coating after removal from the growth chamber.

For the TEM study, both plan-view and cross-sectional specimens were prepared. For plan-view TEM, 2.5 × 2.5 mm sections were cut from the as-grown sample with a diamond saw. The substrate was then thinned with 600 grit SiC paper to a thickness of 65 μm and subsequently polished with 0.3 μm Al_2O_3 suspended in water. This polished side was then dimpled with a steel ball coated with 1 μm diamond paste until the sample was less than 10 μm thick at the center of the crater. After affixing this sample to a 3 mm diameter Ta support ring, ion milling from the substrate side with 6 kV Ar^+ was used to thin the sample until perforation occurred. Cross-sectional TEM (XTEM) samples were prepared in a similar manner. In this case, sections were obtained by cutting perpendicular to the plane of the film after gluing the substrate to silicon buffer layers to form a sandwich. Thinning of the sample was achieved as described for plan-view TEM samples, and the dimpling crater was carefully aligned to ensure that perforation of the specimen during ion milling occurred very near the diamond film.

III. VERIFICATION OF THE DIAMOND PHASE

Verification of the diamond phase constitutes a substantial fraction of the present manuscript due to the relatively "young" nature of this area of low pressure, gas phase diamond synthesis, and the associated skepticism regarding the achievement of true diamond. Therefore, the films grown in this study were evaluated in terms of their composition, structure, and bonding via several characterization techniques in order to verify that true diamond (as opposed to "diamond-like" material) had actually been obtained. By evaluating the films in this manner, the properties of this CVD diamond can be compared to those of natural diamond or conventional high pressure synthesized diamond. Such an evaluation can also aid in determining if graphite or amorphous carbon has been incorporated in significant quantities into the diamond film. This is important since the conucleation of these phases with diamond is a severe problem if such parameters as temperature, pressure, and methane concentration are not optimized during the growth process.

A. Composition

The composition of the films examined in this research was evaluated via AES utilizing a JEOL JAMP 30 Auger microprobe and via SIMS utilizing a Cameca IMS 3f direct imaging microprobe. AES indicated that the surface of the film was composed of 88% C, 5.5% Si, and 6.5% O, as shown in Fig. 2(a). (Quantification of these impurities was obtained by measuring the peak-to-peak heights of the differentiated spectra and applying
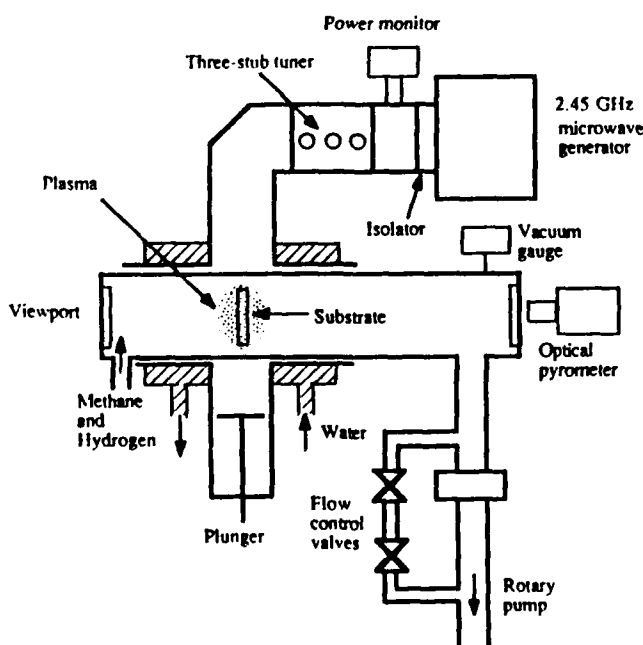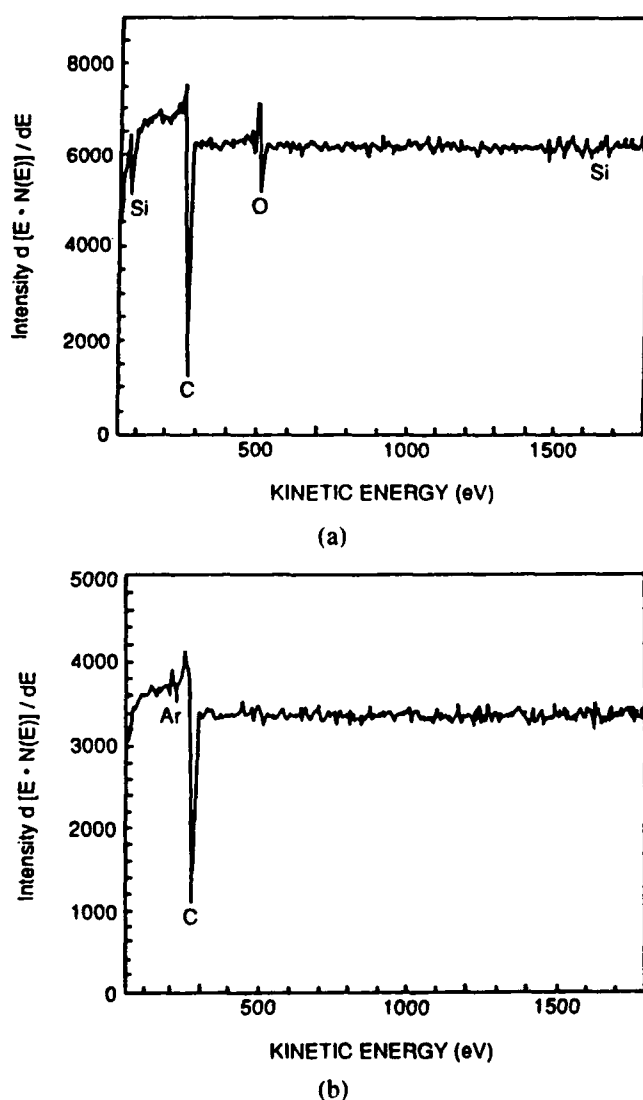
FIG. 2. (a) Broad Auger spectrum of diamond film before argon sputtering, showing the presence of Si and O on the surface. (b) Broad Auger spectrum of diamond film after argon sputtering, showing the absence of Si and O in the bulk of the film.

known sensitivity factors.[27]) Furthermore, the location of the Si peak energy at 84 eV indicates that it is bound to the oxygen. If the silicon were bound to carbon or in an elemental state, the peak energy would be shifted to ~94 eV.[27] Therefore, an oxide of silicon is present on the surface of the as-grown film. However, after argon sputtering for ~30 s at 3 kV and 30 mA, it was found that the only element present within the detection limits of this technique (~0.1% for most elements[28] except H which is virtually undetectable) was carbon, as shown in Fig. 2(b). We speculate that these surface impurities originated from the quartz reaction chamber during shutdown procedures of the microwave system, since they are not observed in the bulk of the film.

The results from the AES are encouraging; however, they do not yield any information about trace impurities due to the sensitivity limitations of the technique. Therefore, SIMS analysis, which is much more sensitive than AES, was conducted utilizing an oxygen primary beam to identify these trace impurities. Molecular filtering was utilized to avoid interference from molecular as opposed to elemental species, and relative isotope abundances were used to identify elements whenever possible. The films examined were found to be composed of mostly carbon with various amounts of H, O, Al, Si, Ca, and Cu present throughout the film. Furthermore, chemical maps of the Si, O, and Al indicated they were segregated in regions up to several microns in diameter.

Unfortunately, accurate quantification of SIMS data is not possible without standards. Since such standards were not available for the present research, accurate amounts of these trace impurities are not yet known. However, a very rough approximation obtained by neglecting matrix effects and utilizing published ion yield data[29] indicated that none of the impurities was present at concentrations greater than 1%, and all but the H and O were less than 0.1%. (The higher O content is due to O implantation from the primary O-beam utilized in this study.) This qualitatively correlates with the AES data. However, it should be pointed out that the regions where impurities were segregated (<5 μm) are "averaged" over the area of the primary beam (~150 μm), and thus local concentrations may be higher. Regardless, none of these elements was detected in the AES study of the film after sputtering.

B. Structure

As shown in Fig. 3, the structure of the films was confirmed to be that of diamond using selected area diffraction (SAD) in a Hitachi H-800 transmission electron microscope. A plan-view bright-field TEM image and the associated SAD pattern are seen in Fig. 3(a). The plane spacings of the film determined from this SAD pattern are shown in Fig. 3(b). These measurements were calibrated using the silicon substrate as a reference. The reported ASTM values for natural diamond are also shown in this figure for comparison. Note the excellent agreement between the plane spacings measured for the film vs those reported for natural diamond. X-ray diffraction was also used to measure plane spacings of the diamond film, and the results of this work agree within experimental error with the electron diffraction data.

C. Bonding

Although the films have been shown to be composed almost entirely of carbon and the diamond cubic structure has been verified in the films, this is not sufficient evidence to label the films "diamond." This is because electron and x-ray diffraction which were used in this research to identify the diamond structure are not sensitive to small amounts of amorphous components within the films. Furthermore, amorphous carbon containing significant π-

(a)

Observed hkl	Reported d(Å)	(ASTM 6-675) d(Å)
111	2.060	2.060
220	1.265	1.261
311	1.073	1.0754
400	0.896	0.8916
331	0.814	0.8182

(b)

FIG. 3. (a) Bright-field TEM micrograph of a diamond film with SAD pattern inset. (b) Interplanar spacings calculated from the SAD pattern in (a) with reported ASTM spacings for natural diamond.

type bonding is a common CVD product.[30-32] Therefore, it must be shown that this type of amorphous material does not exist in significant quantities within the film. Furthermore, many of the unique and desirable characteristics of diamond are a result of the sp^3 bonding which forms the diamond structure. Therefore, the true nature of the bond type in the film must be determined. This can be accomplished by examining the interband transition and K-shell ionization regions of the electronic structure of the films using AES and EELS, as described below.

The AES results described in this section were obtained using a Perkin-Elmer Physical Electronics electron gun and double pass cylindrical mirror analyzer. The beam voltage used was 1.5 kV, and the beam current was kept at 0.5 μA to minimize beam damage. The samples were not pretreated in any way, and long exposure to the atmosphere had occurred prior to analysis. The examinations were confined roughly to the center regions of the sample to avoid exciting the Si substrate exposed at the edges of the sample.

The binding energy of core electrons in diamond vs graphite or amorphous carbon has been shown to shift less than 1 eV,[36] which is too small to observe in most conventional electron spectrometer systems utilized for AES and XPS. Furthermore, charging of the substrate during AES and XPS is difficult to assess quantitatively and also causes energy shifts, thus adding further ambiguity to binding energy measurements. However, the AES fine structure of the C KLL peak has been shown to be sensitive to these three allotropes of carbon and is not affected significantly by charging.[37] This is analogous to fine structure differences which have been used to identify the presence of metal carbides vs elemental metal species.[38] In the case of diamond and graphite, this fine structure has been explained by a band structure model correlating the experimental peaks with peaks in the calculated density of states in the respective band structures. Therefore, in an AES system with moderate resolution (~1 eV in the present case), the shape of the fine structure on the low energy side of the carbon KLL peak can be used to distinguish among diamond, graphite, and amorphous carbon, as shown below.

Differentiated carbon KLL Auger spectra are shown in Fig. 4. Figure 4(a) illustrates the C KLL fine structure for a typical CVD film. Inset in this figure are the spectra for natural diamond, graphite, and amorphous carbon from Lurie and Wilson.[37] It can be seen that diamond, which contains only sp^3 bonds, yields a very different fine structure from graphite and amorphous carbon which both contain sp^2 bonding. Direct comparison of these spectra with the spectrum obtained from the films analyzed in the present study reveals that the diamond film yields a fine structure very similar to natural diamond. That is, the intensity of the fine structure peak closest to the primary C KLL peak is greater than the peak located at a slightly lower energy. The situation is reversed for graphite, as seen by Lurie and Wilson's results in the inset as well as by a pyrolytic graphite sample examined in the present research and shown in Fig. 4(b). Amorphous carbon yields a "smeared" fine structure relative to diamond and graphite, as also shown in the inset. Therefore, it appears that the surface of this film is composed of diamond (sp^3) type bonding. It should be noted that the sensitivity of this technique (i.e., the concentration of sp^2 bonding which is necessary before it will be detected) is not currently known, but research of known concentrations of graphite in diamond is underway to attempt to determine its sensitivity.
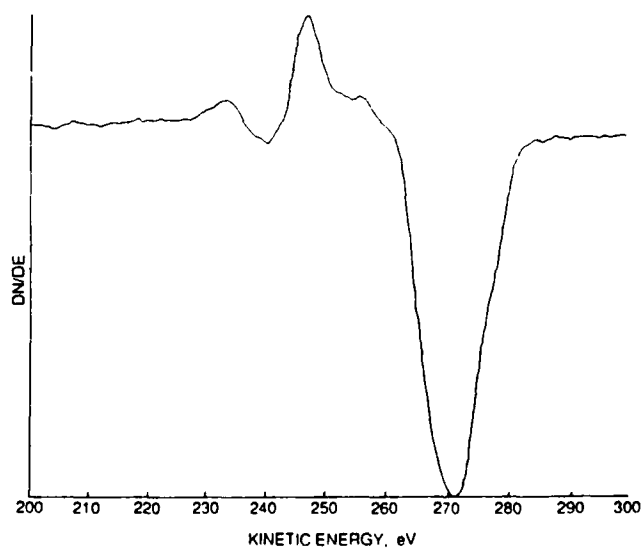
An interesting change in the surface bonding was observed after argon sputtering. This is significant because argon sputtering is commonly used for substrate cleaning

(a)

(b)

(c)

FIG. 4. (a) Auger spectrum about the C *KLL* energy, showing fine structure of diamond film with inset spectra from Lurie and Wilson.[37] (b) Auger spectrum about the C *KLL* energy, showing fine structure obtained on pyrolytic graphite in this research. (c) Auger spectrum about the C *KLL* energy, showing fine structure of a diamond film after sputtering for 30 s with a rastered (9 × 9 mm) Ar^{+} beam (V = 1.5 kV, I = 2.5 μA).

prior to CVD deposition of many materials. Figure 4(c) is an energy scan taken about the C *KLL* peak after sputtering for only 30 s with a rastered (9 × 9 mm^2) Ar$^+$ beam of relatively low accelerating voltage and beam current (V = 1.5 kV, I = 2.5 μA). Comparison of this spectrum to that shown for graphite in Fig. 4(b) reveals that the argon sputtering has caused the shape of the AES fine structure to appear more graphitic. That is, the lower energy peak intensity is much greater than the intensity of the peak closest to the major carbon peak, which is reversed from what was observed for diamond. This is an indication that the argon sputtering has increased the sp^2 bonding component at the surface of the film. Research is ongoing to determine the depth of this damage after sputtering and to determine if subsequent annealing of this surface in hydrogen can revert the surface to its original diamond state.

In order to verify the conclusion presented above that the film is composed of diamond-type bonding and to determine that this bonding is present not only at the surface but also in the bulk of the film, EELS in the transmission mode was conducted on a Philips 400 TEM equipped with a field emission gun and Gatan electron spectrometer. The accelerating voltage used in these measurements was 100 kV. Energy losses due to excitation of core level electrons (K-shell ionization) which appear at higher energies in the EELS spectrum can be used to identify different phases of carbon because the position and shape of this region of the spectrum is strongly dependent on the type of bonding present. The energy loss spectrum obtained from the diamond film about the carbon K-edge is shown in Fig. 5. The reference spectra[39] inset in this figure illustrate two important features in terms of identifying the diamond phase. First, the energy of the carbon K-edge in the diamond film (measured at one-third of the peak height of the absorption edge) is at 291 eV, which is characteristic of natural diamond. This is significant because the K-edge energies for natural diamond, graphite, and amorphous carbon are approximately 291, 286, and 284 eV, respectively. Second, the shape of the K-shell ionization region for the spectrum obtained on the diamond film in Fig. 5 is characteristic of that of diamond. That is, no peak is observed below 291 eV, and an additional peak is observed at higher energies. Therefore, the film has been shown to contain diamond, sp^3 type bonding by both EELS and AES.
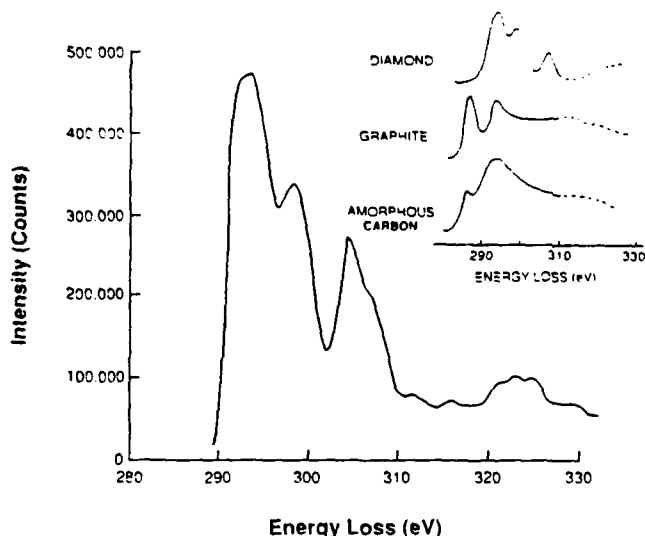
FIG. 5. EELS spectrum near the K-shell ionization energy from a single diamond grain in the Philips 400 TEM with reference spectra obtained from amorphous carbon, graphite, and diamond by Egerton[39] inset.

It should be noted that Raman spectroscopy was also performed on these samples to verify the presence of diamond bonding and is the subject of separate publications.[22,23] It is sufficient to say here that a diamond 1332 cm^{-1} Raman peak was observed for these samples, thus verifying the presence of diamond bonding. For the samples grown with higher methane concentrations, especially 2.0%, other peaks indicating amorphous C and microcrystalline graphite impurities were also observed. Due to the large difference in scattering cross sections between diamond and graphite,[40] this may or may not indicate a significant sp^2 bonding component. Unfortunately, as in the case of AES and EELS, experimental correlation between Raman peak intensity and percentage of non-diamond component in a film has not yet been accomplished. For more details on the Raman analysis of these and other samples, the reader should consult Refs. 12, 14, 15, 19, 20, 22, 23, 40, and 41.

In summary of Sec. III, the films grown from a methane/hydrogen gas mixture by microwave plasma enhanced CVD have been examined in terms of composition, structure, and bonding. They were found to be composed almost entirely of carbon except at the surface where significant amounts of silicon and oxygen were present. Both the structure and bonding in the films were identical to those found in natural diamond within the resolution of the techniques employed. Therefore, it has been demonstrated that the films are comprised of the diamond phase. Future research will be directed to determining the amount of sp^2 bonding which may be present as an impurity.

IV. SURFACE MORPHOLOGY AND DEFECT STRUCTURES

Scanning electron microscopy was utilized to examine the surface morphology of the samples. In general, a

highly faceted, polycrystalline film was observed, as illustrated by Fig. 6; however, deviations from this faceting were observed near the edges of the samples, as shown in Fig. 7(a–c). For example, the center region of a 2 cm × 1 cm sample grown with 1.0% CH_4 in H_2 is shown in Fig. 7(a). In a region 2.5 mm from the edge of the sample shown in Fig. 7(b), the diamond is less faceted, and a mixture of microcrystalline and cauliflower-type particles is prevalent behind the faceted grains which have decreased in concentration. In Fig. 7(c), which is from an area within 0.5 mm of an edge of the sample, the large facets have disappeared entirely, and the cauliflower texture is all that is observed. Such a cauliflower texture is believed to be caused by an increased concentration of sp^2 bonding in the film, as suggested by Raman data.[26] Such an abrupt change in morphology on a single substrate is believed to be due to changes in the local growth conditions, especially temperature, on different areas of the sample.

Along with location on the sample, surface morphology is a strong function of methane concentration in the feed gas. For all of the methane concentrations studied in the present research, the samples were predominantly covered by well-faceted crystals up to ∼1 μm in size. At 0.3% CH_4, threefold {111} facets dominated the morphology, as shown in Fig. 8(a); however, at 1.0% and 2.0% CH_4, fourfold {100} facets were dominant [see Fig. 8(b)]. This implies that in the lower concentrations the {100} planes are the faster growing planes, and in the higher concentrations the {111} planes grow fastest. Previous research on these films utilizing Raman spectroscopy[22,26] has shown that the sp^2 bonding component is greater in the films grown with 2.0% CH_4 in H_2 than the films grown with 0.3% CH_4 in H_2 although no quantification has been possible to date. Several other phenomena were apparent during this surface morphology evaluation. Surface steps were present on both the {111} and {100} facets, suggesting a
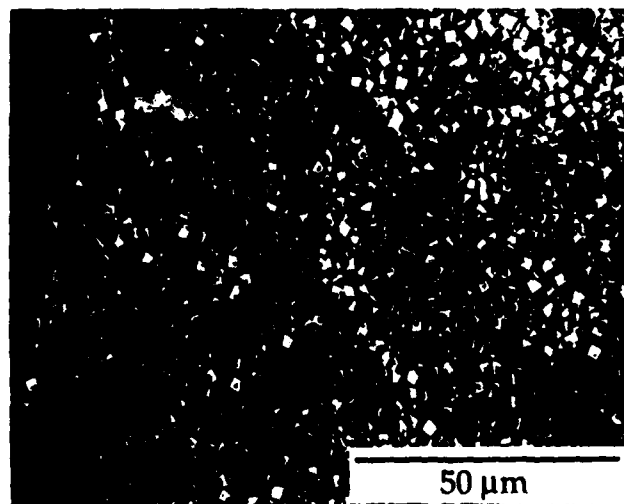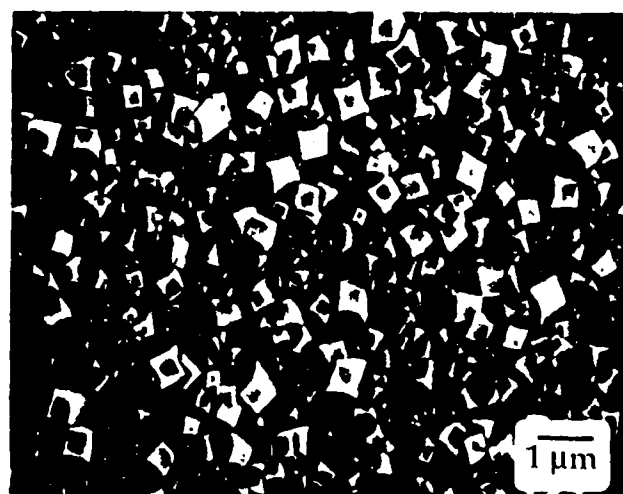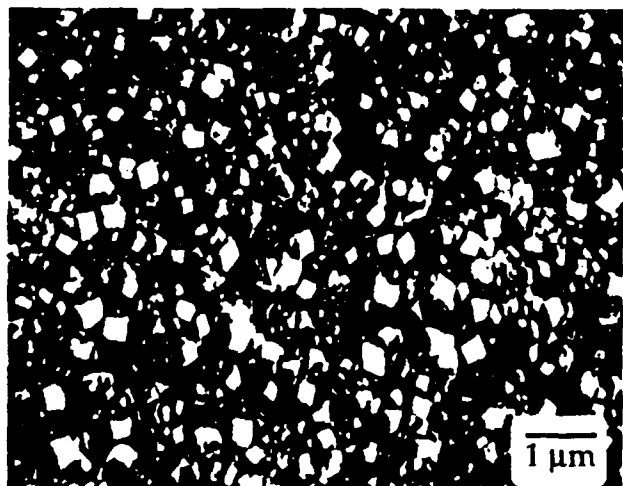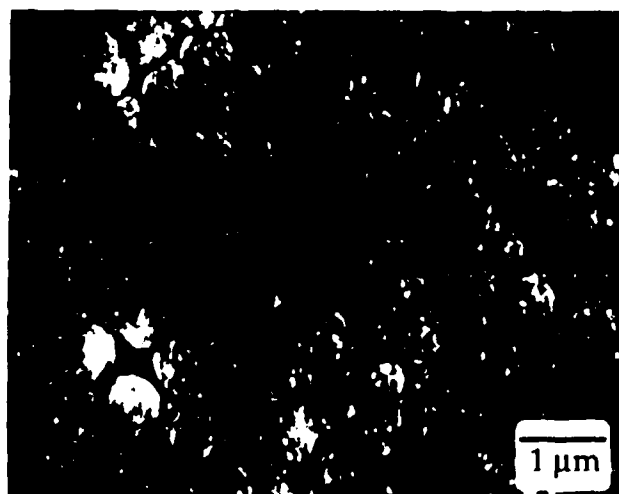

FIG. 6. SEM micrograph of a typical well-faceted diamond film.

(a)

(a)

(b)

(b)

FIG. 8. (a) SEM micrograph of a diamond film exhibiting 3-fold particles, indicative of {111} planes. (b) SEM micrograph of a diamond film exhibiting 4-fold particles, indicative of {100} planes.
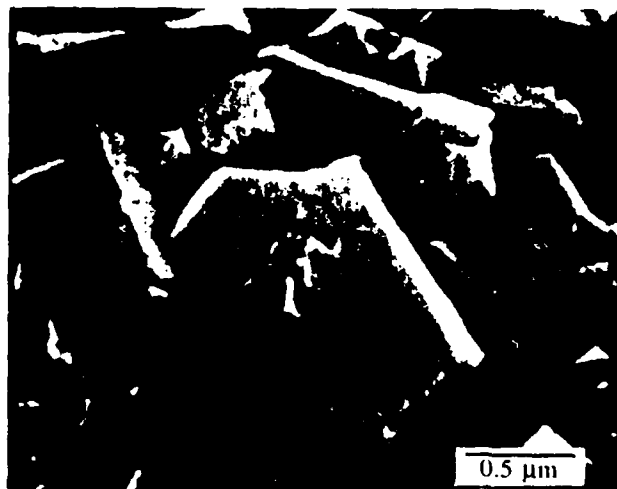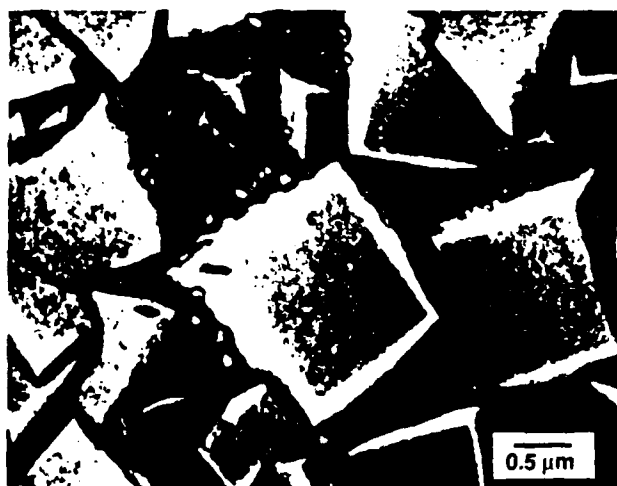

(c)

FIG. 7. (a) SEM micrograph of the center region of a 2 cm × 1 cm sample grown with 1.0% CH₄ in H₂. (b) SEM micrograph of the diamond film 2.5 mm from the edge of the sample (c) SEM micrograph of the diamond film within 0.5 mm of an edge of the sample

two-dimensional growth mode for the diamond on diamond. Secondary nucleation was observed on the {111} facets and appeared to have a definite orientational relationship to the parent grain. On the {100} dominated films, secondary nucleation was observed primarily between the grains, in which case its orientation was random. Finally, films grown at the lower methane concentrations were found to contain many more multiply twinned particles than those grown at higher methane concentrations.

Transmission electron microscopy (TEM) was utilized for the examination of defect structures in the diamond films. Previous investigations have shown that planar defects including {111} stacking faults and {111} twins are quite common in natural diamond, high pressure–high temperature synthesized diamond, and shock-wave synthesized diamond.[42-46] Dislocations and dislocation structures have been studied extensively, and platelet defects associ-

ated with the presence of aggregates of foreign atoms (e.g., nitrogen) have also been examined in great detail.[47-49] However, relatively few TEM examinations of CVD diamond films have been reported.[11,24,25] Therefore, a significant effort has been devoted to plan view and cross-sectional TEM of these diamond films in the present research.

A plan view TEM micrograph of a diamond film is shown in Fig. 9. Qualitatively, a variety of defects can be seen in this material. The contrast reversal at point (a) with respect to the surrounding areas indicates a twinned region which is relatively large compared with the majority of twins found in this material, as discussed later. Dislocations are observed at (b), and small triangular defects believed to be stacking fault tetrahedra are present at (c). Finally, a grain boundary is indicated by (d). No phase other than diamond was observed during the TEM study.

Twinning was the most predominant defect observed in all of the diamond samples. Figure 10 is a TEM bright-field [10(a)], dark-field [10(b)] pair of a single diamond grain viewed along the [011] direction in a plan-view sample of a diamond film grown at 0.3% CH$_4$. A high density of twins (visible as dark lines) is observed in Fig. 10(a) on the two {111} planes which are in a diffracting condition in this orientation. The dark-field image shown in Fig. 10(b) was obtained using a (111) spot from one set of the twins, causing them to appear bright in this micrograph. Additional information regarding the nature of these twins was obtained from careful examination of a diffraction pattern shown in Fig. 11 obtained from this grain in the SAD mode. The two sets of twins have given rise to the twin spots located at one-third of the distance between the major spots from the untwinned material, as indexed on this figure. Streaking of the diffraction pattern normal to the {111} planes is also observed. Such streaking

0.1 μm

(a)

0.1 μm

(b)

FIG. 10. TEM bright-field (a), dark-field (b) pair of a single diamond grain viewed along the [011] in a plan-view sample of a diamond film grown at 0.3% CH$_4$.

0.1 μm

FIG. 9. Electron micrograph of single diamond grain exhibiting (a) twins, (b) dislocations, (c) stacking fault tetrahedra, and (d) a grain boundary.

can be attributed to the presence of either stacking faults or coherent twin boundaries.

A preliminary HRTEM examination of these twins was accomplished on a JEOL 200 CX microscope. Figure 12 is an HRTEM micrograph of a single diamond grain from the same sample studied in Figs. 10 and 11. Since the diamond grain is in a [011] orientation, {111} cross-fringes of 2.05 Å spacing are visible. Note that within 100 Å, the diamond has twinned three times. (The mirror plane for each twin is indicated by an M on the micrograph.)

The diamond films were also examined via cross-sectional TEM (XTEM). Figure 13 is an XTEM micrograph of a diamond film grown at 2.0% CH$_4$. Notice the columnar type growth which the grains appear to have undergone. The dark areas which are associated with defects and/or strain in the film appear to fan out from a small
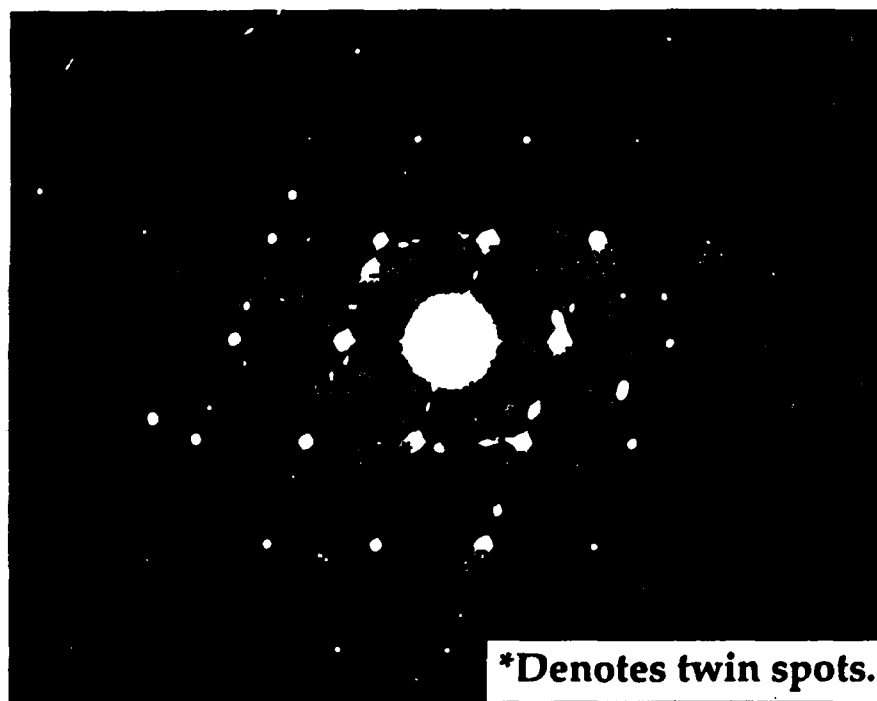
FIG. 11. Diffraction pattern obtained in SAD mode from the grain shown in Fig. 10. The two sets of twins have given rise to the twin spots located at one-third of the distance between the major spots from the untwinned material, as indexed by labels marked with asterisks centered about the corresponding diffracted spots.
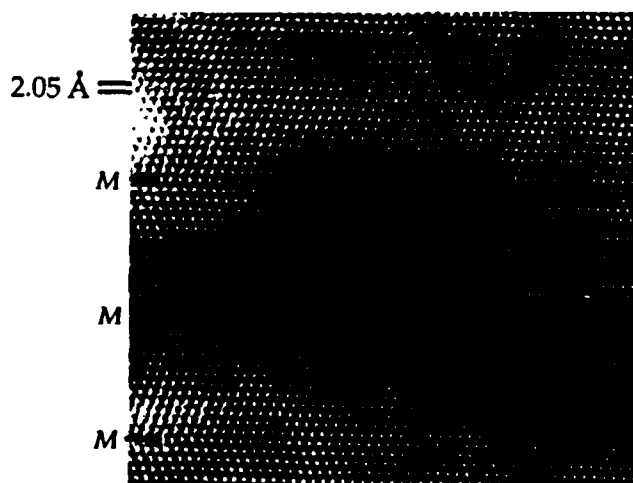

FIG. 12. HRTEM micrograph of a single diamond grain where {111} cross-fringes of 2.05 Å spacing are visible. Several twins are visible and the mirror planes for each are indicated by an M on the micrograph.

FIG. 13. XTEM micrograph of film grown in 2.0% CH_4/H_2, showing fanning out of defects from the diamond-silicon interface.

region at the surface, implying a single nucleation site for the grain. This supports the general observations that the CVD diamond undergoes 3-D rather than 2-D growth and that film adherence is usually rather poor. A higher magnification of this film and a film grown at 0.3% CH_4 are shown in Figs. 14(a) and 14(b), respectively. The density of defects (indicated by the dark regions in the micrograph) in the 2.0% CH_4 film [Fig. 14(a)] is significantly higher than that observed in the XTEM micrograph of the 0.3% CH_4 film [Fig. 14(b)]. The dark areas appear to be much less dense in the 0.3% CH_4 film, probably due to the

lower growth rate at these lower methane concentrations which allows a less defective and/or less strained film to form. This observation may also be related to a decreased sp^2 bonding component which was observed during Raman spectroscopy,[22,26] but more research is necessary to confirm this hypothesis.

Closer examination of the diamond/silicon interface of films grown at 2.0% and 0.3% CH_4/H_2 reveals significant differences in the nature of this interface. In Fig. 14(a), the apparent interface layer is actually due to ion milling damage caused by the presence of the interface and the very

(a)

FIG. 15. XTEM micrograph of diamond film grown in 0.3% CH_4/H_2, showing 50 Å layer of β-SiC at the interface.

(b)

FIG. 14. (a) XTEM micrograph of diamond film grown in 2.0% CH_4/H_2, showing increased density of defects in the diamond film. (b) XTEM micrograph of diamond film grown in 0.3% CH_4/H_2, showing lower defect density in the diamond film.

different milling characteristics of the diamond film and the silicon substrate. This was confirmed by the absence of a second phase in this region during microdiffraction and the observation that no depth was apparent in this layer during TEM examination (i.e., this feature is confined to the surface of the TEM specimen). Therefore, it is believed to be an amorphous surface layer caused by interaction of the ion milling beam with the interface during sample preparation.[50] On the other hand, a sample grown at 0.3% CH_4 yields an obvious interfacial layer approximately 50 Å thick, as shown in Fig. 15. This is easily distinguished from an ion milling damage layer by the defect contrast observed as dark lines in the layer and the depth which was apparent parallel to the electron beam in this re-

gion, indicating it is not simply a surface artifact. Furthermore, a SAD pattern from this region shown in Fig. 16 indicated that this interfacial layer was β-SiC. The alignment of the Si(111) and SiC(111) diffraction spots indicates that in the region of this SAD the β-SiC buffer layer is a single crystal, epitaxial with the Si substrate (i.e., β-SiC(111)‖Si(111), β-SiC[110]‖Si[110]). This is not surprising since epitaxial β-SiC layers have been grown on Si(111) substrates by thermal CVD.[51] However, it is also known that the quality of an epitaxial layer of β-SiC on Si(111) is relatively poor. This is apparent in the present research in Fig. 16 by the smearing out of spots (indicating residual strain) and the alternating dark and light areas in the layer (see Fig. 15), which are believed to be caused by various defects and strain associated with (i) the poor lattice and thermal coefficient of expansion match between Si and SiC, (ii) the fact that growth conditions were not optimized for the formation of the SiC in the present research, and (iii) growth of β-SiC on Si(111), which has been shown by previous investigators to be of relatively poor quality.[51]

Several other interesting observations can be made by carefully analyzing the SAD pattern in Fig. 16. First, although the diamond film is known to be polycrystalline, this diffraction pattern indicates that one of the grains (labeled grain #1) observed here is actually in a twinned epitaxial relationship with the Si substrate. That is, diamond (111)‖Si(111) and diamond [0$\bar{1}$1]‖Si[01$\bar{1}$]. Thus, two of the diamond (111) spots are seen to be aligned with Si(111) spots while the other two (111) spots for this grain are reflected across the [111] direction from where one would expect for "conventional" epitaxy. The Si substrate and diamond grain are related by a mirror plane located at the diamond/Si interface in this case. Diamond grain #2 in this micrograph is rotated ~34° about the [110] direction relative to the [110] direction in the Si substrate. This will

(a)

- Silicon
- β–SiC
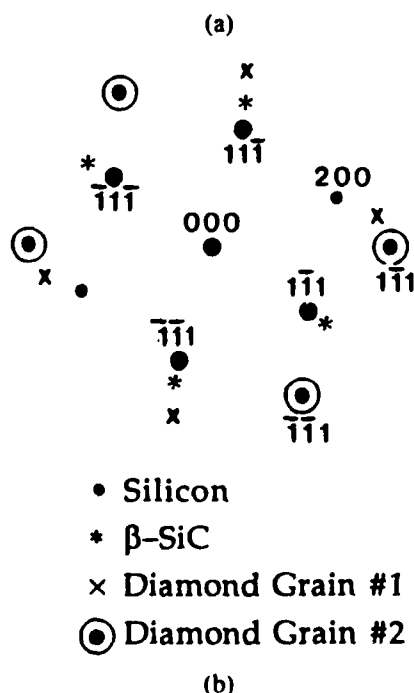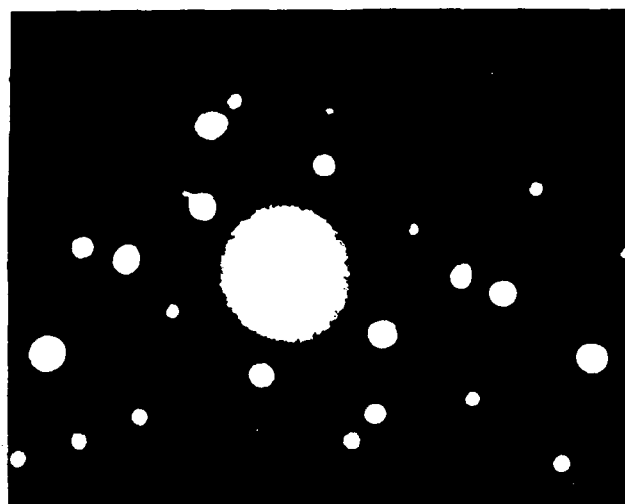- x Diamond Grain #1
- ⊙ Diamond Grain #2

(b)

FIG. 16. (a) Diffraction pattern obtained in SAD mode from the region shown in Fig. 15. (b) Indexed schematic diagram of SAD pattern shown in (a).

give rise to a grain boundary where these two grains meet. HRTEM has recently verified this "twinned epitaxy" and the presence of the SiC buffer layer and is currently being utilized to understand grain boundaries and defects in the films. This HRTEM will be the subject of another publication in the near future.

V. SUMMARY

Several conclusions have been drawn from the present research: (i) Films grown from a methane/hydrogen gas mixture by microwave plasma enhanced CVD were determined to be comprised almost entirely of diamond in terms of composition, structure, and bonding. (ii) The surface

morphology of the diamond films has been observed to be a function of position on the sample surface and methane concentration in the feedgas. That is, well-faceted diamond crystals were observed near the center of the sample whereas an apparently non-faceted cauliflower texture was found very close to the sample edges, presumably due to temperature variations. Regarding the methane concentration dependence, for 0.3% CH_4 in H_2, threefold {111} facets were dominant, while at 1.0% and 2.0% CH_4 in H_2 fourfold {100} facets were dominant. (iii) A high defect density within individual diamond crystals was observed. The defects observed include {111} type twins, {111} stacking faults, dislocations, and grain boundaries. (iv) XTEM of a diamond film grown at 0.3% CH_4 has revealed a 50 Å epitaxial layer of β–SiC at the diamond-silicon interface. However, no evidence for any buffer layer of β–SiC was observed on a diamond film grown at 2.0% CH_4. (v) Local regions of "twinned epitaxy" have been observed in the films, indicating that the substrate orientation does appear to play a role in the growth of some of the diamond grains.

REFERENCES

[1] Landolt and Börnstein, *Numerical Data and Functional Relationships in Science and Technology* (Springer-Verlag, 1987).
[2] J. E. Field, *Properties of Diamond* (Academic Press, London, 1979).
[3] V. K. Bazhenov, I. M. Vikulin, and A. G. Gontar, Sov. Phys. Semicond. **19** (8), 829 (1985).
[4] B. V. Derjaguin, B. V. Spitsyn, A. E. Gorodetsky, A. P. Zakharov, L. I. Bouilov, and A. E. Aleksenko, J. Crystal Growth **31**, 44 (1975).

[5]B. V. Deryagin, D. V. Fedoseev, N. D. Polyanskaya, and E. V. Statenkova, Sov. Phys. Crystallogr. 21 (2), 239 (1976).

[6]B. V. Deryagin, V. G. Lyuttsau, D. V. Fedoseev, and V. A. Ryabov, Sov. Phys. Dokl. 15 (1), 58 (1970).

[7]D. V. Fedoseev, V. P. Varnin, and B. V. Deryagin, Sov. Phys. Dokl. 15 (8), 787 (1971).

[8]M. W. Geis, presented at the Third Annual SDIO/IST-ONR Diamond Technology Initiative Symposium, Crystal City, VA, July (1988).

[9]H. Nakazawa, Y. Kanazawa, M. Kamo, and K. Osumi, Thin Solid Films 151 (2), 199 (1987).

[10]B. Singh, Y. Arie, A. W. Levine, and O. R. Mesker, Appl. Phys. Lett. 52 (6), 451 (1988).

[11]S. Matsumoto and Y. Matsui, J. Mater. Sci. 18, 1785 (1983).

[12]A. Sawabe and T. Inuzuka, Thin Solid Films 137, 89 (1986).

[13]S. Matsumoto, J. Mater. Sci. Lett. 4, 600 (1985).

[14]Y. Sato, M. Kamo, and N. Setaka, in High Tech Ceramics, edited by P. Vincenzini (Elsevier Science Publishers B.V., Amsterdam, 1987).

[15]K. Kobashi, K. Nishimura, Y. Kawate, and T. Horiuchi, J. Vac. Sci. Technol. A 6 (3), 1816 (1988).

[16]H. Kawarada, K. S. Mar, and A. Hiraki, Jpn. J. Appl. Phys. 26 (6), L1032 (1987).

[17]M. Kamo, Y. Sato, S. Matsumoto, and N. Setaka, J. Cryst. Growth 62, 642 (1983).

[18]Y. Mitsuda, Y. Kojima, T. Yoshida, and K. Akashi, J. Mater. Sci. 22, 1557 (1987).

[19]P. K. Bachmann, W. Drawl, Diane Knight, R. Weimer, and R. F. Messier, in Diamond and Diamond-Like Materials Synthesis, edited by G. H. Johnson, A. R. Badzian, and M. W. Geis (Materials Research Society, 1988).

[20]C. P. Chang, D. L. Flamm, D. E. Ibbotson, and J. A. Mucha, J. Appl. Phys. 63 (5), 1744 (1988).

[21]Y. Saito, S. Matsuda, and S. Nogita, J. Mater. Sci. Lett. 5, 565 (1986).

[22]R. J. Nemanich, R. E. Shroder, J. T. Glass, and G. Lucovsky, to be published in the Proc. 19th Int. Conf. on the Physics of Semiconductors, Warsaw, Poland, August 1988.

[23]R. J. Nemanich, J. T. Glass, G. Lucovsky, and R. E. Shroder, J. Vac. Sci. Technol. 6 (3), 1783 (1988).

[24]H. Kawarada, K. S. Mar, J. Suzuki, T. Ito, H. Mori, H. Fujita, and A. Hiraki, Jpn. J. Appl. Phys. 26 (11), L1903 (1987).

[25]B. E. Williams, J. T. Glass, R. F. Davis, K. Kobashi, and Y. Kawate, in Diamond and Diamond-Like Materials Synthesis, edited by G. H.

Johnson, A. R. Badzian, and M. W. Geis (Materials Research Society, 1988).

[26]K. Kobashi, K. Nishimura, Y. Kawate, and T. Horiuchi, Phys. Rev. B 38 (6), 4067 (1988).

[27]Handbook of Auger Electron Spectroscopy (JEOL Ltd., Tokyo, 1982).

[28]L. C. Feldman and J. W. Mayer, Fundamentals of Surface and Thin Film Analysis (North-Holland, New York, 1986).

[29]H. A. Storms, K. F. Brown, and J. D. Stein, Anal. Chem. 49 (13), 2023 (1977).

[30]S. Berg and L. P. Andersson, Thin Solid Films 58, 117 (1979).

[31]D. C. Ingram, J. A. Woollam, and Bu-Abbud, Thin Solid Films 137, 225 (1986).

[32]J. C. Angus, Thin Solid Films 142, 145 (1986).

[33]O. Matsumoto, H. Toshima, and Y. Kanzaki, Thin Solid Films 128, 341 (1985).

[34]M. J. Mirtich, J. S. Sovey, and B. A. Banks, NASA Tech. Briefs, p. 139, May/June (1986).

[35]T. Mori and Y. Namba, J. Vac. Sci. Technol. A 1 (1), 23 (1983).

[36]F. R. McFeely, S. P. Kowalczyk, L. Ley, R. G. Cavell, R. A. Pollak, and D. A. Shirley, Phys. Rev. B 9 (12), 5268 (1974).

[37]P. G. Lurie and J. M. Wilson, Surf. Sci. 65, 476 (1977).

[38]H. H. Madden, J. Vac. Sci. Technol. 18 (3), 677 (1981).

[39]R. F. Egerton and M. J. Whelan, Philos. Mag. 30, 739 (1974).

[40]S. A. Solin and A. K. Ramdas, Phys. Rev. B 1 (4), 1687 (1970).

[41]N. Wada and S. A. Solin, Physica B 105, 353 (1981).

[42]G. S. Woods, Philos. Mag. 23, 473 (1971).

[43]G. S. Woods, Philos. Mag. 34 (6), 993 (1976).

[44]L. F. Trueb, J. Appl. Phys. 39 (10), 4707 (1968).

[45]C. Phaal and G. Zuidema, Philos. Mag. 14 (127), 79 (1966).

[46]Y. Moriyoshi, M. Kamo, N. Setaka, and Y. Sato, J. Mater. Sci. 18, 217 (1983).

[47]P. Humble, Proc. R. Soc. London, A 381, 65 (1982).

[48]P. Humble, D. F. Lynch, and A. Olsen, Philos. Mag. A 52 (5), 623 (1985).

[49]P. Humble, J. K. Mackenzie, and A. Olsen, Philos. Mag. A 52 (5), 605 (1985).

[50]C. H. Carter, R. F. Davis, and S. R. Nutt, J. Mater. Res. 1 (6), 811 (1986).

[51]H. P. Liaw and R. F. Davis, J. Electrochem. Soc. 12 (131), 3014 (1984).

384

J. Mater. Res., Vol. 4, No. 2, Mar/Apr 1989

SURFACE ANALYSIS OF DIAMOND NUCLEATION ON SILICON AND ELECTRON MICROSCOPY OF THE DIAMOND/SILICON INTERFACE

B. E. WILLIAMS, D. A. ASBURY AND J. T. GLASS
Department of Materials Science and Engineering
North Carolina State University
Raleigh, NC 27695-7907

ABSTRACT. The nucleation of diamond films grown by microwave plasma chemical vapor deposition on silicon substrates has been examined by Auger electron spectroscopy (AES), x-ray photoelectron spectroscopy (XPS) and electron microscopy. Furthermore, cross sectional transmission electron microscopy (XTEM) was utilized to examine the diamond/silicon interface. The immediate (< 5 minutes) formation of a cubic SiC buffer layer was observed prior to the growth of a detectable diamond film. This SiC layer was too thin to be observed (< 10 monolayers) in XTEM when methane concentrations in the feedgas were relatively high (2.0%) but was observable via AES and XPS even at 3.0% CH_4. At low concentrations (0.3% CH_4) the SiC layer was relatively thick (~50Å) and easily observed in XTEM.

Introduction

Diamond is an excellent candidate material for use in both electronic and wear resistant coating applications due to its unique combination of exceptional properties.[1-3] Regarding electronic applications, these properties include high hole and electron mobilities (2000 and 1800 $cm^2 \cdot V^{-1} \cdot sec^{-1}$, respectively), a high breakdown voltage, high carrier drift velocities, and a much higher thermal conductivity (from 1000 to 10,000 W/m-K) than even copper, which is considered a good thermal conductor. Diamond films may thus be utilized as heat sinks on which to mount various electronic devices fabricated from more conventional semiconductors such as Si and GaAs or directly for the fabrication of microwave devices as well as devices to be employed in high power, high current density, high temperature and/or high radiation flux applications. Recent attempts to grow diamond films for such potential applications have been very encouraging. Researchers have deposited polycrystalline diamond films via RF-plasma CVD,[4] microwave plasma CVD,[5] and hot filament CVD[6] as well as various modifications of these techniques. However, in order to reach the true potential of diamond in many of the aforementioned electronic applications, high quality single crystal films will be necessary on economical non-diamond substrates. Therefore, it is important to develop an understanding of the nucleation of diamond on substrates of interest. The present paper investigates such nucleation on "scratched" single crystal Si substrates which have been the most extensively utilized substrates to date.

Experimental

The diamond films analyzed in this research were grown on 2 cm by 1 cm n-type Si (111) substrates immersed in a CH_4/H_2 plasma created by a 2.45 GHz microwave source. A schematic of the deposition system is shown in Figure 1. Details of the system have been given elsewhere.[7] The substrate temperature as measured by an optical pyrometer was maintained at approximately 800°C by controlling the microwave power (which was typically 300 - 350 watts). No corrections were made for emissivity changes or for the quartz window; therefore, this temperature is an approximation. The total pressure in the chamber was maintained at 30 Torr, and only the CH_4/H_2 ratio in the feedgas was varied for the films studied in this work (between 0.3 and 2.0% CH_4 in H_2).

Fig. 1. Schematic diagram of microwave plasma CVD system used for the deposition of diamond films.

Prior to growth, the commercially polished silicon substrates were scratched with 0.25 μm diamond paste for one hour in order to increase the nucleation density of the diamond particles which make up the film. The substrates were then ultrasonically cleaned in acetone, ethanol, and distilled water. For the preparation of plan-view TEM specimens, 2.5 X 2.5 mm sections were cut from the as-grown sample with a diamond saw. The substrate was then thinned with 600 grit SiC paper to a thickness of 65 μm and subsequently polished with 0.3 μm Al_2O_3 suspended in water. This polished side was then dimpled with a steel ball coated with 1 μm diamond paste until the sample was less than 10 μm thick at the center of the crater. After affixing this sample to a 3 mm diameter Ta support ring, ion milling from the substrate side with 6 kV Ar^+ was used to thin the sample until perforation occurred. To remove as much ion milling damage as possible, the sample was then milled with 3 kV Ar^+ for an additional 15 minutes. Cross-sectional TEM (XTEM) samples were prepared in a similar manner. In this case, sections were obtained by cutting perpendicular to the plane of the film after gluing the substrate to silicon buffer layers to form a sandwich. Thinning of the sample was achieved as described for plan-view TEM samples, and the dimpling crater was carefully aligned to ensure that perforation of the specimen during ion milling occurred very near the diamond film. For the TEM reported in this research, a Hitachi H-800 operated at 200 kV and a Philips 430 operated at 300 kV were utilized.

The surface analysis was conducted in a custom built multi-technique analysis system containing Auger electron spectroscopy (AES), x-ray photoelectron spectroscopy (XPS), electron energy loss spectroscopy (EELS), reverse view low energy electron diffraction (RVLEED) and electron stimulated desorption (ESD) capabilities.

The Auger and XPS spectra were recorded using a Riber MAC 2 semidispersive electron energy analyzer which has a resolution of 0.3 eV to 4 eV. The resolution ΔE of the spectrometer is constant over the entire range of kinetic energies. For Auger spectroscopy, the analyzer was modulated at 8 kHz and differentiated spectra were obtained using a lock-in amplifier. The XPS was obtained using the Mg anode of a dual anode (Mg/Al) x-ray source, and spectra were recorded in pulse counting mode. The system is attached through ultrahigh vacuum (UHV) to a diamond microwave plasma CVD system and thus able to conduct in vacuo analysis of such films. However, the present results were obtained ex situ, thus samples were exposed to the atmosphere prior to analysis.

Results and Discussion

NUCLEATION OF DIAMOND ON SILICON

A transmission electron micrograph of diamond nucleation on Si is shown in Figure 2. In this case, the diamond growth was stopped after 45 minutes of growth using 1.0% CH_4 in H_2. Three interesting observations can be made from this data. First, the diamond is found to nucleate in a highly three dimensional, particulate manner. This is due to the very high surface energy of diamond which favors C-C as opposed to C-Si bonding, thus yielding 3-D nucleation and growth.[8] Next, the particles are also seen to vary in size indicating that nucleation probably does not occur all at one

time. Rather, new particles continue to nucleate while previously nucleated particles undergo significant growth. Another explanation for the observed results is that the growth rate of the particles varies substantially. However, given the broad range of particle sizes observed, this explanation seems unlikely. Finally, "scratches" can also be seen in these micrographs as bright lines. Some of the particles are seen to nucleate along these scratches; however, others appear to nucleate without the aid of any scratches. More research is necessary to understand the role of the scratches, but it appears from these results that they are an aid to nucleation density rather than a necessary condition.

Fig. 2. Plan-view TEM micrograph of diamond particles nucleated on (111) silicon.

To further evaluate the nucleation of diamond on Si, a series of samples grown for 5, 15, 30, 120 and 360 minutes with 3.0% CH_4 in H_2 were examined with XPS and AES. Scanning electron microscopy was also conducted and is shown for the 30 and 120 minute samples in Figure 3. The formation of a film is shown to occur by the intergrowth of discrete particles. C and Si concentrations from XPS correlate well with the observed particle coverage. XPS spectra for the 5 minute and 120 minute (2 hr.) growths are shown in Figure 4. The carbon film and silicon substrate are observed, as well as oxygen contamination. In addition to the XPS peaks of the elements, x-ray excited Auger peaks of the oxygen and carbon are visible. After 2 hours of growth the sample is seen to consist of mostly C with only small concentrations of Si and O remaining. The oxygen is believed to be due to the native oxide formed on the Si during atmospheric exposure prior to analysis.
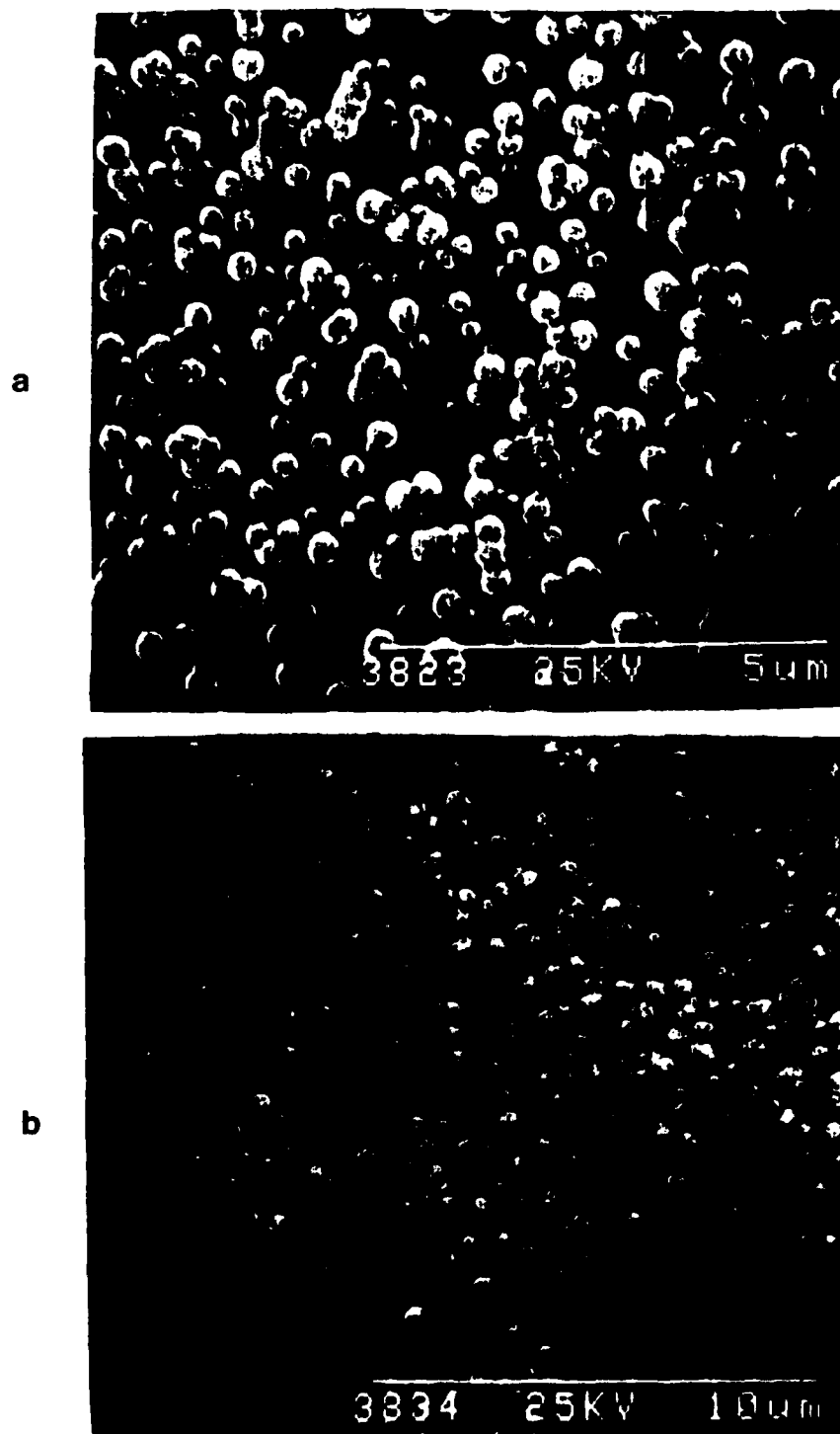
Fig. 3. SEM micrographs of diamond grown on silicon using 3.0% CH$_4$/H$_2$ for (a) 30 min. and (b) 120 min.
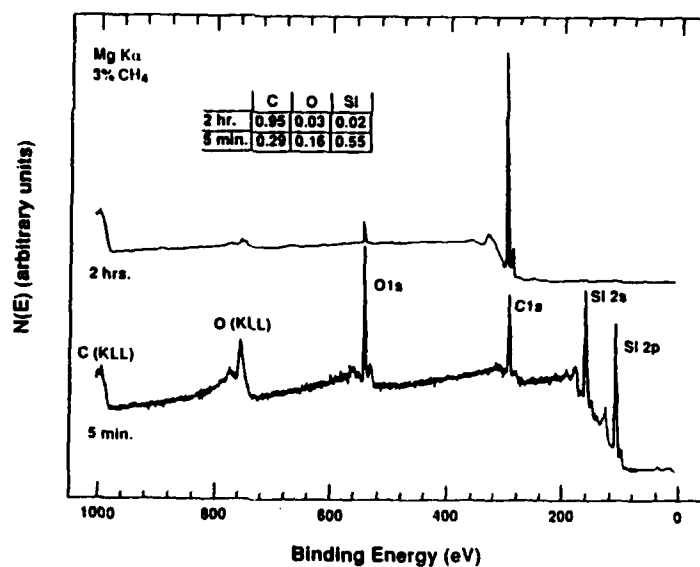
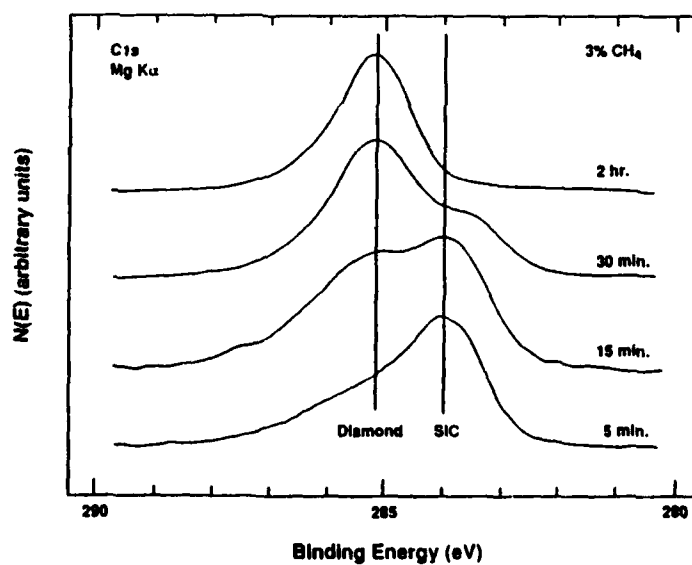Fig. 4. XPS spectra obtained from diamond films grown with 3.0% CH_4/H_2 for 5 min. and 120 min.

Fig. 5. XPS C1s spectra obtained after growth times of 5 min., 15 min., 30 min., and 2 hrs. using 3.0% CH_4/H_2.

Examining the carbon 1s , XPS peak more closely (Figure 5), an interesting observation is made. The first carbon peak to become visible is due to SiC.[9] This is followed by the slow increase in intensity of the diamond C 1s peak as growth proceeds. Although the formation of a SiC layer between the diamond film and the silicon substrate might be considered a somewhat obvious result, two major points make this observation interesting. First, formation of the SiC layer is extremely rapid relative to the formation of a discernable diamond layer. The plasma plays a critical role in this SiC formation since the growth temperature is much lower than generally used in the formation of such films by thermal CVD.[10] Second, the formation of a SiC layer has not been observed during XTEM of such films grown with relatively high methane concentrations as discussed later in this paper.

These results were verified by examining the fine structure of the carbon *KLL* Auger peak of these samples as shown in Figure 6. After 15 minutes of growth, this fine structure has the typical shape of a silicon carbide. After 2 hrs., the shape has become very similar to that obtained from bulk diamond.[11]

Fig. 6. AES C *KLL* spectra as a function of growth time. A characteristic SiC peak shape is present during the early stages of growth.

Thus, it appears that diamond is actually growing on a very thin layer of SiC rather than directly on the Si substrate. Unfortunately, it is not believed by the present authors that a similar statement can be made about the nucleation of the diamond. That is, it may still be possible that the initial nucleus of the diamond forms on Si but

due to the different growth modes for SiC and diamond, coupled with a rapid initial SiC growth rate, only the SiC is detectable. The SiC is nucleating as a true film, thereby rapidly covering the surface and yielding a strong initial XPS and AES signals. The diamond, however, is growing as small particles scattered over the surface, yielding a small signal due to the low areal coverage on the surface. As time continues, the SiC growth becomes diffusion limited since Si from the substrate is necessary. Thus the SiC growth begins to slow whereas the diamond continues to grow without limitations. After some period of time the diamond particles begin to grow up over the SiC layer, and thus yield the majority of the XPS and AES signal. It appears from the electron microscopy discussed in the following section that with high methane concentrations in the feedgas this overgrowth occurs relatively rapidly, thus yielding a thin SiC layer, whereas at lower concentrations a thicker SiC layer is able to form. Regarding the question of whether the diamond nucleates on Si or SiC, the authors believe that this question is still open and will remain so until further electron microscopy, field ion microscopy or scanning tunneling microscopy is performed during the initial stages of diamond nucleation.

THE DIAMOND-SILICON INTERFACE

To obtain more information about the nature of the diamond-silicon substrate interface, the samples were examined with cross-sectional transmission electron microscopy. Micrographs of films grown at 2.0% CH_4 and 0.3% CH_4 in H_2 are shown in Figures 7(a) and 7(b), respectively. The density of defects and/or the amount of
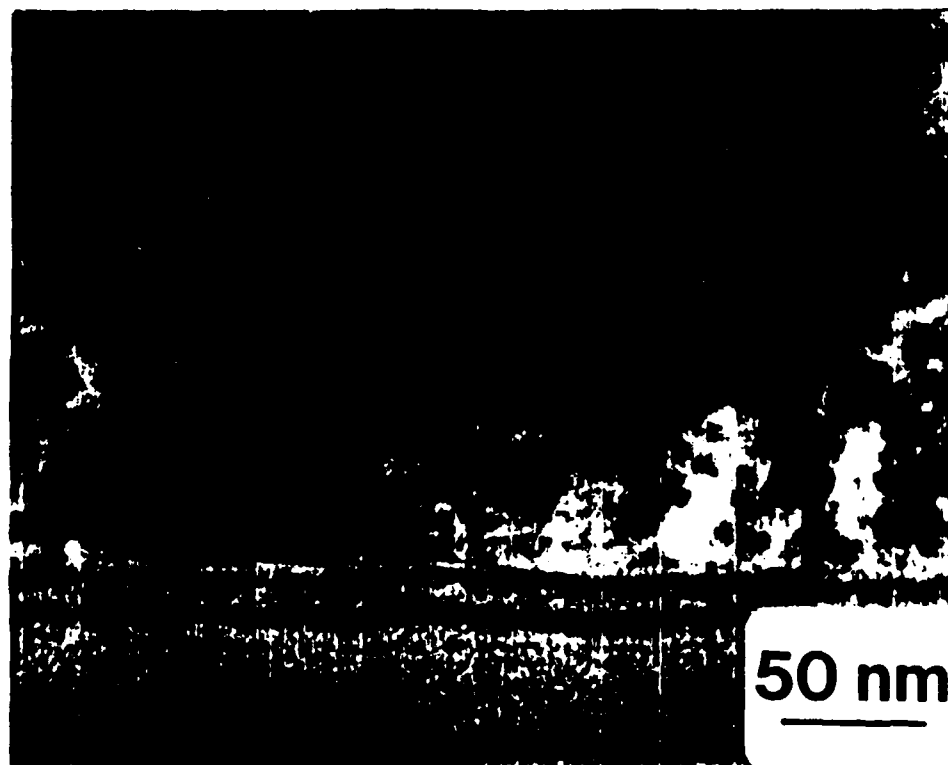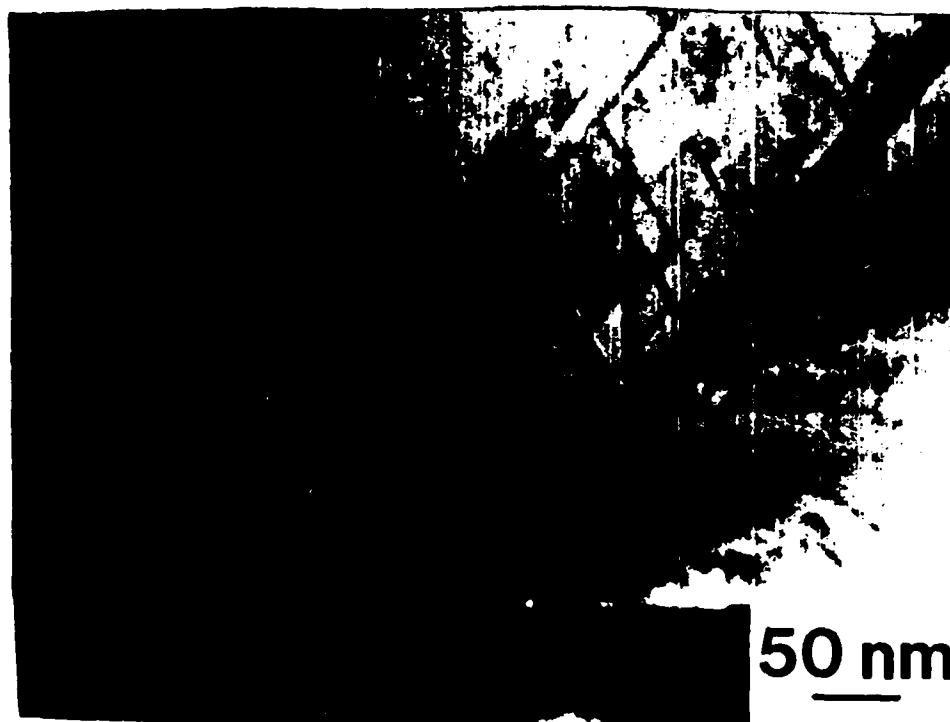

50 nm

Fig. 7. (a)   XTEM micrograph of diamond film grown in 2.0% CH_4/H_2, showing increased density of defects in the diamond film.

(b)   XTEM micrograph of diamond film grown in 0.3% CH_4/H_2 showing lower defect density on the diamond film.

elastic strain (indicated by the dark regions in the micrograph) in the 2.0% CH_4 film [Figure 7(a)] is significantly higher than that observed in the XTEM micrograph of the 0.3% CH_4 film [Figure 7(b)], probably due to the lower growth rate at these lower methane concentrations which allows a less defective and/or less strained film to form. This observation may also be related to a decreased sp^2 bonding component which was observed during Raman spectroscopy,[12,13] but more research is necessary to confirm this hypothesis.

Closer examination of the diamond/silicon interface of films grown at 2.0% and 0.3% CH_4/H_2 reveals significant differences in the nature of this interface. In Figure 7(a), only an ion milling damage layer is observed, caused by the presence of the interface and the very different milling characteristics of the diamond film and the silicon substrate. This was confirmed by the absence of a second phase in this region during microdiffraction and the observation that no depth was apparent in this layer during TEM examination (i.e., this feature is confined to the surface of the TEM specimen). Therefore, it is believed to be an amorphous surface layer caused by interaction of the ion milling beam with the interface during sample preparation.[14] On the other hand, a sample grown at 0.3% CH_4 yields an obvious interfacial layer approximately 50 Å thick as shown in Figure 8. Due to the imaging contrast optimized to observe defects in the diamond, this layer was not visible in Figure 7(b); however, it can be observed readily in Figure 8. This is easily distinguished from an ion milling damage layer by the defect contrast observed as dark lines in the layer and the depth which was apparent parallel to the electron beam in this region,

indicating it is not simply a surface artifact. Furthermore, a SAD pattern from this region indicated that this interfacial layer was β-SiC. The alignment of the Si(111) and SiC(111) diffraction spots indicated that in the region of the SAD the β-SiC buffer layer was a single crystal, epitaxial with the Si substrate (i.e., β-SiC(111)||Si(111), β-SiC[110]||Si[110]). The presence of this layer is confirmed by high resolution XTEM as shown in Figure 9. Fringes for the Si and SiC(111) planes can be observed and appear to be aligned, indicating an epitaxial relationship between the Si and SiC.

Fig. 8. XTEM micrograph of diamond film grown in 0.3% CH_4/H_2 showing 50Å layer of β-SiC at the interface.

The absence of the SiC layer in the sample grown with the higher concentration of CH_4 (i.e., 2% CH_4) may be due to the more rapid growth rate of the diamond in these samples. This may "cap" the Si before an SiC layer detectable in the TEM has time to form. After the diamond has covered the Si, the high bond strength and "kinetic stability" (i.e. large activation energy required to transform the diamond) of the

Fig. 9. High resolution XTEM micrograph of diamond film grown in 0.3% CH_4/H_2. Note the cross-fringes visible in both the silicon substrate and the β-SiC layer, indicative of the epitaxial nature of the β-SiC film.

diamond prevents the inter-diffusion of the Si and C, thus limiting the SiC layer thickness. However, it should be remembered that an SiC layer was detected by XPS and AES in a sample grown with a high methane concentration (i.e., 3.0%). This is believed to be due to the increased surface sensitivity of these techniques and suggests that the layer is simply too thin to be detected in the TEM (i.e., less than 5 - 10 monolayers) for the reasons discussed above.

Summary

Diamond films grown by microwave plasma CVD have been examined by AES, XPS and TEM. The surface analysis of a series of samples grown for various times indicated that a detectable SiC layer forms within the first five minutes of growth. Diamond then slowly begins to become detectable until, after two hours of growth, the SiC is no longer observed. In cross sectional electron microscopy, the presence of an epitaxial SiC layer was observed for samples grown with a low CH_4 concentration. However, contrary to the surface analysis results, such a layer was not observed in the samples grown with higher CH_4 concentrations. This is believed to be due to the very thin nature of the SiC layer in this case, probably caused by the diamond film "capping" the substrate more quickly and thus preventing further carburization.

Acknowledgements

References

1. Landolt and Börnstein (1987) Numerical Data and Functional Relationships in Science and Technology, Springer-Verlag.

2. Field, J. E. (1979) Properties of Diamond, Academic Press, London.

3. Bazhenov, V. K., Vikulin, I. M., and Gontar, A. G. (1985) 'Synthetic diamonds in electronics' (review), Sov. Phys. Semicond., **19** (8), 829.

4. Matsumoto, S. (1985) 'Chemical vapour deposition of diamond in RF glow discharge,' J. Mat. Sci. Lett.,**4**, 600.

5. Kamo, M., Sato, Y., Matsumoto, S., and Setaka, N. (1983) 'Diamond synthesis from gas phase in microwave plasma,' J. Cryst. Growth, **62**, 642.

6. Matsumoto, S., Sato, Y., Kamo, K., and Setaka, N. (1982) 'Growth of diamond particles from methane-hydrogen gas,' J. Appl. Phys., **21**, 483.

7. Kobashi, K., Nishimura, K., Kawate, Y., and Horiuchi, T. (1988) 'Synthesis of diamonds by use of microwave plasma chemical-vapor deposition: Morphology and growth of diamond films,' Phys. Rev. B, **38** (6), 4067.

8. Kern, R., LeLay, G., and Metois, J. J. (1979) Chapter 3, in E. Kaldis (eds.) Current Topics in Materials Science Volume 3, North Holland Publishing Co.

9. Wagner, C. D., Riggs, W. M., Davis, L. E., Moulder, J. F., and Muilenberg, G. E. (1979) Handbook of X-ray Photoelectron Spectroscopy, Perkin-Elmer, Eden Prairie, MN.

10. Liaw, P. and Davis, R. F. (1985) 'Epitaxial Growth and Characterization of β-SiC Thin Films,' J. Electrochem. Soc. 132, 642.

11. Williams, B. E. and Glass, J. T. (1989) 'Characterization of diamond thin films: Diamond phase identification, surface morphology, and defect structures,' J. Mater. Res, **4** (2), 373.

12. Nemanich, R. J., Shroder, R. E., Glass, J. T., and Lucovsky, G. 'Precursor Structures in the Formation of Diamond Films,' Proceedings of Physics of Semiconductors, Poland, Aug. 1988.

13. Kobashi, K., Nishimura, Kawate, Y., and Horiuchi, T. (1988) 'Synthesis of diamonds by use of microwave plasma chemical-vapor deposition: Morphology and growth of diamond films,' Phys. Rev. B **38** (6), 4067.

14. Carter, C. H., Davis, R. F., and Nutt, S. R., 'Transmission electron microscopy of process-induced defects in β-SiC thin films,' J. Mater. Res. **1** (6), 811.

Electron Microscopy of Vapor Phase Deposited Diamond

B. E. Williams, H. S. Kong, and J. T. Glass

Department of Materials Science and Engineering

North Carolina State University

Raleigh, NC 27695-7907

Thin carbon films grown from a low pressure methane-hydrogen gas mixture by microwave plasma enhanced CVD have been examined by electron microscopy. Previously reported transmission electron microscopy (TEM) of the diamond films[1] has shown that the majority of diamond crystals have a very high defect density comprised of {111} twins, {111} stacking faults, and dislocations. In this study, high resolution electron microscopy (HREM) has been utilized to lattice image individual defects in these polycrystalline diamond films. Interpretation of the images from these defects is not trivial and reported image simulations have been utilized to further understand these defects. Five fold multiply twinned particles have also been examined and it was found that the 7.5° misfit present in such particles has been accommodated at the twin boundaries rather than by elastic deformation. This creates a twin boundary coincident with a low angle grain boundary which has been termed a "tilted twin boundary". The density of defects in these particles is generally high; however, a dramatic reduction in the defect density near the twin boundaries was observed. This defect reduction is significant because if its origin can be determined, this information may be useful in producing higher quality diamond films.

I. Introduction and Background

Diamond has potential for use in both electronic and wear resistant coating applications due to its high hardness, strength, thermal conductivity, electron saturated drift velocity, hole and electron mobilities, chemical and thermal stability, radiation hardness, and optical transmission.[2-4] Researchers throughout the world are currently attempting to grow single crystal films of diamond using low pressure (i.e., less than one atmosphere) gases to make the fabrication of electronic devices which utilize these outstanding properties feasible. Such research has been encouraged by recent results which indicate that epitaxial diamond films can be grown on diamond substrates.[5-8] However, microcracking and poor surface morphologies after several microns of growth are still major concerns in this homoepitaxy. Furthermore, for thin film devices of diamond to be economically viable, heteroepitaxial growth is believed to be necessary. Previous investigations[9-13] have only yielded highly defective, polycrystalline films when non–diamond substrates are utilized. The research presented in this paper is part of a continuing effort to understand defect structures and particle morphologies in such polycrystalline CVD diamond. This understanding will yield information on the nucleation and growth of these films which will, in turn, aid researchers in attempts to achieve heteroepitaxial growth of high quality diamond.

The surface morphologies and defect structures in CVD diamond have been reported previously.[1, 14, 15] In general, highly faceted polycrystalline films (average grain size ≈1 μm) have been observed; however, deviations from this faceting were also present depending on location on the substrate and the methane concentration in the feedgas. Well-faceted diamond crystals were observed near the center of the sample whereas a less faceted, cauliflower texture was observed near the edge of the

sample, presumably due to variations in temperature across the surface of the sample. Regarding methane concentration effects, three-fold (111) faceted diamond crystals were predominant in a film grown with 0.3% CH_4 in H_2 while four-fold (100) facets were observed in films grown with 1.0% and 2.0% CH_4 in H_2. Cyclic growth patterns of these facets due to secondary nucleation have also been reported.[16] Transmission electron microscopy of the diamond films[1] has shown that the majority of diamond crystals have a very high defect density comprised of (111) twins, (111) stacking faults, and dislocations. The presence of these crystallographic defects (twins, stacking faults, and dislocations) in CVD diamond is not surprising since natural and high pressure synthesized diamond have also been observed to have high concentrations of these defects.[17, 18] In the present research, high resolution TEM (HREM) has been used to examine these defects on an atomic scale. The interpretation of HREM micrographs is not trivial and is also addressed in the present manuscript as it relates to the diamond films which were examined.

Along with the various defects discussed above, multiply twinned particles (MTPs) of diamond were also observed by HREM in the present study. Particles nucleated in the gas phase and electrodeposited particles of a variety of materials have been shown to form MTPs. Several different types of MTPs exist,[19] the most common being; (i) a single twin separating particles into two halves which are the mirror image of each other, (ii) pseudopentagonal particles (known as a decahedral MTP) containing five tetrahedra sharing a common [110] axis and each twinned relative to its neighbor and (iii) an icosahedral particle bounded by 20 (111) planes composed of 20 tetrahedra sharing a common apex. All of these types have been observed in CVD diamond;[10] however, only one other HREM investigation of the atomic positions has previously been attempted.[20] The present paper will conduct such a study on decahedral diamond MTPs which were found to be the most

common type in the diamond CVD films examined. Such MTPs have previously been found in various FCC metals such as Fe, Ni, Pt,[21] Cu,[22] Ag,[23] and Au.[24, 25] Silicon[19, 26] and Ge[27], both comprised of the diamond structure, have also been shown to crystallize in these multiply twinned configurations.

Prior to presenting the results of the present research, it is necessary to discuss the nature of decahedral MTPs observed in various materials by previous investigators. Decahedral MTPs have pseudopentagonal character because they are comprised of five tetrahedra joined by a common [110] edge. Thus, when viewed parallel to this [110] direction, these particles appear to have five fold symmetry. (This has given rise to another name sometimes used for these particles - "five fold MTPs.") However, when five tetrahedra are joined in this manner, they cannot completely fill 360°. This is because the ideal angle between the (111) planes bounding each tetrahedron is 70.5°; therefore the five adjacent tetrahedra make up a total angle of 352.5° leaving a 7.5° mismatch. At the core of the MTP this mismatch may be accommodated by elastic strain in the lattice but as the particle grows, this strain becomes too great and a boundary forms to accommodate this misfit. For example, in Si, core diameters were found to consistently be on the order of 4nm in decahedral MTPs.[19] In the core, one of the tetrahedra was elastically strained to accommodate most of the 7.5° misfit. After the particle reached the 4 nm diameter, a low angle grain boundary was formed in one of the tetrahedra. An elastically strained core has also been observed recently in diamond MTPs.[20] In this case the misfit was distributed over four of the five tetrahedra rather than confined to a single one. No boundary accommodating the misfit was observed in the particles studied in that report, which is contrary to the particles studied in the present research as discussed later.

Most agree that MTPs form when substrate particle interaction is relatively weak since otherwise the substrate will determine atomic arrangements rather than the particle nucleus. (In fact, crystal growth theory[28] shows that poor particle/substrate interaction causes three dimensional particle growth, and MTPs are an extreme case of this phenomenon.) Several different theories have been suggested regarding the formation of MTPs. A balance between strain energy, surface energy and twin boundary energy has been used to discuss the stability of various forms of small metallic twinned particles.[29] Decahedral MTPs have been explained[22] by an impurity atom of the proper size which acts as a nucleus around which five atoms from the particle cluster in a modified close packed arrangement. If particle growth maintains this initial configuration, a five fold MTP is formed. Another speculation is that the initial nucleus is created by a minimization of surface energy and a lack of surface mobility causes this structure to continue even after it is energetically unfavorable. In the case of vapor phase deposited diamond, the different MTP configurations have been related to different hydrocarbon compounds which could act as nuclei.[10] Each is an exact duplicate of the smallest possible core region of the various MTPs. As a first order approximation, these compounds can be viewed simply as hydrogen terminated diamond of the smallest possible dimensions. Since diamond is known to be hydrogen terminated during vapor phase growth this explanation appears reasonable. However, it is not likely in the case of the FCC metal MTPs due to the absence of such precursor molecules. For this reason a new theory has been suggested[20] involving the nucleation of five fold MTPs at an edge dislocation which is nearly perpendicular to the substrate surface. The atomic structure at the termination of this edge dislocation appears to be consistent with the HREM micrographs of the MTP core. However, this mechanism cannot account for MTPs nucleated in the vapor phase.

Various mechanisms may be important depending on the material, growth parameters, substrate, growth process, etc. This is supported by (i) the variety of proposed theories which appear quite reasonable, (ii) the numerous materials observed to form MTPs, and (iii) the different orientations and morphologies of MTPs. They have been observed to nucleate with either (111) or (001) nuclei.[24] Particles which appear to be cut in half by the substrate have also been observed. Thus, it appears that no single theory is yet able to describe the formation of MTPs in all observed cases. The section on MTPs in the present manuscript discusses the character of five fold diamond MTPs and the misfit boundaries therein.

II. Experimental

Details of the microwave plasma enhanced CVD system used to grow the diamond films in this research have been reported elsewhere.[14] In general, microwaves from a 2.45 GHz power supply were guided through an isolator and a three stub tuner to a quartz tube reaction chamber. The diamond films analyzed in this research were grown on 2 cm by 1 cm n-type Si (111) substrates immersed in a CH_4/H_2 plasma created by the microwave source. The approximate substrate temperature as measured by an optical pyrometer was maintained at approximately 800°C by controlling the microwave power (which was typically 300–350 watts). The total pressure in the chamber was maintained at 30 Torr, and the CH_4/H_2 ratio in the feedgas for the films studied in this work was 0.3% CH_4 in H_2.

Prior to growth, the commercially polished silicon substrates were scratched with 0.25 μm diamond paste for one hour in order to increase the nucleation density of the diamond particles which make up the film. The substrates were then ultrasonically cleaned in acetone, ethanol, and distilled water. For the preparation of plan-view TEM specimens, 2.5 × 2.5 mm sections were cut from the as-grown

sample with a diamond saw. The substrate was then thinned with 600 grit SiC paper to a thickness of 65 μm and subsequently polished with 0.3 μm Al_2O_3 suspended in water. This polished side was then dimpled with a steel ball coated with 1 μm diamond paste until the sample was less than 10 μm thick at the center of the crater. After affixing this sample to a 3 mm diameter Ta support ring, ion milling from the substrate side with 6kV Ar^+ was used to thin the sample until perforation occurred. To remove as much ion milling damage as possible, the sample was then milled with 3kV Ar^+ for an additional 15 minutes.

For the conventional TEM (bright field and dark field) reported in this work, a Hitachi H-800, Philips 400 with FEG, and a Philips 430 were utilized. The high resolution TEM (HREM) was accomplished on a JEOL 200CX equipped with a top entry stage and a LaB_6 filament operated at 200 kV. The HREM micrographs were obtained by orienting individual diamond crystals (typically 1μm in size) to [011] where two sets of {111} fringes were visible at 800,000x in the microscope. No objective aperture was used when recording these images.

III.   Results and Discussion

In general, the interpretation of HREM lattice images is quite difficult and depends on a number of experimental parameters. However, the correct interpretation of the HREM images obtained in this work was aided by *a priori* information about the diamond structure. For example, the [110] projection of this structure with lattice parameter a=3.568 Å is depicted in Fig. 1a. The lattice spacings of several planes are indicated on the micrograph but the spacing of the (400), 0.89 Å, is below the resolution of the images obtained in this research. Thus, the pairs of atoms separated by the (400) spacing in this projection will not be resolved. Fig. 1b is a projection of the diamond lattice which would be observed assuming a resolution

sufficient to observe the (111) planes of spacing 2.06 Å but not the (400) planes. The structure in Fig. 1b is representative of the images obtained in this work. It is interesting to note that such images are identical to those which would be obtained from an FCC lattice. For certain defects, (111) twins and intrinsic stacking faults in particular, the loss in resolution produces no change in the symmetry of the defect.[30] The *abc* notation utilized to designate the (111) planes in this case has been thoroughly discussed by Hornstra.[31]

Twins and Stacking Faults

In the diamond structure, the perfect crystal can be identified by the presence of *abcabc* type stacking as indicated in Fig. 1. In a twinned crystal, the normal stacking sequence is disturbed on a single layer which is known as the twin (or mirror) plane. Then the stacking sequence becomes *abcba* where the *c* plane is the mirror plane. A schematic of such a defect is shown in Fig. 2a where the mirror plane is designated with an *M* on the figure. Fig. 2b is a HREM of a region in a diamond crystal where a single (111) twin plane is present. In this case, it does not matter if we are imaging the atomic columns as bright or dark because the symmetry of the defect remains the same. Such twins were observed throughout the diamond films; however, in some regions their density was too high to measure using conventional TEM techniques (i.e., multiple twin planes within 50 (111) spacings), whereas other local regions, up to ~2μm in diameter, were relatively twin-free. Thus, due to their inhomogeneous nature, accurate quantification of the twin density was not possible.

In addition to twins, numerous (111) stacking faults were observed in these films. However, the high density of other defects, especially twins, made it difficult to image the stacking faults using conventional bright field TEM. This problem was

avoided by using weak beam dark field imaging and HREM. Fig. 3a shows a representation of a [111] intrinsic stacking fault in the diamond structure viewed in a [110] projection at the resolution obtained in the present HREM research. In Fig. 3b, an intrinsic stacking fault on a (111) plane is labelled SF on the micrograph. Note that in this region of the crystal, three twins (denoted by M) have also occurred. This is representative of the high defect density observed in certain regions of the CVD diamond.

The twins and stacking faults noted above are important defects in CVD diamond because their density is extremely high; thus it is expected that they will play an important role in the electronic properties of diamond films. High densities of these planar defects have also been observed in natural diamond crystals.[17, 18] Their presence in CVD diamond films can be attributed to the relative ease with which they can be nucleated on the surface when the growth plane is (111). A 60° rotation of a single atom on the growth surface creates a hexagonal nucleus (boat configuration),[32] which when extended on the growth surface forms either a twin or a stacking fault depending on the position of the atoms in the next plane formed. Because only next nearest neighbors are affected by the rotation, this defect has a relatively low formation energy. This low energy of formation thus explains the extremely high density of these planar defects which is observed on (111) faceted crystals such as MTPs. Such defects are more difficult to nucleate on (100) planes, and lower defect densities have in fact been observed experimentally in (100) faceted films.[33] Thus, in order to eliminate these defects in CVD diamond films it may be necessary to choose growth conditions which favor (100) faceted films.

In addition to conventional images of stacking faults, an interesting variation of these images was observed in the HREMs of the CVD diamond films as shown in Fig. 4. In this case, the (111) planes in the lattice appear to be stacked on top of one

another, i.e. in an *aaa* type arrangement. In region A of Fig. 5, this is observed over four (111) planes of the lattice, and in region B a shift has occurred causing only three atomic planes to be stacked in this manner. It is tempting to attribute this observation to an unusual defect associated with the unique nature of carbon bonding, i.e., an sp^2 or sp^1 layer within the sp^3, diamond matrix. However, a similar structure has been observed in Si HREMs and was shown to be due to a simple stacking fault when viewed under certain conditions of sample thickness, beam defocus, and beam energy. This same phenomena is presumed to be the cause of the present images. The shift observed in the present case between regions A and B in this micrograph is related to changing sample thickness along the fault. The only differences between the Si case and the present case are the particular values of the beam defocus, beam energy, and sample thickness giving rise to this phenomena.

Due to the numerous intersections of twins and stacking faults on different planes, it is worthwhile to examine such interactions more closely. In order to determine the nature of the interaction of the two stacking faults shown in Fig. 5, a Burgers circuit was constructed around their intersection. This follows the method used by Krivanek to examine the structure of extrinsic stacking faults in silicon produced by oxidation.[34] However, when this was done in the present case the Burgers circuit closed upon itself, indicating an absence of any Burgers vector component parallel to the plane of the micrograph. Thus, at the intersection, only a [110] dislocation could be present which would be perpendicular to the plane of the micrograph and thus undetectable in this orientation. This is consistent with the presence of a stair-rod dislocation which has a $\frac{1}{6}$[110] Burgers vector. Such a dislocation is formed by the combination of the two partial dislocations which bound the stacking faults. Although the mechanism of this formation is not known

in the present case it is likely that it is created when twinned regions on two different (111) planes meet during growth.

The intersection of twins was also a common observation in this material. In Fig. 6, a twin labelled A on the micrograph appears to have climbed across several planes to avoid crossing another twin labelled B. Although there are various distortions and apparent secondary twins and stacking faults which complicate the situation, the primary observation is that twin B terminates at the position labelled C on the micrograph instead of crossing the other twin boundary. These intersections are interesting since it has been shown by Dahmen[35] et al. that hexagonal silicon can be formed at twin intersections formed by the hot indentation of silicon. However, in order to form a hexagonal component, two (111) twins must completely cross each other. For this to occur, the region of twin intersection must undergo a shear transformation which results in the formation of a hexagonal phase; however, in the present study, this has not been observed. In fact, twin boundaries appear to climb to adjacent planes in order to avoid cross-twinning when they meet another twin. Therefore, no evidence has been seen for the presence of a hexagonal form of diamond in the present samples. This may be due to the origin of the twins and/or the high bond strength of the diamond. That is, the twins are believed to be formed during growth and are not related to a shear deformation mechanism. Furthermore, even if thermal stresses are present during sample cooling, the high strength of the diamond lattice may prevent the shear mechanism.

Multiply Twinned Particles

A TEM micrograph of a five fold MTP is shown in Fig. 7. Fig. 7(a) is a bright field micrograph showing the five growth sectors comprised of tetrahedra bounded

by {111} planes sharing a common [110] axis and twinned relative to each other. The electron beam is parallel to a [110] direction. Fig. 7(b) is a weak beam dark field micrograph imaged by using a (111) diffracted spot. Twinned regions within the sectors which are in a diffracting condition appear bright (as streaks) since the twinning brings these regions back into the centered diffracting spot. A small secondary sector is also shown twinned relative to its neighbors and labelled as A in the micrograph. Perhaps the most interesting observation from this micrograph is the absence of defects near four of the five major twin boundaries which separate the sectors. In general, many defects of the types discussed earlier in this paper are found within each sector as seen by the strong lines of contrast in the micrographs. Twins on intersecting {111} planes parallel to the major twin boundaries separating the tetrahedra are most visible. However, in the regions near at least 4 of the 5 major twin boundaries, the defect density is significantly reduced. This appears to be more obvious at some boundaries than at others. The explanation for this phenomenon is believed to be related to the nature of these boundaries and will be discussed in following paragraphs.

A HREM micrograph of the core of a five fold MTP and a schematic of the growth sectors are shown in Figs. 8a and 8b. Contrary to the previous HREM investigation[20] a very irregular core is observed due to interactions with secondary twins and apparent "wandering" of the primary twins. One of the five major twin boundaries was, in fact, not a single twin boundary at all. Rather, it is an extended boundary consisting of multiple parallel twins. This is indicated on the schematic in Fig. 8b and can also be seen in the HREM of the core region shown in Fig. 8a. It is speculated that at the true nucleus of the MTP a perfect core exists; however, as the particle grows the core is distorted. In this way, the overall five fold symmetry is maintained by the earlier growth; however, due to sample preparation for the TEM,

only the irregular core which is some distance from the nucleus is left for observation. This is shown schematically in Fig. 9. If this were not the case (i.e., if the irregular core was actually the nucleus) it is difficult to envision why a five fold MTP would form and none of the nucleation mechanisms previously discussed would be applicable.

As previously discussed, a five fold MTP must accommodate approximately 7.5° of misfit. In the central core of the particle this misfit has been shown to be accommodated by elastic strain. At the center of the elastically strained core region the five twin boundaries come together, forming a defect which has been referred to as a star disclination.[36] In the case of Si, a low angle grain boundary then forms in one of the sectors as the particle grows larger than some critical diameter. In some cases, the MTPs have been seen to be unstable after a second critical size,[25] transforming to irregular shapes presumably due to the strain from this misfit. In the present case, the particle shown in Fig. 8 accommodated most of its misfit in two of the five major twin boundaries present as shown schematically in Fig. 10. The angles between (111) planes is also shown in this schematic and indicates that within the error of the measurement (~0.2°), the misfit is located entirely at these twin boundaries. (A perfect tetrahedron contains an angle of 70.5° between the (111) planes.) To accommodate this misfit these two twin boundaries contain series of dislocations. An HREM of the boundary accommodating most of the misfit in the present case is shown at two different magnifications in Figs. 11a and 11b. Approximate locations of dislocations are indicated by the arrows. The frequency of these dislocations is related to the amount of misfit which is accommodated at the twin. Based on a repeat distance of eight spacings between these dislocations a misfit angle of approximately 7.18° can be calculated by simple geometric considerations.

This correlates well with the angle of 7.0° (Fig. 10) measured directly from the (111) planes in the growth sectors.

The presence of dislocations along the twin boundary may be viewed as the superposition of a low angle grain boundary and a twin boundary. Thus, a more descriptive name is perhaps a "tilted twin boundary" (TTB). Although the dislocations occur at the termination of a (111) plane in the TTB, conventional Burgers vector analysis is not applicable for these dislocations since they are located between two crystals with different orientations(i.e., twinned relative to each other). The O-lattice theory,[37] which interprets a crystalline interface as a dislocation network, can be utilized to extend Burgers vector analysis to this case. The dislocations within a crystal boundary are defined as the intersections of the boundary surface with the O-lattice cell walls. However, a detailed analysis of this kind is beyond the scope of the present manuscript.

An interesting phenomenon which occurs at these tilted twin boundaries is shown in Fig. 11b. It can be seen that a twin has intersected the TTB in the region labelled A, causing it to change direction locally in order to maintain its low energy configuration. This change allows the TTB to follow the (1̄11) plane in the twinned crystal but causes significant distortion of the lattice in the untwinned crystal located across the TTB from the twin. A boundary dislocation can be seen eight (111) lattice spacings below the intersecting twin where the TTB has recovered from the distortion caused by the intersecting twin. In the intersecting region it is not appropriate to discuss dislocation frequency because the (111) planes are no longer in a low angle relationship. As in the case of intersecting twins studied by Dahmen,[35] at the intersection of the TTB and the secondary twin it appears that the (1̄11) plane of the sector is matching with the (1̄15) of the twinned region as shown schematically in Fig. 12.

It was observed in relation to Fig. 8 that near some of the major twin boundaries in a five fold MTP the defect density is greatly reduced compared to the central regions of each of the twin sectors. This is a very interesting observation which may provide insight into achieving higher quality diamond growth when the mechanistic causes of this phenomenon are thoroughly understood. Although the study necessary for such an understanding is beyond the scope of the present research, some speculations are useful. This phenomenon may be related to the nature of the tilted twin boundaries in the MTP. That is, in a TTB there are a series of dislocations to accommodate the misfit present in the MTPs. These dislocations may form at the expense of the internal defects near the boundary. Similarly, dislocations of opposite sign can annihilate each other and a series of dislocations can eliminate a microtwin. Thus, although the details are not understood at this time, it may be that the interactions of the TTB and the dislocations therein with the surrounding matrix material significantly decrease the defect density nearby. It is also possible that the presence of the TTBs helps alleviate stresses during growth by decreasing the confinements or constraints on the crystal in this region. That is, the presence of a semi-free boundary in this region dissipates some of the stresses which occur during growth due to improper incorporation of atoms, thermal fluctuations, etc. This may eliminate the need for defects to form in this region in order to accommodate these stresses. The major problem with these approaches is that the "defect-free" regions appear to be present near boundaries with minimal dislocation densities (i.e., near the "perfect" twin boundaries rather than just near the tilted twin boundaries). This suggests that the "growth geometry" near the twin boundaries may be responsible. For example, this boundary may be acting as a nucleation site which does not allow twinned diamond (i.e., boat vs chair configurations) to form. This could be likened to off-axis growth in epitaxy which prevents double positioning boundaries by constraining the atomic sites which may

incorporate new species. These general speculations are currently being investigated but further refinement is not yet possible. However, it is clear that near some of the major twin boundaries the defect density is greatly reduced. This minimization of defects which naturally occurs in these MTPs may be a clue to a method of decreasing the defect density in diamond films which do not consist of MTPs.

Conclusions

High resolution electron microscopy (HREM) has been utilized to lattice image individual defects in polycrystalline diamond films. Numerous twins and stacking faults were observed, including their intersections. Five fold multiply twinned particles have been observed and it was found that the 7.5° misfit present in such particles has been accommodated at the twin boundaries rather than by elastic deformation. This creates a twin boundary coincident with a low angle grain boundary which has been termed a "tilted twin boundary". The density of defects in these particles is generally high; however, a dramatic reduction in the defect density near the twin boundaries was observed. This defect reduction is significant because if its origin can be determined, this information may be useful in producing higher quality diamond films.

Acknowledgements

List of Figures

12. Schematic diagram of the above region showing matching of the (1$\bar{1}$5) of the twinned region with the (1$\bar{1}$1) of the other sector.

References

1. B. E. Williams and J. T. Glass, J. Mater. Res. 4, 373 (1989).

2. Landolt and Börnstein, *Numerical Data and Functional Relationships in Science and Technology* (Springer-Verlag, 1987).

3. J. E. Field, *Properties of Diamond* (Academic Press, London, 1979).

4. V. K. Bazhenov, I. M. Vikulin and A. G. Gontar, Sov. Phys. Semicond. 19, 829 (1985).

5. B. V. Derjaguin, B. V. Spitsyn, A. E. Gorodetsky, A. P. Zakharov, L. I. Bouilov and A. E. Aleksenko, J. Cryst. Growth 31, 44 (1975).

6. B. V. Deryagin, D. V. Fedoseev, N. D. Polyanskaya and E. V. Statenkova, Sov. Phys. Crystallogr. 21, 239 (1976).

7. M. W. Geis, presented at *The Third Annual SDIO-IST/ONR Diamond Technology Initiative Symposium*, Crystal City, VA, 1988.

8. H. Nakazawa, Y. Kanazawa, M. Kamo and K. Osumi, Thin Solid Films 151, 199 (1987).

9. B. Singh, Y. Arie, A. W. Levine and O. R. Mesker, Appl. Phys. Lett. 52, 451 (1988).

10. S. Matsumoto and Y. Matsui, J. Mater. Sci. 18, 1785 (1983).

11. A. Sawabe and T. Inuzuka, Thin Solid Films 137, 89 (1986).

12. S. Matsumoto, J. Mater. Sci. Lett. 4, 600 (1985).

13. Y. Sato, M. Kamo and N. Setaka, in *High Tech Ceramics*, edited by P. Vincenzini (Elsevier Science Publishers, B. V., Amsterdam, 1987).

14. K. Kobashi, Phys. Rev. B 38, 4067 (1988).

15. B. E. Williams, J. T. Glass, R. F. Davis, K. Kobashi and Y. Kawate, MRS Proc. (1988).

16. K. Kobashi, K. Nishimura, K. Miyata, Y. Kawate, J. T. Glass and B. E. Williams, SPIE Proc. (1988).

17. B. Lawn, Y. Kamiya and A. R. Lang, Philos. Mag. 12, 177 (1965).

18. T. Evans and P. Rainey, Proc. R. Soc. London, A 344, 111 (1975).

19. S. Iijima, Jpn. J. Appl. Phys. 26, 365 (1987).

20. J. Narayan, A. R. Srivatsa, M. Peters, S. Yokota and K. V. Ravi, Appl. Phys. Lett. 53, 1823 (1988).

21. A. J. Melmed and D. O. Hayward, J. Chem. Phys. 31, 545 (1959).

22. H. S. Peiser, Acta Cryst. 17, 774 (1964).

23. J. Smith, F. Ogburn and C. J. Bechtoldt, J. Electrochem. Soc. 115, 371 (1968).

24. S. Ino and S. Ogawa, J. Phys. Soc. Jpn. 22, 1365 (1967).

25. T. Komoda, Jpn. J. Appl. Phys. 7, 27 (1968).

26. S. Iijima, Jpn. J. Appl. Phys. 26, 357 (1987).

27. J. Narayan, to be published in Appl. Phys. Lett. (1989).

28. R. Kern, G. L. Lay and J. J. Metois, in *Current Topics in Materials Science*, edited by E. Kaldis (North-Holland Publishing Company, 1979).

29. S. Ino, J. Phys. Soc. Jpn. 27, 941 (1967).

30. A. Olsen and J. C. H. Spence, Philos. Mag. A 43, 945 (1981).

31. J. Hornstra, J. Phys. Chem. Solids 5, 129 (1958).

32. J. C. Angus, Science (1989).

33. R. E. Clausing, L. Heatherly, K. L. More and G. M. Begun, presented at *International Conference on Metallurgical Coatings*, San Diego, CA, 1989.

34. O. L. Krivanek and D. M. Maher, Appl. Phys. Lett. 32, 451 (1978).

35. U. Dahmen, C. J. Hetherington, P. Pirouz and K. H. Westmacott, submitted to Scripta Met. (1988).

36. R. De Wit, Phys. C: Solid State Phys. 5, 529 (1972).

37. J. Weertman and J. R. Weertman, *Elementary Dislocation Theory* (Macmillan, New York, 1964).
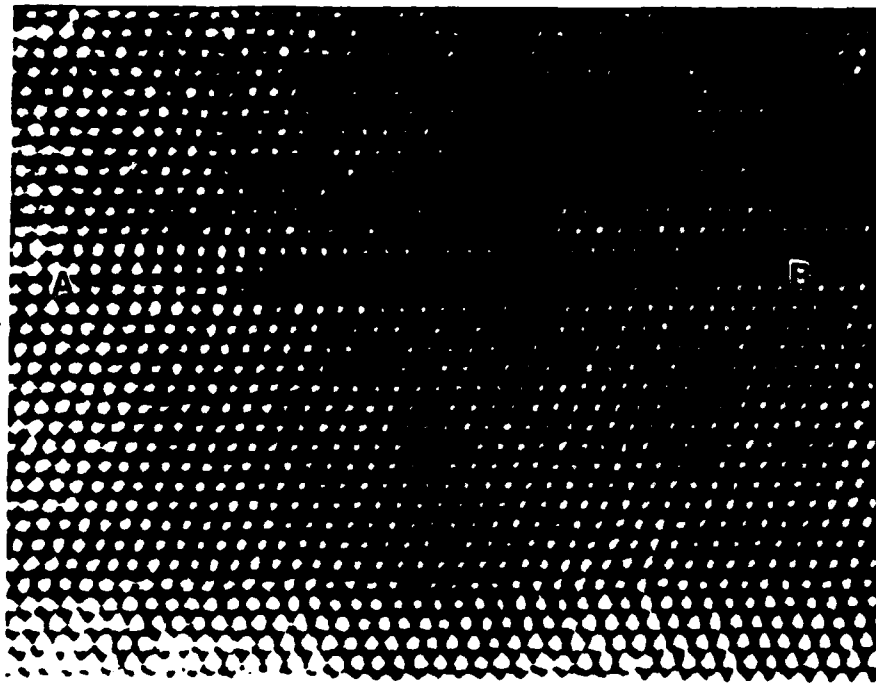
Figure 1.

a)

M

A

B

C

B

A

b)

2.06 Å

M

Figure 2.

a)

b)

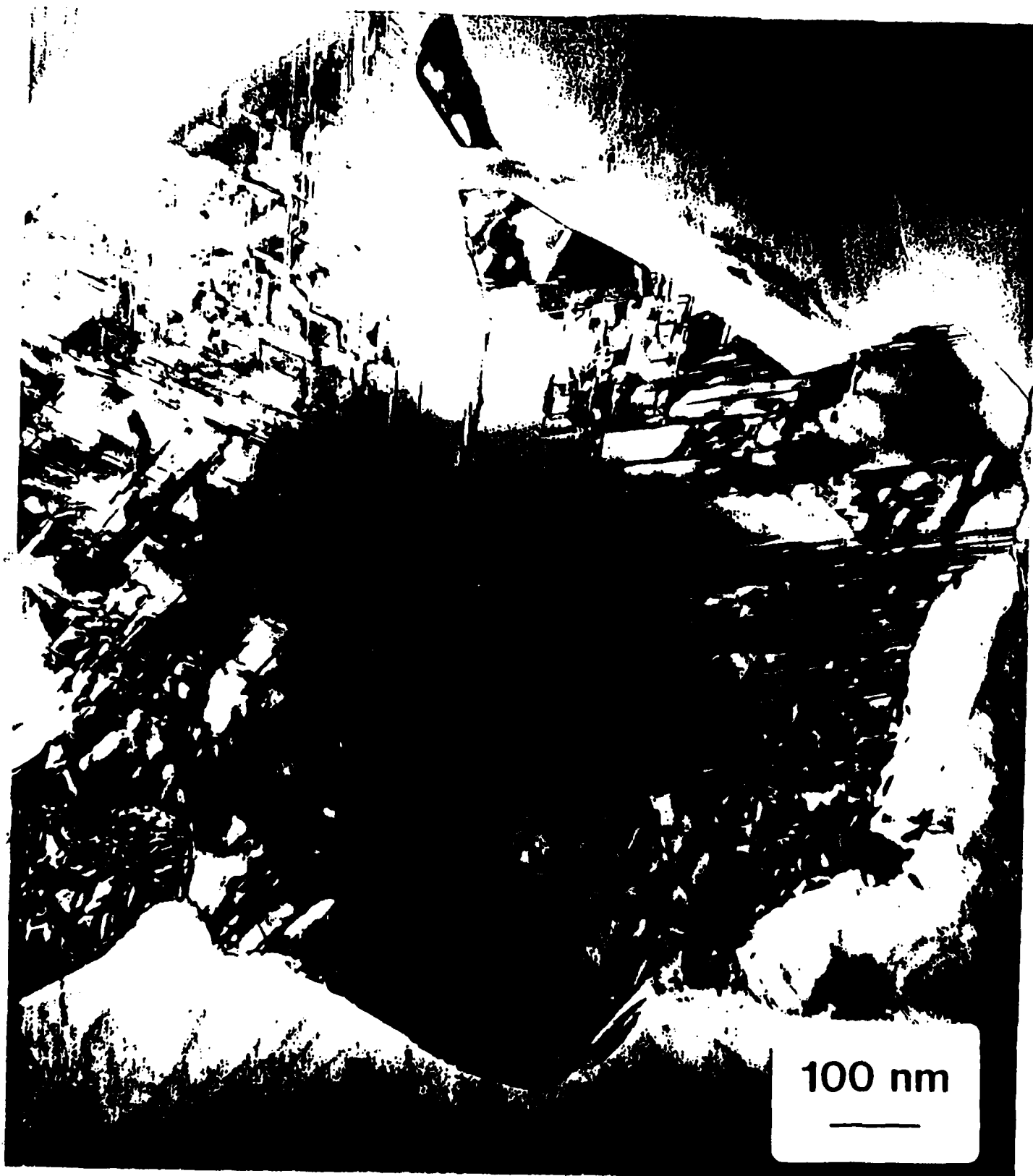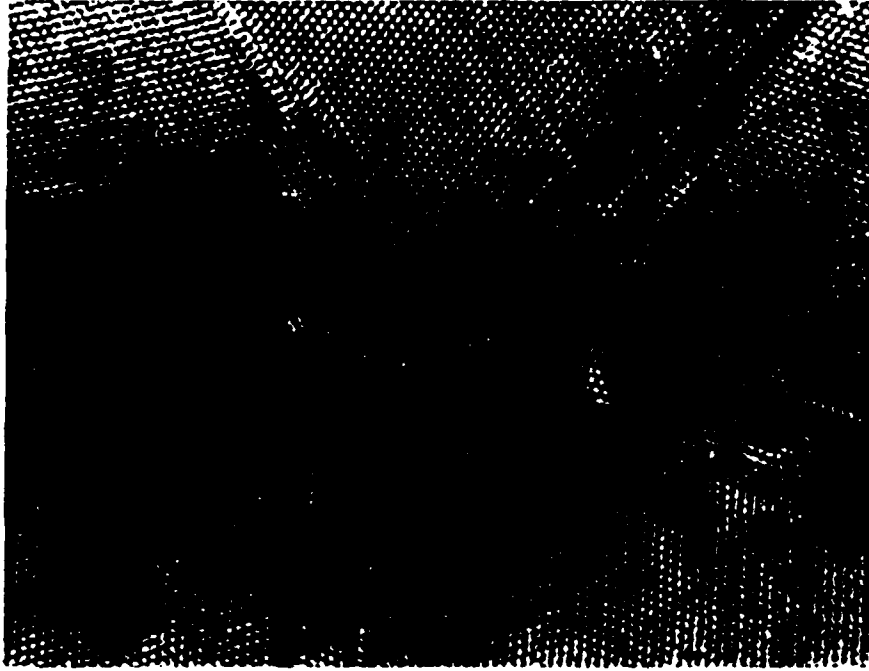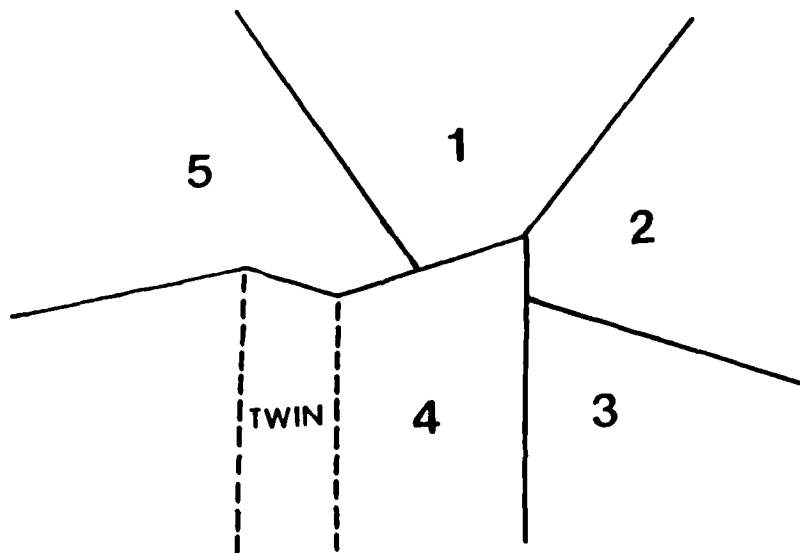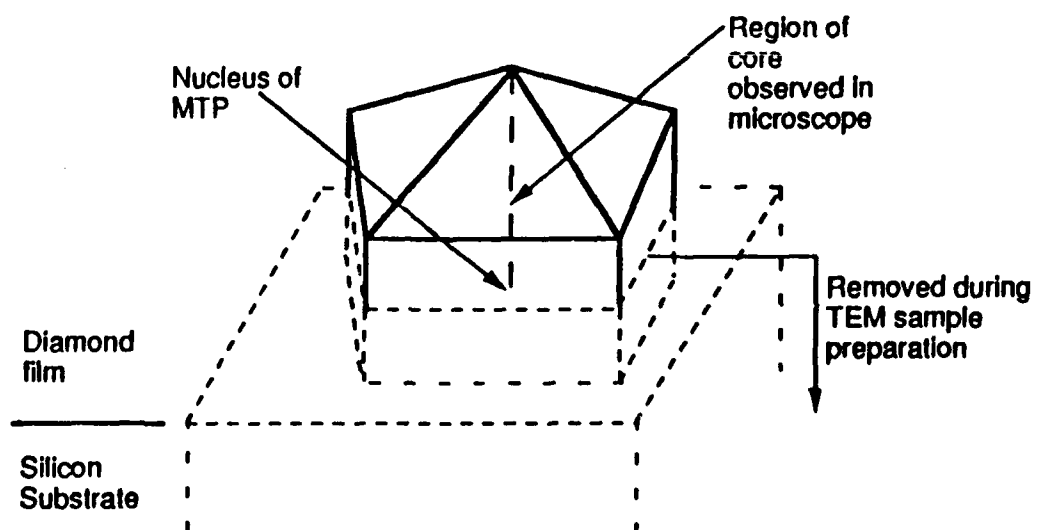Figure 3.

Figure 4.

Figure 6.

100 nm

Figure 7(a).

100 nm

Figure 7(b).

a)

b)

Figure 8.

Figure 9.

Figure 10.

a)

b)

Figure 11.

Figure 12.

PRECURSOR STRUCTURES IN THE FORMATION OF DIAMOND FILMS

R. J. Nemanich, R. E. Shroder, J. T. Glass and G. Lucovsky

Department of Physics and Department of Materials Science and Engineering
North Carolina State University
Raleigh, NC 27695-8202
USA

The carbon bonding configurations of films prepared by plasma excited deposition of methane diluted with hydrogen are examined by Raman spectroscopy. In the limits of methane concentrations less than 1% the films show predominant diamond character while for methane concentrations greater than 3%, Raman spectra are similar to those of microcrystalline or disordered graphite. At concentration of 2%, near the onset of diamond formation, a new feature is detected which exhibits a frequency similar to that expected for amorphous or microcrystalline diamond.

It is well known that graphite is the stable solid state crystalline form of carbon at ambient temperature and pressure. Recent advances in CVD growth methods have demonstrated, however, the formation of films with crystalline diamond structures.[1,2] Other studies have shown that it is possible to dope diamond crystals. With the high electron mobility and wide bandgap of diamond, the new advances suggest that these films may form the basis for future high temperature semiconductors.

Successful growth techniques have used mixtures of hydrocarbon gases and hydrogen in various CVD methods. Under different deposition conditions, the films exhibit properties characteristic of graphite or diamond. Raman spectroscopy has proved to be one of the most useful experimental characterizations of the carbon bonding configurations in the films.[3,4] In this study we employ Raman scattering characterization of a series of films prepared under various deposition conditions. The focus is to determine the atomic bonding configurations of the carbon in the films.

Films were prepared by plasma excited CVD process. Methane was diluted with hydrogen and excited with microwaves. The microwaves heated the substrate to ~800°C and caused a plasma of the gases around the sample. Because of the high substrate temperature, the films exhibited less than 1 at % H. The pressure in the chamber was ~30 torr with a flow of 100 sccm. For methane concentrations less than 1% film growth rates of ~0.2μm/hr were obtained while for methane concentrations >2 %, growth rates of 1μm/hr were obtained. The films were all deposited on Si<100> substrates which had been polish roughened to increase the nucleation density.

The Raman spectra were obtained in a backscatter configuration using 514.5nm Ar ion laser radiation. The scattered light was dispersed with a computer controlled triple monochromator and detected with a photomultiplier.

An important aspect of the Raman spectra is that the modes due to 3-fold coordinated bonding in crystalline, microcrystalline and amorphous graphite occur at a higher frequency than the characteristic $1332cm^{-1}$ mode of crystalline diamond.[4] This is because the 3-fold coordinated materials exhibit stronger bonding between nearest neighbors than 4-fold coordinated diamond. The spectrum of microcrystalline graphite
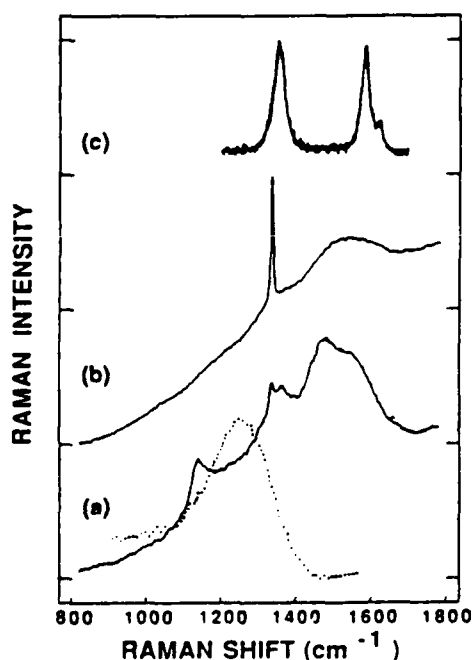
Fig. 1 The Raman spectra of carbon films on Si produced by CVD. Samples a) and b) were deposited using microwave CVD while sample c was produced using remote plasma enhanced CVD. The dotted line represents the Raman spectrum of amorphous tetrahedrally coordinated diamond and was obtained by scaling the spectrum of a-Si to the diamond frequency.
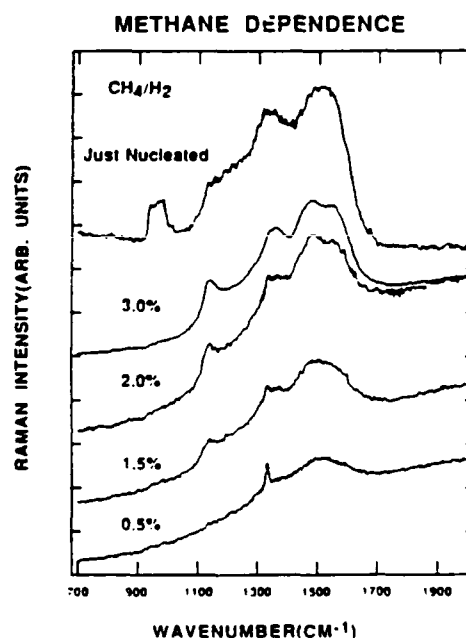
Fig. 2 The Raman spectra of carbon films produced with different methane concentrations. The just nucleated film shows incomplete coverage.

exhibits a peak at 1355cm^{-1} which is close in frequency to that of diamond. Extensive studies have correlated this feature with a peak in the density of states of graphite [5], and it is further noted that the highest frequency mode of diamond is at ~1332cm^{-1} and would require a stress of over 50 kbar to shift to 1355 cm^{-1} [6].

We consider now the results of a series of carbon films produced by the microwave CVD growth process. The results are shown in Fig. 1. One of the most striking aspects is that the spectrum of the sample produced at 0.5% methane is dominated by a peak at 1332cm^{-1} which is an indication of crystalline diamond formation. The broad peak centered at 1500cm^{-1} is similar to that of amorphous graphite. We would suggest that this indicates the presence of disordered 3-fold coordinated carbon. An important aspect that is not evident in the spectrum is that there is a broad luminescence background which displays a strong peak at ~1.68eV. Previous studies have assigned a similar feature to the neutral vacancy in diamond. Since graphitic regions would act as non-radiative recombination centers, the presence of luminescence suggests that well ordered diamond regions are larger than the exciton size.

The samples produced at higher methane concentrations are dominated by a series of spectral components extending from 1300 to 1600 cm^{-1}. Close examination of the film produced with 2% methane indicates that the feature at 1332cm^{-1} is weakly present as are features centered at 1355, 1500 and 1590 cm^{-1}. The 1355 and 1590 cm^{-1} features are similar to the features of microcrystalline graphite [4,5], and indeed the sample produced by low pressure remote plasma CVD is dominated by these features. The feature at 1500 cm^{-1} is similar to amorphous graphite and indicates the presence of these structures. Thus these features indicate the presence of 3-fold bonded carbon structures in addition to the diamond structures. Previous measurements have found that the absolute cross section of graphite is 50 times stronger than that of diamond [7], thus the samples may still exhibit a large percentage of diamond.

One spectral feature that cannot be simply accounted for is that at 1140cm^{-1}. This feature is most evident for conditions were the onset of crystalline diamond formation is detected. The Raman spectra of a series of samples with similar preparation conditions but different methane ratios are shown in Fig. 2. The spectrum of a just nucleated film which has incomplete surface coverage is also shown. At lower methane concentrations where diamond film growth dominates, the feature is no longer detected. For very thin film depositions (Fig 2d) the 1140 cm^{-1} feature becomes very broad. Thus the 1140 cm^{-1} feature occurs at the onset of diamond formation, and appears to be a precursor to the formation of crystalline diamond.

While amorphous tetrahedral semiconducting films of Si and Ge have been produced for many years, amorphous tetrahedrally coordinated C films have not been produced and measured. Because the phonon dispersion curves of Si and diamond are similar in general form, we can use the spectra of a-Si to model the expected results for the Raman spectrum of "amorphous diamond." The Raman spectra of a-Si has been scaled by the ratio of the Raman frequencies of crystalline diamond and silicon (ie. 1332/520), and the results are also shown in Fig. 1. An important aspect is that the peak due to amorphous or microcrystalline 4-fold coordinated carbon will occur at frequencies less than $1332cm^{-1}$. The $1140cm^{-1}$ feature exhibits a strong correspondence to that of "amorphous tetrahedral carbon." A similar analysis of microcrystalline diamond would yield a peak at a similar frequency for microcrystalline domains <50Å. We suggest that this feature then is due to the presence of disordered 4-fold carbon.

The $1140cm^{-1}$ feature is most evident for less than ideal diamond growth conditions. The samples have considerable 3-fold carbon concentrations and grow with higher deposition rates than ideal growth conditions. It is likely that the disordered diamond structures form on graphitic surfaces and then act as nucleation sites for crystalline diamond growth.

ACKNOWLEDGEMENT

REFERENCES

[1]   B.V. Spitsyn, L.L. Bouilov and B.V. Derjaguin, J. Cryst. Growth 52, 219(1981).

[2]   S. Matsumato, Y. Sato, M. Tsutsumi, N. Setaka, J. Mat. Sci. 17, 3106 (1982).

[3]   K. Suzuki, A. Sawabe, H. Yasuda and T. Inuzuka, Appl. Phys. Lett. 50, 728 (1987).

[4]   R.J. Nemanich, J.T. Glass, G. Lucovsky and R. Shroder, J. Vac. Sci. Tech. A6, 1783 (1988).

[5]   R.J. Nemanich and S.A. Solin, Phys. Rev. B20, 392 (1979).

[6]   A. Jayaraman, Rev. Mod. Phys. 55, 65 (1983)

[7]   N. Wada and S.A. Solin, Physica 105 B, 353 (1981).

Bias Controlled Chemical Vapor Deposition of Diamond Thin Film

Y. H. Lee, P. D. Richard, K. J. Bachmann and J. T. Glass

Department of Materials Science and Engineering,

North Carolina State University, Raleigh, N. C. 27695-7907

Abstract

The growth of diamond films on (001) Si substrates by bias controlled chemical vapor deposition is described. The film quality as judged by Raman spectroscopy and scanning electron microscopy depends strongly on the biasing conditions. Under low current reverse bias conditions, highly facetted cubooctahedral diamond growth exhibiting a single sharp Raman line at 1332 cm^{-1} was obtained, while biasing in high current conditions which created a plasma resulted in multiply twinned, microcrystalline growth incorporating sp^2 bonded carbon into the diamond film.

Diamond films and particles have been grown by various deposition methods such as thermal dissociation chemical vapor deposition (CVD)[1,2], plasma assisted CVD[3,4], electron assisted CVD[5,6], RF sputtering[7] and ion beam deposition.[8] A major direction in diamond research has been towards achieving high growth rates for coating-orientated technology.[5,6,9] Also, attempts are underway to obtain the heteroepitaxial deposition of single crystalline films on Si and various metal and compound substrates. In both of these key areas, charged species, especially electrons, may play a significant role during the hot filament CVD of diamond. For example, electrons may damage the surface of diamond[10,11] or they may accelerate the decomposition of H_2 and CH_4[5], yielding opposite effects in terms of film quality. In the present research a controlled bias is applied to the substrate and the filament to examine such effects. The conditions which result in a clean, facetted growth morphology and a sharp Raman spectra characteristic of pure diamond are described.

Figure 1a is a schematic of the experimental arrangement of the Bias Controlled Chemical Vapor Deposition (BCCVD) system utilized in the present research which is similar to conventional thermal CVD systems reported in the literature.[1,2] However, means have been added for independent biasing of the substrate and the filament with regard to the grounded walls of the growth chamber. A gas mixture of methane and hydrogen is introduced above a hot tungsten filament. The ratio of methane to hydrogen can be set from 0% to 10% independently of total flow (25 to 400 sccm) and pressure (0.5 to 13 kPa). Below the filament the substrates rest upon a removable 55 mm diameter molybdenum holder which is mounted on a boron

nitride encapsulated substrate heater. A linear manipulator allows the position of the substrate with respect to the filament to be varied between 8 and 75 mm.

In this particular series of experiments, only the bias was varied. The methane ratio was fixed at 3% , total flow at 100 sccm, and pressure at 3.3 kPa. Also filament temperature (T_f) was adjusted to 1930°C, substrate temperature held at 850°C and filament to substrate distance set at 8 mm. Silicon (001) substates polished with 0.25 μm diamond paste, were used as a standard substrate. The deposited films were characterized by scanning electron microscopy (SEM) and Raman spectroscopy.[12,13]

Initial experiments involved the variation of the filament bias voltage and substrate bias voltage independently relative to the grounded chamber. However, it was found that the current depended primarily on the potential difference (ΔV) between the filament and substrate due to the highly resistive path to the chamber walls which were on the order of 3 cm away. The current is plotted relative to this ΔV in Figure 1b. As expected, the system behaves like a diode[14]due to the high temperature of the filament which easily ejects electrons vs. the low temperature of the substrate which does not allow the electrons to escape easily. Thus, "forward" bias (positive ΔV in Fig. 1b) occurs when the substrate is held at a positive potential relative to the filament. At high reverse and forward bias the sudden increase in current and its hysterysis indicate the formation of a DC plasma. Furthermore, a weak glow was observed under reverse biasing conditions when the filament was turned off.

Typical SEM micrographs of the deposited diamond particles and films on the Si substrates are also shown in Figure 2. The potential difference between the substrate

and the filament is given in the figure caption. Different biasing conditions introduced differences in the growth morphology. Under conditions which created a DC plasma during forward bias [i.e., more positive substrate voltage, V_s, and a negative current I (electrons flowing into substrate)] and reverse bias (more positive filament voltage, V_f) multiply twinned[15], microcrystalline particles are dominant as shown in Figures 2a and d, respectively. In addition, under the reverse bias plasma conditions, nucleation was very nonuniform suggesting that nucleation sites have been altered in some way, inhibiting nucleation. In contrast, for the case of reverse biasing below the plasma forming region (i.e., low current reverse bias, figure 2c) and in the case of a grounded potential (i.e., $\Delta V=0$) only highly facetted cubooctahedral particles are observed.

The corresponding Raman spectra shown in Figure 3 indicate that in the low current reverse biasing condition (Figure 3c), only the 1332 cm^{-1} diamond line is observed. The broad band normally located at ~1500 cm^{-1} associated with a sp^2 bonded graphitic phase is absent. Furthermore, this sample exhibited a full width at half maximum (FWHM) of the 1332 cm^{-1} Raman peak which is more narrow (≤ 5 cm^{-1}) than any of the other samples. On the other hand, samples grown under conditions which generated a plasma contain a significant sp^2 component as shown in Figures 3a and 3d. Research is continuing to determine possible causes of this phenomena.

From these results, we conclude that biasing which creates a DC plasma significantly deteriorates the film quality. In contrast, low current reverse biasing conditions which reduce electron flux suppress the formation of an sp^2 bonded phase. It is supposed that this is due to a decrease in electron and ion bombardment

of the sample during the low biasing conditions which minimizes surface damage during growth. It may also be possible that electron flux from the substrate and substrate holder surface accelerates the decomposition of H_2 into atomic hydrogen in the vincity of the surface, and thereby suppress the sp^2 bonded phase. The quantitative analysis of these films is currently in progress.

References

[1] S. Matsumoto, Y. Sato, M. Tsutsami, and N. Setaka, J. Mater. Sci. **17**, 3106 (1982).

[2] S. Matsumoto, Y. Sato, M. Kamo, and N. Setaka, J. Appl. Phys. **21**, 483 (1982).

[3] R. Mania, L. Stobierski and R. Pampuch, Cryst. Res. and Technology **16**, 785 (1981).

[4] M. Kamo, Y. Sato, S. Matsumoto, and N. Setaka, J. Cryst. Growth **62**, 642 (1983).

[5] A. Sawabe and T. Inuzuka, Appl. Phys. Lett. **46**, 146 (1985).

[6] A. Sawabe and T. Inuzuka, Thin Solid Films **137**, 89 (1986).

[7] A. Hiraki, T. Kawano, Y. Kawakami, M. Hayashi and T. Miyasato, Solid State Commun. **50**, 713 (1984).

[8] A. Aisenberg and R. Chabot, J. Appl. Phys. **42**, 2953 (1971).

[9] Y. Hirose and Y. Terasawa, Jpn. J. Appl. Phys. **25**, L519 (1986).

[10] Y. Mizokawa, T. Miyasato, S. Nakamura, K. M. Geib and C. W. Wilmsen, Surf. Science **182**, 431 (1987).

[11] S. Pepper, Appl. Phys. Lett. **38**, 344 (1981)

[12] D.S. Knight and W. B. White, J. Mater. Res., **4**, 385 (1989).

[13] K. Kobashi, K. Nishimura, Y. Kawate, and T. Horiuchi, Phys. Rev. B, **38**, 4067 (1988)

[14] W. Yarbrough, Private Communicatons, Pennsylvania State University.

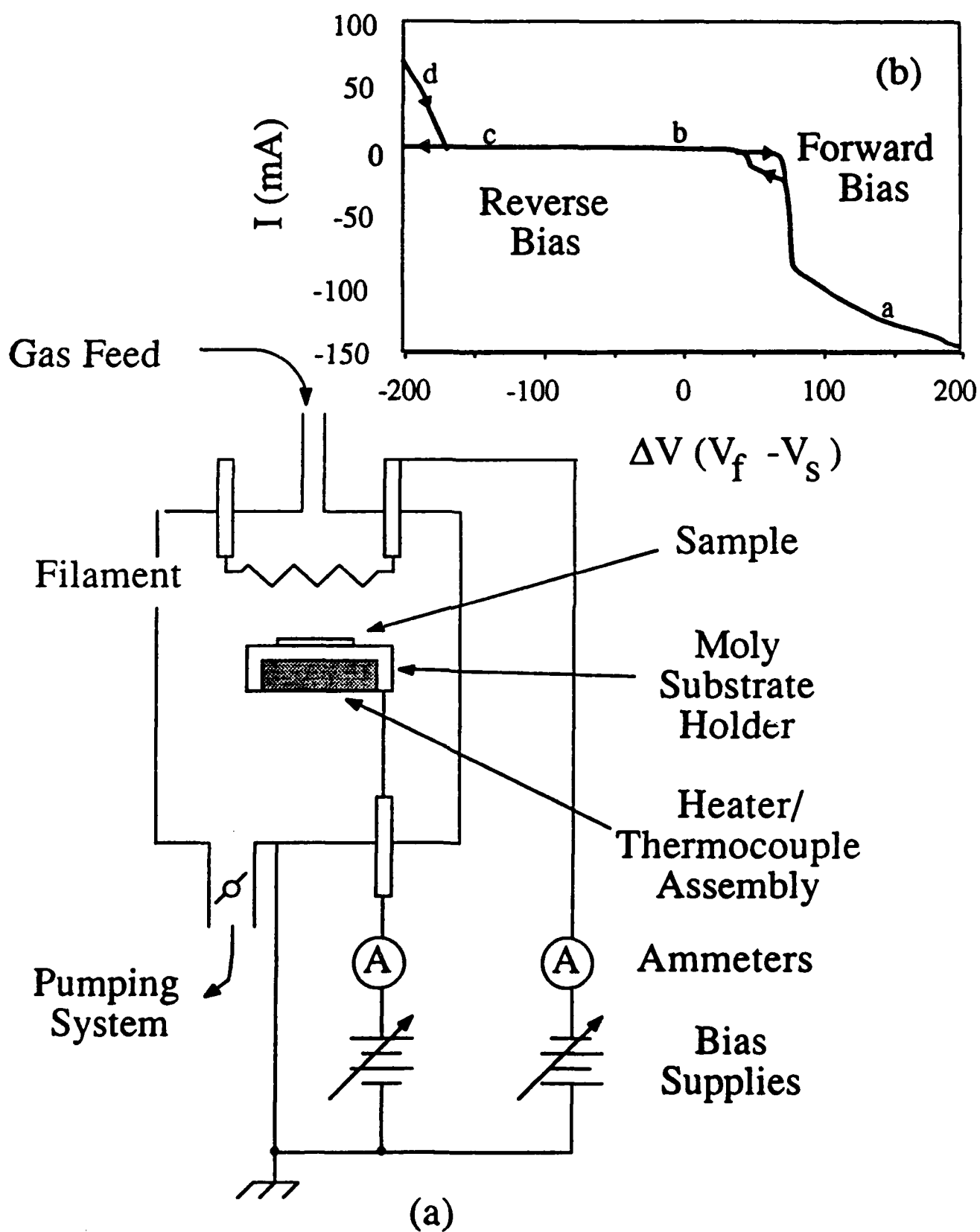[15] S. Matsumoto, Y. Matsui, J. Mater. Sci. **18**, 1785 (1983)

Figure Captions

Fig. 1. (a)Schematic diagram of BCCVD system which is similar to a hot filament CVD system to which biasing capabilities have been added.

(b)I-V characteristic of BCCVD System showing the diode nature of this arrangement. Samples are labelled on the plot as a, b, c, and d.

Fig. 2. SEM images of diamond thin films on Si grown for 3 hours under different biasing conditions: (a) $V_f = 0$ V, $V_s = 150$ V, I $\approx$ -125 mA, (b) $V_f = 0$ V, $V_s = 0$ V, I $\approx$ -10 μA, (c) $V_f = 150$ V, $V_s = 0$ V, I $\approx$ 5 μA, (d) $V_f = 180$ V, $V_s = 0$ V, I $\approx$ 60 mA.

Fig. 3. Raman spectra of diamond thin films grown under different biasing conditions. Sample designations (a) - (d) are the same as in figure 2. FWHM of (a) 14.0 cm^{-1}, (b) 5.7 cm^{-1}, (c) 5.0 cm^{-1}, (d) 13.0 cm^{-1} (Raman conditions: .5145 nm Ar+ laser, 2 cm x 2 mm sampling area, 2 cm-1 slit width).

(b)

I (mA)

Reverse Bias

Forward Bias

$\Delta V (V_f - V_s)$

Gas Feed

Filament

Pumping System

Sample

Moly Substrate Holder

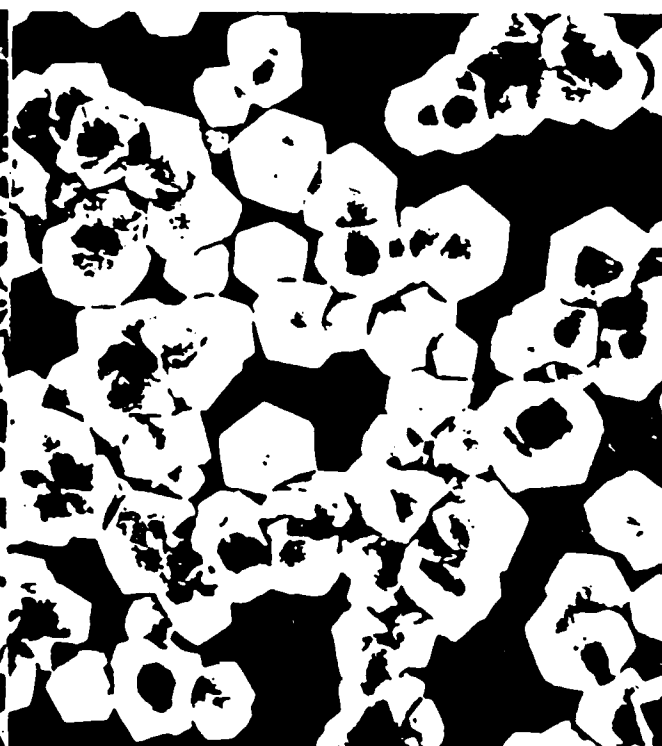Heater/ Thermocouple Assembly

Ammeters

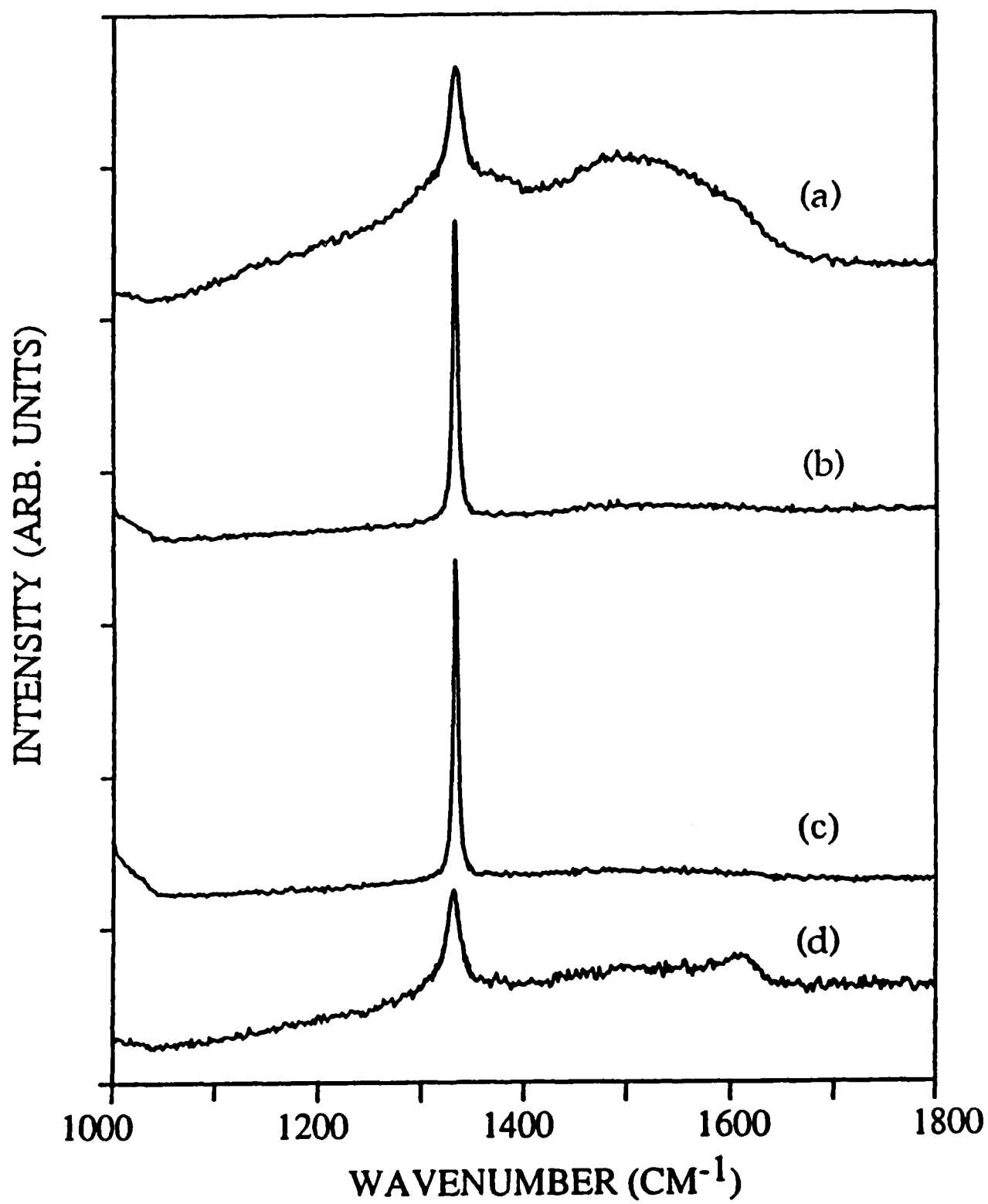Bias Supplies

(a)

(a)

(b)

(c)

(d)

5 μm

Electrical Properties of B Doped CVD Grown Polycrystalline Diamond Films

K. Nishimura*, K. Das, J. T. Glass, K. Kobashi**, R. J. Nemanich***, Department of Materials Science and Engineering, North Carolina State University, Raleigh, NC. 27695-7907, USA
* Visiting scientist from Kobe Steel, Ltd., Japan
** Electronics Research Laboratory, Kobe Steel Ltd., Takatsukadai 1-chome, 5-5, Nishiku, Kobe, Japan, 652
***Department of Physics, North Carolina State University, Raleigh, NC, 27695-8202, USA

ABSTRACT. B doped diamond films were synthesized by microwave plasma CVD. and the crystal quality and the electrical properties were investigated. From SEM. clear facets were observed and X-ray diffraction data showed that only the diamond phase was present. Raman spectroscopy verified the presence of diamond and indicated that the crystal quality increased when B is incorporated in the films up to 400 ppm. SIMS analysis showed that on the order of $10^{20}/cm^3$ (564 ppm) of B was incorporated in the diamond film with a gas phase B/C ratio of 400 ppm. Electrode patterns of Pt were fabricated on the films and electrical properties were investigated. Undoped diamond films showed rectifying contacts with small leakage currents and B doped diamond films with a B concentration of 400 ppm showed ohmic behavior. The B in these films had small activation energies, which indicates that impurity band conduction plays an important role.

1 Introduction

Diamond can be considered a semiconductor with a very wide band gap (≈ 5.4 eV) and ha., a variety of useful properties [1]-[3], such as high: (a) thermal conductivity (2,000 W/K m), (b) carrier mobility, (c) breakdown voltage, (d) drift velocity, and (e) radiation hardness. Therefore, it is expected to be useful for power devices, high speed devices, and devices used at high temperature and in radiation intensive environments. As a consequence, many articles on the electrical properties of bulk semiconductive diamond have been published .[4]-[7] Unfortunately, the scarcity and expense of such diamond, as well as the necessity of utilizing thin films for many of the aforementioned devices, has limited the continued research and development of this area. Recently, however, renewed interest has been generated by the successful chemical vapor deposition (CVD) of diamond by various vapor phase methods.[8]-[10] In fact, it has been shown that semiconductive p type diamond films can be grown when B is introduced into the films.[11]-[13] These achievements are key technologies for the fabrication of devices and has further accelerated research in this area. However, although numerous studies of the electrical properties of bulk diamond have been conducted, the electrical properties of

B doped polycrystalline diamond films have not been investigated thoroughly. Thus, in the present research, B doped diamond films were grown by microwave CVD and investigated by scanning electron microscopy (SEM), X ray diffraction, Raman spectroscopy, Secondary Ion Mass Spectroscopy (SIMS), current-voltage characteristics (I-V characteristics), and resistivity measurements.

2 Experimental

B doped diamond films were grown on polycrystalline Al_2O_3 substrates with dimensions of 20 mm X 10 mm by microwave plasma CVD. Al_2O_3 substrates were employed due to their high resistivity which allowed electrical measurements to be made without influences from the substrates. The detailed features of this apparatus, experimental procedures and preparation of substrates are given in reference [14]. To grow B doped diamond films, CH_4, H_2 and B_2H_6 gases were employed. The concentration of CH_4 was 0.5 % and B_2H_6 concentrations ranged from 1 ppm to 0.1 ppm in the gas phase, which are equal to B/C ratios from 400 ppm to 40 ppm. For the remainder of this paper, B concentrations will be given as ppm of B relative to C in the gas phase as determined by mass flow measurements. The growth temperature was 800 °C and the gas pressure was 31.5 Torr. The films were deposited for 7 hours and the film thickness obtained was approximately 1.4 µm.

These specimens were cut into 5 mm X 5 mm samples using a diamond saw and then cleaned in H_2SO_4 at approximately 70°C for 10 minutes, followed by a conventional RCA clean.[15] As a final cleaning step, specimens were dried in an oven at 120 °C for 5 minutes to eliminate moisture on the diamond films, otherwise, the Pt metal utilized for electrical contacts (see below) would sometimes separate from the diamond when an ultrasonic cleaning was performed.

Electrode patterns were fabricated on the diamond films by conventional photolithography and Pt electrodes were deposited on the films by RF sputtering. The RF power was 100 W and the gas pressure was 10 mTorr. The film thickness of the deposited Pt was about 2,000 Å. Lift-off was utilized to achieve the final pattern consisting of circular dots with diameters of 100 µm separated from the surrounding metal by an open annulus. Electrical ground was made on the same side of the specimen. There are several reasons for choosing Pt as the contact material: (a) Pt has a large work function (5.7 eV) [16], thus it should facilitate the achievement of ohmic contacts on p type diamond films [16], (b) Pt is inert in air, therefore, should yield stable contacts and, (c) perhaps most importantly, Pt yielded the minimum contact resistivity of the metals which were investigated for the present study, including as-deposited Ni, Al and $TaSi_2$.

To obtain atomic B concentration, B was implanted into undoped diamond films synthesized by the same growth conditions as B doped CVD grown films and they were used as standards during SIMS measurements.

3 Results and Discussions

3.1 MATERIAL CHARACTERIZATION

Surface morphology was observed via scanning electron microscopy (S-530, Hitachi Co.). Figure 1 shows the surface morphology of a B doped diamond film with a B/C ratio of 400 ppm. Clear (111) facets and five fold multiply twinned particles can be seen. It was found that, for B/C ratios from 0 to 400 ppm, no differences in this morphology could be observed. Furthermore, X-ray diffraction indicated that diamond was the only structure present in the films up to 400 ppm of B. However, when the B/C ratio was greater than 4,000 ppm, the shapes of particles became irregular and the size decreased. Additional X-ray diffraction peaks believed to be due to graphite were also observed as the B concentration was increased above 400 ppm. Details of the surface morphology of B doped diamond films are published in a separate article.[17] Similar research has been conducted by Y. Sato et. al..[12]

Figure 1. Surface Morphology of B doped diamond films on an Al_2O_3 substrate. The B/C ratio in gas phase was 400 ppm.

Laser Raman spectroscopy was used to investigate the crystal quality of the B doped diamond films. The diameter of the laser beam was 100 μm X 2 mm and the wave length used was 5145 A. Figure 2 shows Raman spectra obtained from B doped diamond films with different B concentrations. It can be seen that the Raman peak increased relative to the intensity of the sp^2 peak as the B concentration increased. Furthermore, the full width half maximum of the diamond sp^3 Raman peak decreased. This indicates that doping with B increases the quality of the diamond films. This may be a gas species effect due to the B_2H_6 or may be a surface effect during growth caused by B incorporation at the growth surface. Although speculation of the mechanism is possible, more experiments are necessary before any conclusions can be made.

The Raman peak position characteristic of diamond was located at 1,337 cm^{-1} for the undoped diamond films. This position is shifted by 5 cm^{-1} from the same peak in most natural diamonds which occurs at 1,332 cm^{-1}. This suggests that a residual compressive stress is present in the film.[18] When the films were doped with B. the peak position was shifted to even higher wave numbers ($\approx$4 cm^{-1} at 400 ppm of B) than for undoped diamond films, implying that B doping increases the residual compressive stress or changes the domain size which can also affect the peak position.[19]
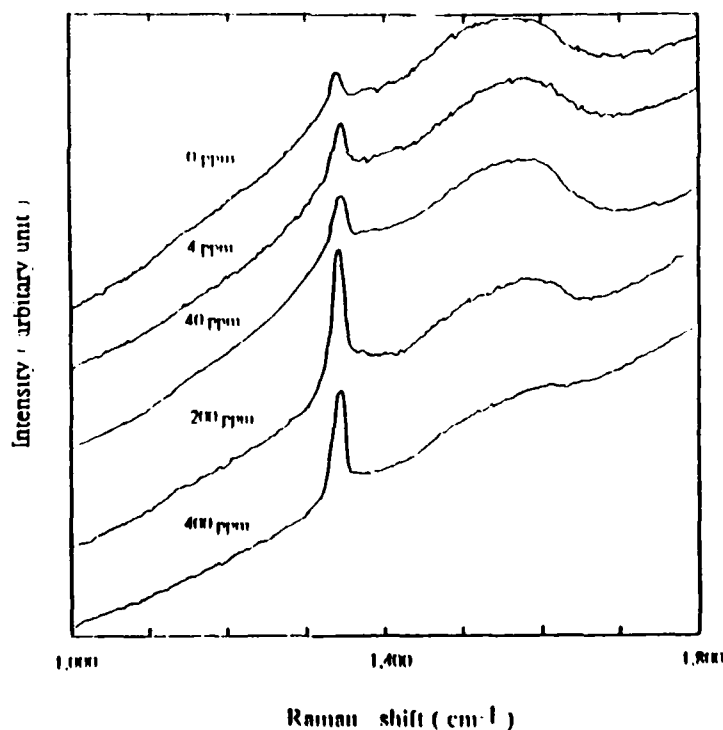

Figure 2. Raman spectra of undoped diamond and B doped diamond films. 1,332 cm^{-1} peak from diamond and a broad peak near 1,550 cm^{-1} caused by sp^2 components are observed. Crystal quality appears to increase with doping.

SIMS depth profiles (Fig.3) were obtained for diamond films containing different concentrations of boron. The apparatus used was a Cameca Co., IMS 3F instrument and an O^{2+} beam with 15 keV was used as the primary ion source. The sputtered area was about 180 μm X 180 μm and the sampled area was 60 μm in diameter. Figure 3 shows depth profiles of B doped and undoped diamond films. These profiles indicate that the interface between the Al_2O_3 substrates and the diamond films is sharp, thus, interdiffusion of C and B appears to be minimal at the growth conditions employed. It can be seen that the atomic concentration of B decreased when the B_2H_6 concentration in the gas phase was decreased.

Figure 4 shows the relationship between atomic concentration of B in the film and B concentration introduced into in the gas phase as measured by mass flow controllers. The atomic concentration of B decreases when the B_2H_6 concentration in the gas phase decreases. However, the B concentration in the film is greater than the B concentration in the gas phase. For example, the atomic concentration of B was on the order of $10^{20}/cm^3$ (i.e. B/C ratio of 564 ppm in the film) for a B concentration of 400 ppm in the gas phase. This actually means that the B/C ratios in the film are higher than the B/C ratios in the gas phase.
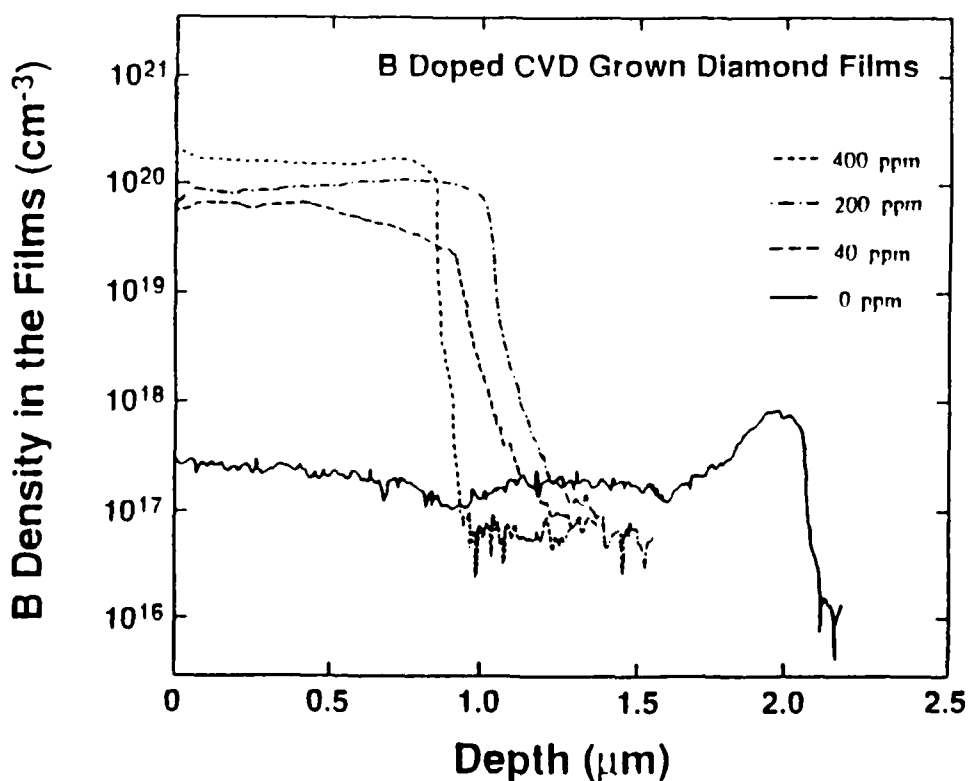

Figure 3. SIMS depth profile of undoped and B doped diamond films. It can be observed that B was distributed homogeneously in the films.

It can be speculated that this is caused by the difference between the sticking coefficients of carbon species and boron species, i.e., the sticking coefficient of boron is larger than the sticking coefficient of carbon at the growth conditions employed. (Note: The B concentration data presented in this manuscript is not corrected by this difference and thus refers to the gas phase B concentration.)

Finally, it should be noted that B was observed even in "undoped" diamond films at an approximate concentration of $5 \times 10^{17}/cm^3$. This indicates that residual B in the growth chamber was incorporated into the undoped diamond films. Therefore, the expression " undoped diamond films " is not accurate in present case, but will be retained in this paper for convenience.

Figure 4. Atomic B concentrations obtained from SIMS data versus B concentrations in the gas phase obtained from SIMS data. B concentrations in the gas phase were obtained from C and B ratios controlled by mass flow meters during synthesis.

3.2 ELECTRICAL PROPERTIES OF DIAMOND FILMS

To obtain I-V characteristics of the films, a semiconductor parameter analyser (Hewlet Packard Co. 4145A) was used. Figure 5 shows I-V characteristics of an undoped diamond film with Pt electrodes. Clear rectifying contacts were obtained and leakage current was 40 nA at approximately 10 V. From the direction of the reverse current, the polarity of this film was determined to be p type. Some contacts had high breakdown voltages near 100 V, however, the current did not rise sharply as is expected for avalanche breakdown phenomena.[16] This "soft breakdown" may be caused by current flow through grain boundaries and defects and/or by generation current. It should be noted that photoconductivity was observed in this undoped sample (Figure 6) when it was illuminated with white light. The reverse and
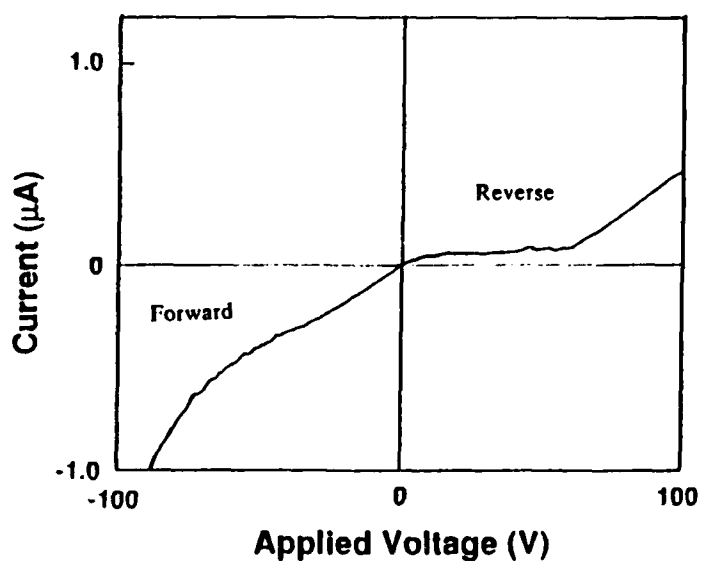
Figure 5. A typical I-V characteristic of an undoped diamond film with Pt electrodes at room temperature. Clear rectifying contacts were obtained and "soft breakdown" was observed.
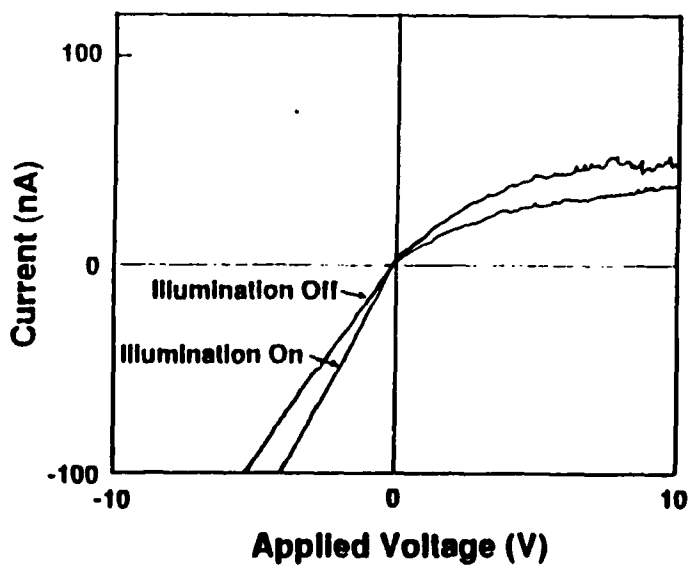

Figure 6. Photoconductivity was observed for the undoped diamond film in white light. Ratios of current gain of photocurrent to the dark current were 46 % and 32 % at 4 V for reverse and forward current, respectively.

forward current increased by ≈46 % and ≈32 %, respectively, at 4 V.

Figure 7 shows the temperature dependence of the I-V characteristics from room temperature to 473 K in air. When the temperature was increased, the leakage current increased and rectification disappeared at 473 K (i.e. ohmic behavior was obtained.). This effect is probably due to the presence of a high density of electrically active defects contributing to a large generation current at higher temperatures.
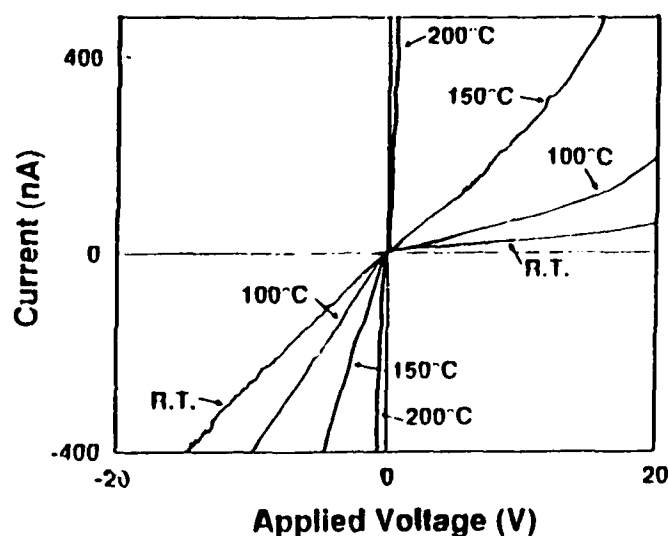

Figure 7. Temperature dependence of the I-V characteristic of the undoped diamond films with Pt electrodes. It can be observed that rectification disappeared at 200 °C and the contact showed an ohmic behavior.

Figure 8 shows the I-V characteristics of a 400 ppm B doped diamond film at various temperatures. In all cases, relatively straight lines are observed, indicating that ideal ohmic behavior is achieved between -5 V and 5 V. This ohmic behavior is believed to be due to tunneling through a thin depletion layer caused by heavy doping. When the absolute value of the applied voltage was over 5 V, the I-V characteristics deviated slightly from ideal ohmic behavior, however, a detailed study of this phenomenon has not been completed.

To obtain values of activation energy, resistivity was measured as a function of a temperature and is shown in Figure 9. The temperature ranged from room temperature to 673 K. The data shows that when temperature increased, resistivity decreased, which indicates that these films are behaving as semiconductors. However, from these data, it can be seen that a straight line was not obtained, thus, more than one activation energy is likely to be present for the charge carriers being measured. Although several activation energies may be present, for simplicity, only two slopes were assumed in this temperature regime as indicated in the figure. The activation energies obtained from this data are shown as a function of B/C ratios in Figure 10. When the B/C ratios increased, activation energies decreased. The maximum activation energy obtained was 0.16 eV for diamond films with the lowest B/C ratio of 40 ppm. These values are much smaller than the value of the acceptor
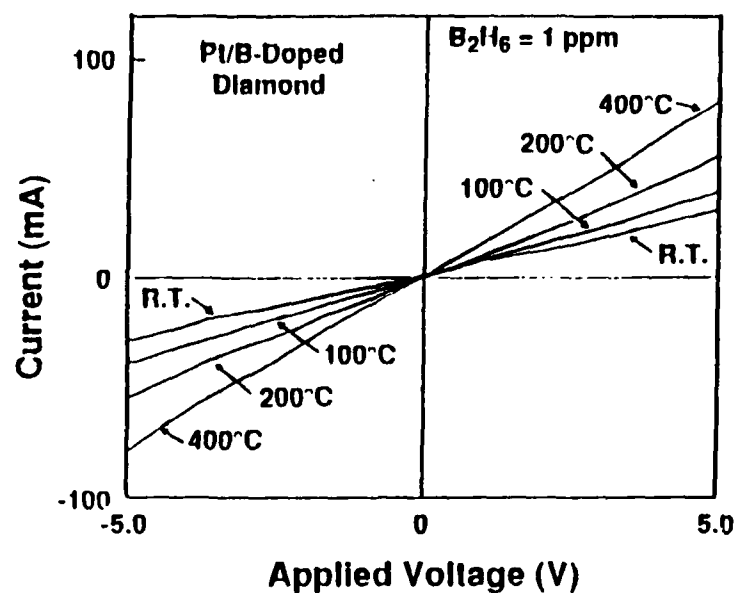
Figure 8. A typical I-V characteristic of a B doped diamond film with Pt electrodes at room temperature. Ohmic contacts were obtained.
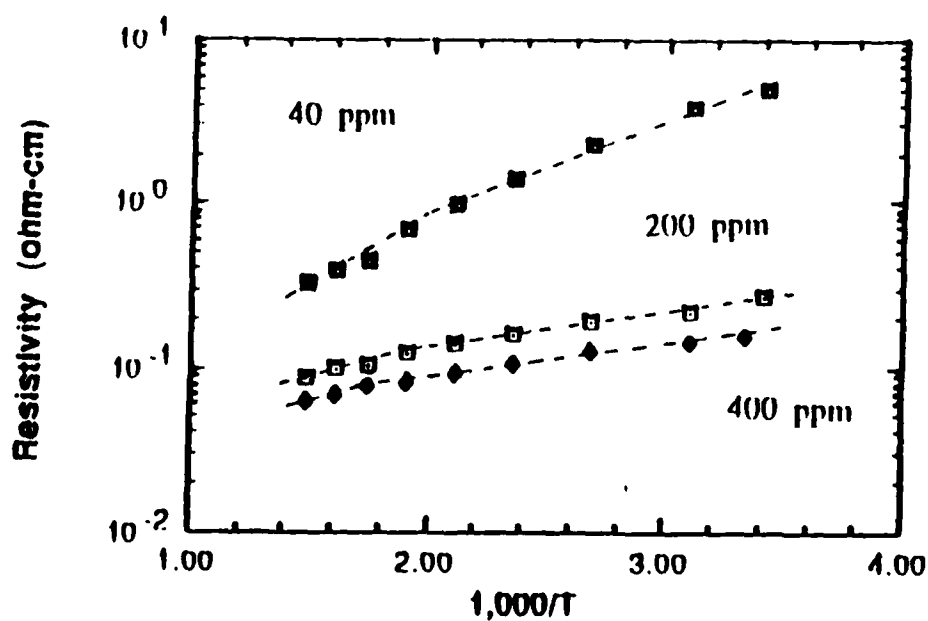

Figure 9. This shows the temperature dependence of resistivity for B doped diamond films from room temperature to 400 °C. B/C ratios were 400, 200, 40 ppm, respectively.

level of B impurities in bulk diamond as determined by photo-absorption (0.35 eV).[6] This suggests that impurity band conduction plays an important role in the films, causing them to behave as heavily doped semiconductors.[20] Such small activation energies due to heavy doping have also been observed in bulk B doped diamonds.[5], [21]. Photoconductivity was not observed in these films in white light which supports the conclusions that these films are heavily doped semiconductors.
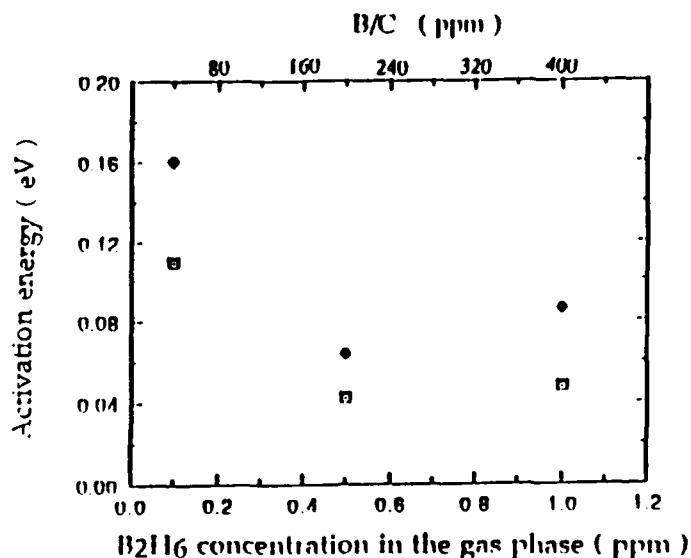
B/C (ppm)

B2H6 concentration in the gas phase (ppm)

Figure 10. Activation energies versus reciprocal temperature for B doped diamond
films were obtained from the higher temperature region (•) and from
the lower temperature region (□). Activation energies became larger
when doping concentration decreased. This trend is observed for
bulk B doped diamonds.[5], [21]

4 Summaries

B doped diamond films were synthesized by microwave plasma CVD, and the crystal quality and the electrical properties were investigated. From SEM, clear facets were observed and X-ray diffraction data showed that only the diamond phase was present. Raman spectroscopy verified the presence of diamond and indicated that the crystal quality increased when B is incorporated in the films up to 400 ppm. SIMS analysis showed that on the order of $10^{20}/cm^3$ (564 ppm) of B was incorporated in the diamond film with a gas phase B/C ratio of 400 ppm. Electrode patterns of Pt were fabricated on the films and electrical properties were investigated. Undoped diamond films showed rectifying contacts with small leakage currents and B doped diamond films with a B concentration of 400 ppm showed ohmic behavior. The B in these films had small activation energies, which indicates that impurity band conduction plays an important role.

5 Acknowledgments

References

[1] J. E. Field (1979) Properties of Diamond, Academic Press, London

[2] V. K. Bazhenov, I. M. Vikulin, and A. G. Gontar' (1985) " Synthetic diamonds in electronics ", **19**, (8), 829

[3] Landolt and Bornstein (1987) Numerical Data and Functional Relationships in Science and Technology, Springer-Verlag

[4] V. S. Vavilov (1975) " Semiconductive Diamond " Phys. Stat. Sol. (a), **31**, 11

[5] A. W. S. Williams, E. C. Lightowlers and A. T. Collins (1970) " Impurity conduction in synthetic semiconductive diamond ", J. Phys. C: Solid St. Phys., **3**, 1727

[6] A. T. Collins and A. W. S. Williams (1971) " The nature of the acceptor center in semiconductive diamond ", J. Phys. C: Solid St. Phys., **4**, 1789

[7] W. B. Wilson (1962) " Evidence for hoppimg transport in B-doped diamond", Phys. Rev., **127**, 5, 1549

[8] S. Matsumoto, Y. Sato, M. Tsutsumi, and N. Setaka (1982) " Growth of diamond particles from methane-hydrogen gas " J. Mater. Sci., **17**, 3106

[9] Y. Hirose and Y. Terasawa (1986) " Synthesis of diamond thin films by thermal CVD using organic compounds ", Jpn. J. Appl. Phys. **25**, L. 519

[10] A. Sawabe and T. Inuzuka (1985) " Growth of diamond films by electron assisted chemical vapor deposition " Appl. Phys. Lett. **46**, 146

[11] D. J. Proferl, N. C. Gardner, and J. C. Angus (1973) " Growth of boron -doped seed crystals by vapor deposition ", J. Appl. Phys., **44**, 4, 1428

[12] Y. Sato, M. Kamo, and N. Setaka (1987) " Growth of semiconductive diamond films by plasma-assisted vapor deposition ", High Tech Ceramics, edited by P. Vincenzini, 1719

[13] B. V. Spitsyn, L. L. Bovilov, and B. V. Derjaguin (1981) " Vapor growth of diamond on diamond and other surface " , J. Cryst. Growth, **52**, 219

[14] K. Kobashi, K. Nishimura, y. Kawate, and T. Horiuchi (1988) " Synthesis of diamonds by use of microwave plasma chemical vapor deposition: morphology and growth of diamond films ", Phys. Rev. B, **38**, 6, 4067

[15] W. Kern and D. A. Puotinen (1970) " Cleaning solution based on hydrogen peroxide for use in semiconductor technology ", RCA Review, June, 187

[16] S. M. Sze (1981) Physcis of Semiconductor Devices, 2nd Edition, John Wiley & Sons, Inc., New York

[17] K. Nishimura, K. Miyata, Y. Kawate, K. Kobashi (1988) " Surface morphology and defect structures in microwave CVD diamond films" '88 Proceeding of SPIE conference in San Diego

[18] D. S. Knight and W. B. White (1989) " Characterization of diamond films by Raman spectroscopy " J. Mater. Res. **4, 2, 385**

[19] Y.M. LeGrice and R. J. Nemanich, Submitted to Materials Research Socety, 1989 Fall meeting, Symposium F

[20] V. I. Fistul' (1969) Heavily doped semiconductors, Plenum press, New york

[21] J. C. Bougoin, J. Krynicki, and B. Blanchard (1979) " Boron concentration and impurity- to- band activation energy in diamond ", Phys. Stat. Sol. (a), **52,** 293

DIAMOND ELECTRONIC DEVICES FOR MICROWAVE AND MM/WAVE APPLICATIONS

P.M. Mock, J.B. Yan and R.J. Trew

ECE Dept., Box 7911

North Carolina State University

Raleigh, NC 27695-7911

(919) 737-2336
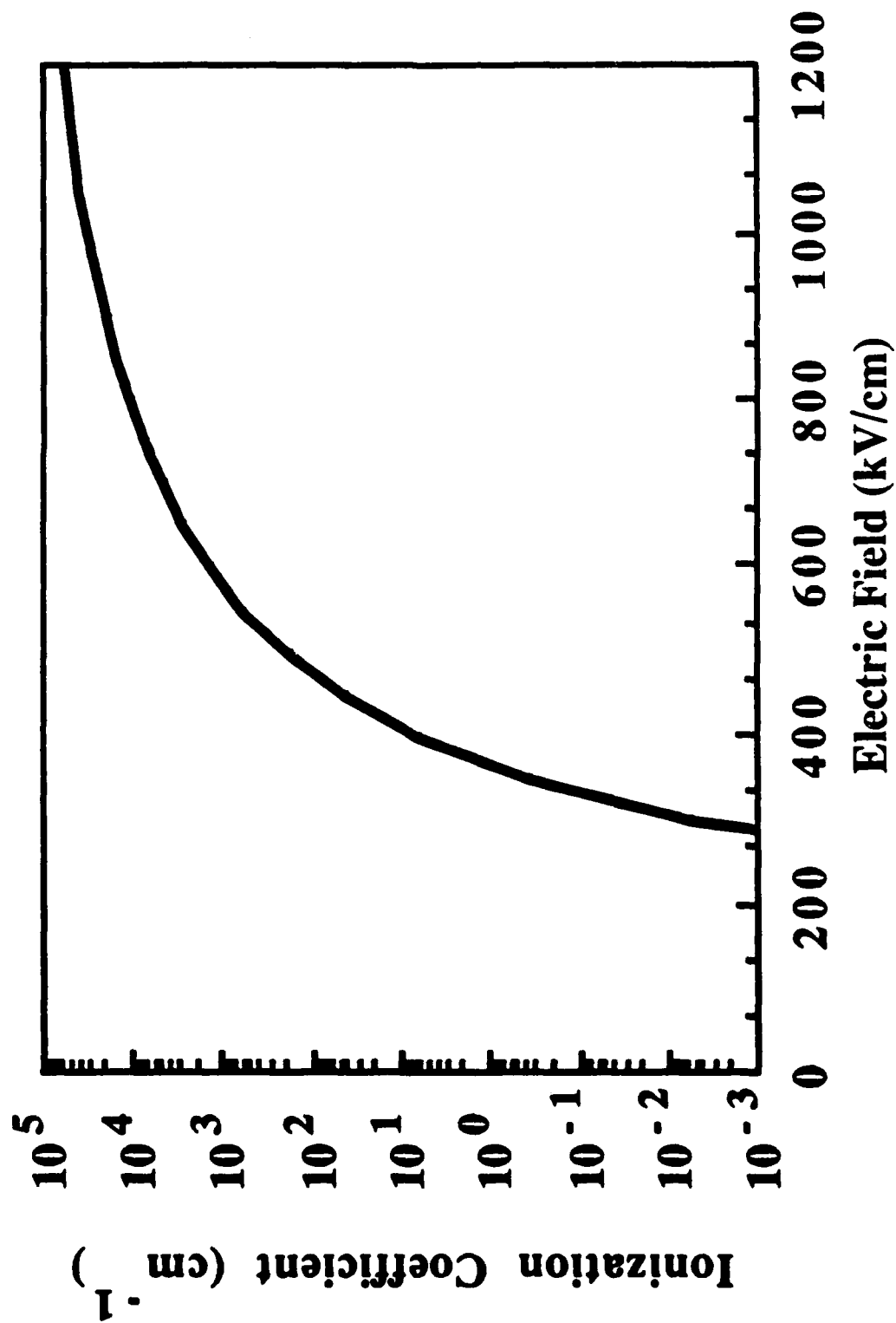
ADVANTAGES OF DIAMOND
FOR MICROWAVE POWER GENERATION

Diamond's large Bandgap (Eg=5.4 eV) allows larger operating voltages and higher power levels.

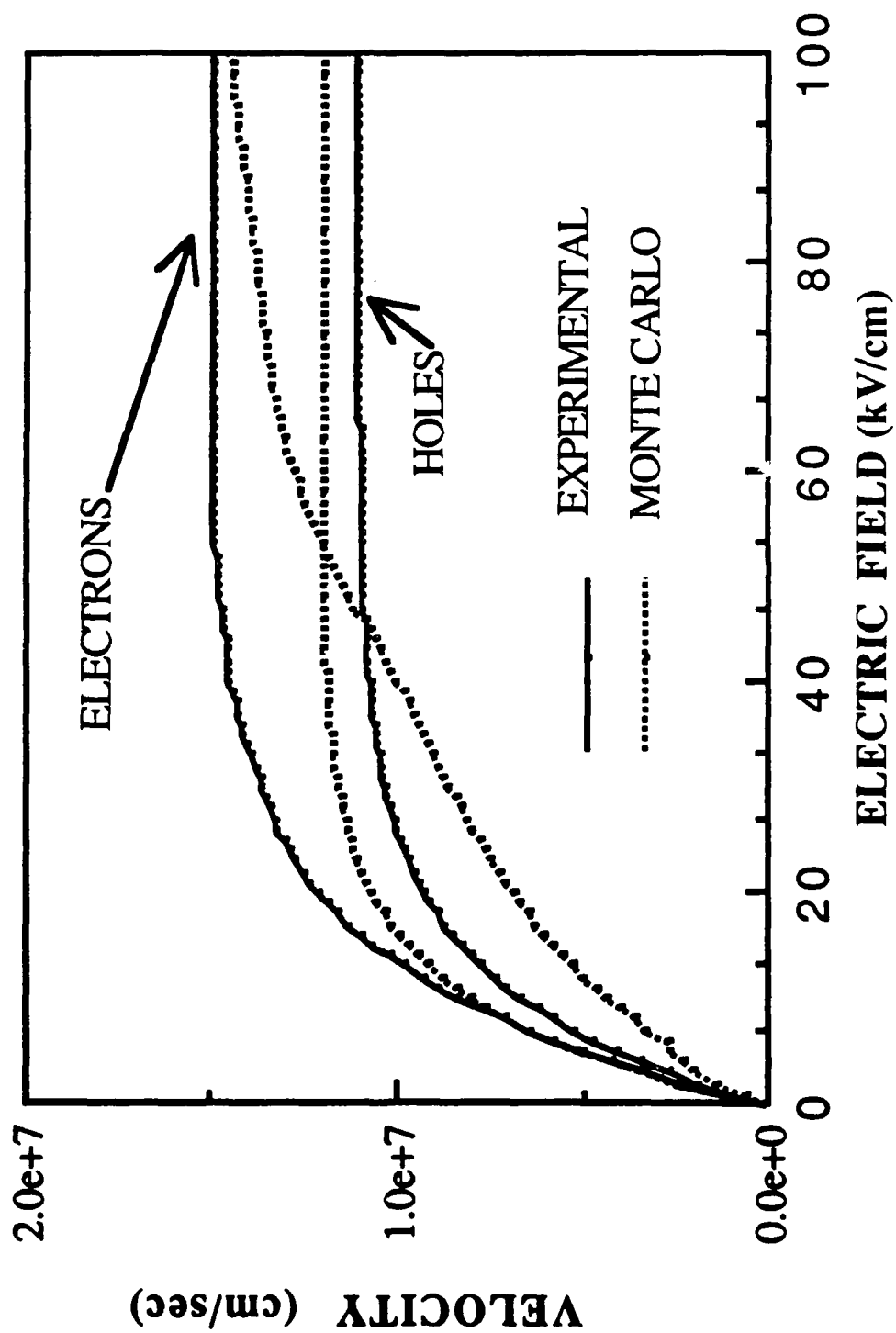The small dielectric constant reduces capacitive loading in diamond devices.

Diamond's high thermal conductivity allows operation at higher power densities than other semiconductors.

The saturated carrier velocities of electrons in diamond (2.7 times that of GaAs) make it a *faster* material and allow diamond devices to operate at higher frequencies.
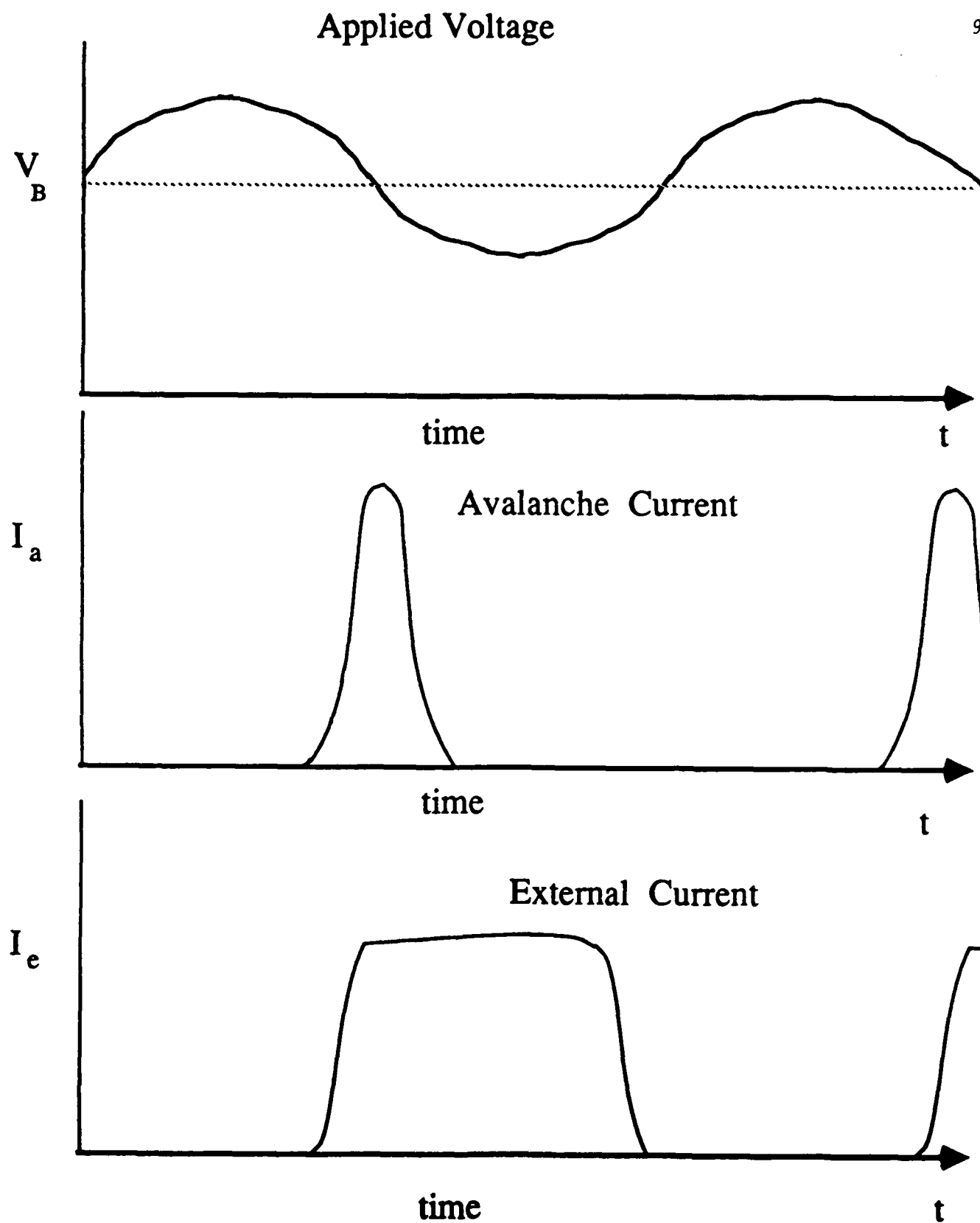
Ionization Coefficient for Diamond

VELOCITY vs ELECTRIC FIELD FOR DIAMOND

IMPATT DIODE POWER GENERATION

IMPact **A**valanche and **T**ransit **T**ime diodes are a source of prime and amplified power over a wide frequency range (1-300 GHz). IMPATTs generate power by employing two process: the generation of carriers within the semiconductor by avalanche multiplication, and the transport of these carriers across a defined distance, within the device, at the saturated drift velocity. These two processes cause the external current to lag behind the applied voltage and thus create an oscilation.

Applied Voltage

Applied Voltage and the Resulting
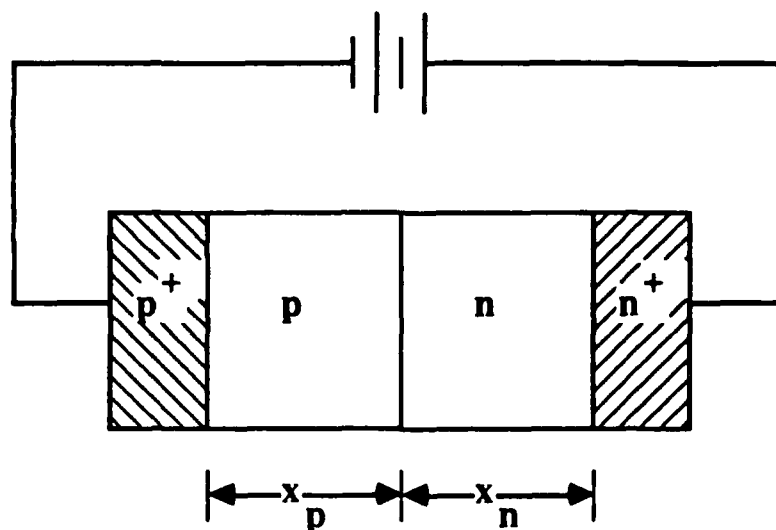Avalanche and External Currents

The Simulation Program

The large-signal simulation program used in this study has successfully described the operation of various Si and GaAs IMPATT diodes. This is a device physics model using carrier transport and avalanche ionization equations. The transport processes in the semiconductor are assumed to be adequately described by drift velocities and diffusion coeffcients that are functions of the electric field. The impact ionization process is represented by ionization coefficients that are also functions of the electric field.

The model accepts data about the diode geometry and doping profile, and then, using appropriate material data, it produces information about the operating characteristics of the diode. The equations in the model are independent of the semiconductor material being used. Two types of solutions are available from the program, ac and dc. A dc solution is provided by forcing the program to converge to a steady state with no ac component in the diode voltage. An RF voltage is impressed on the diode to provide ac solutions. The dc solution primarily provides a starting point for subsequent ac solutions. The priciple output data of the simulation are the diode admittance, efficiency, operating point, and power output. The carrier concentrations, current densities, electric field, and gereration rates are available throughout the RF cycle. This data is used to produce plots, referred to as *snapshots*, for decrete times in the RF cycle.

No computer program can produce output data of higher quality than the input data, so the material data used by the program is as important as the model itself. Transport data used was obtained from published experimental measurements and from Monte Carlo simulations. Ionization coefficients were determined by an analytical equation based on diamond material paramters and were in agreement with experimental results.
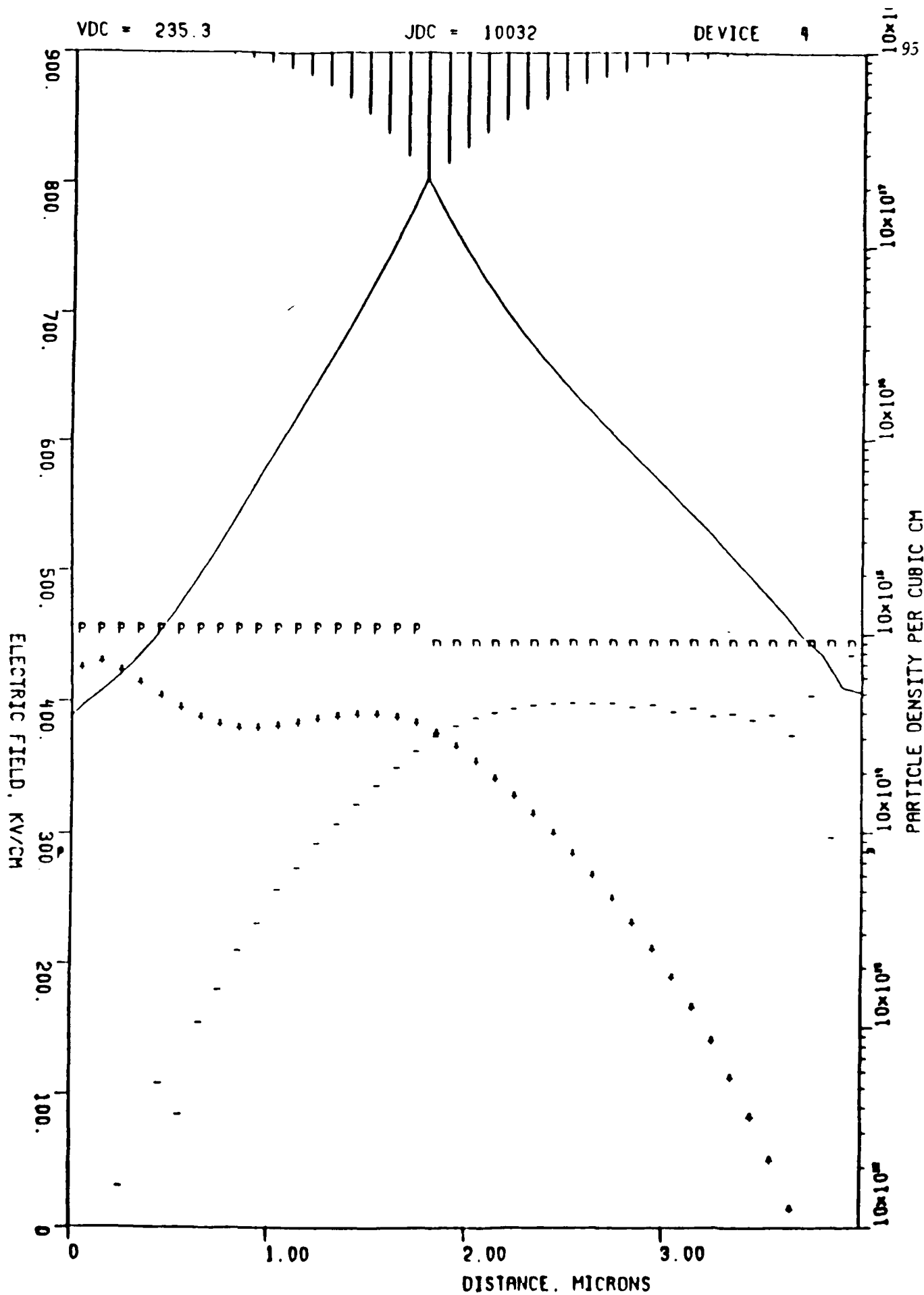
Diamond Impatt Doping Profiles

Freq(GHz)	$p(cm^{-3})$	$n(cm^{-3})$	$x_p(\mu m)$	$x_n(\mu m)$	V_B
35	1.1×10^{16}	9.0×10^{15}	1.80	2.20	235
44	1.5×10^{16}	1.2×10^{16}	1.50	1.80	208
60	2.2×10^{16}	1.8×10^{16}	1.00	1.20	146
94	3.6×10^{16}	3.1×10^{16}	0.80	0.90	124

VDC = 235.3   JDC = 10032   DEVICE   4

Power Generation for 35 Ghz IMPATT

Exp. Data
M. C. Data

CW Power (W)

Freq.(GHz)

Power Generation for 44 GHz IMPATT

Exp. Data
M.C. Data

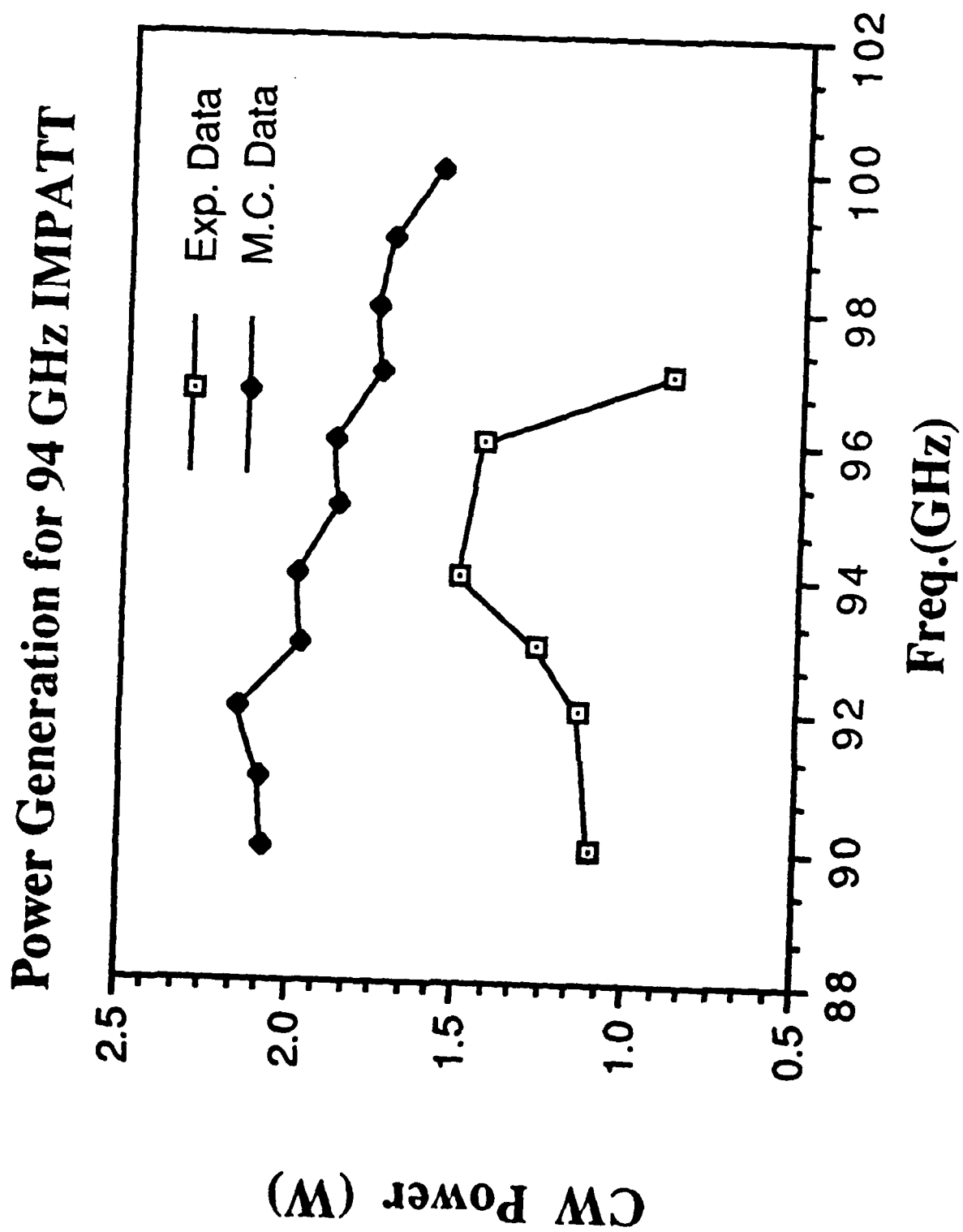CW Power (W)

Freq.(GHz)

Power Gereration for 60 GHz IMPATT

Power Generation for 94 GHz IMPATT

Diode Efficiencies for Different Materials

Power Conversion Efficiency vs **Freq (GHz)**

Legend: Si, InP, GsAs, C

A-J PLANE ANALYSIS: A TECHNIQUE FOR IMPATT DIODE OPTIMIZATION

Output Power for GaAs, Si, InP
and Diamond (C) Diodes
Numbers represent power efficiency (%)
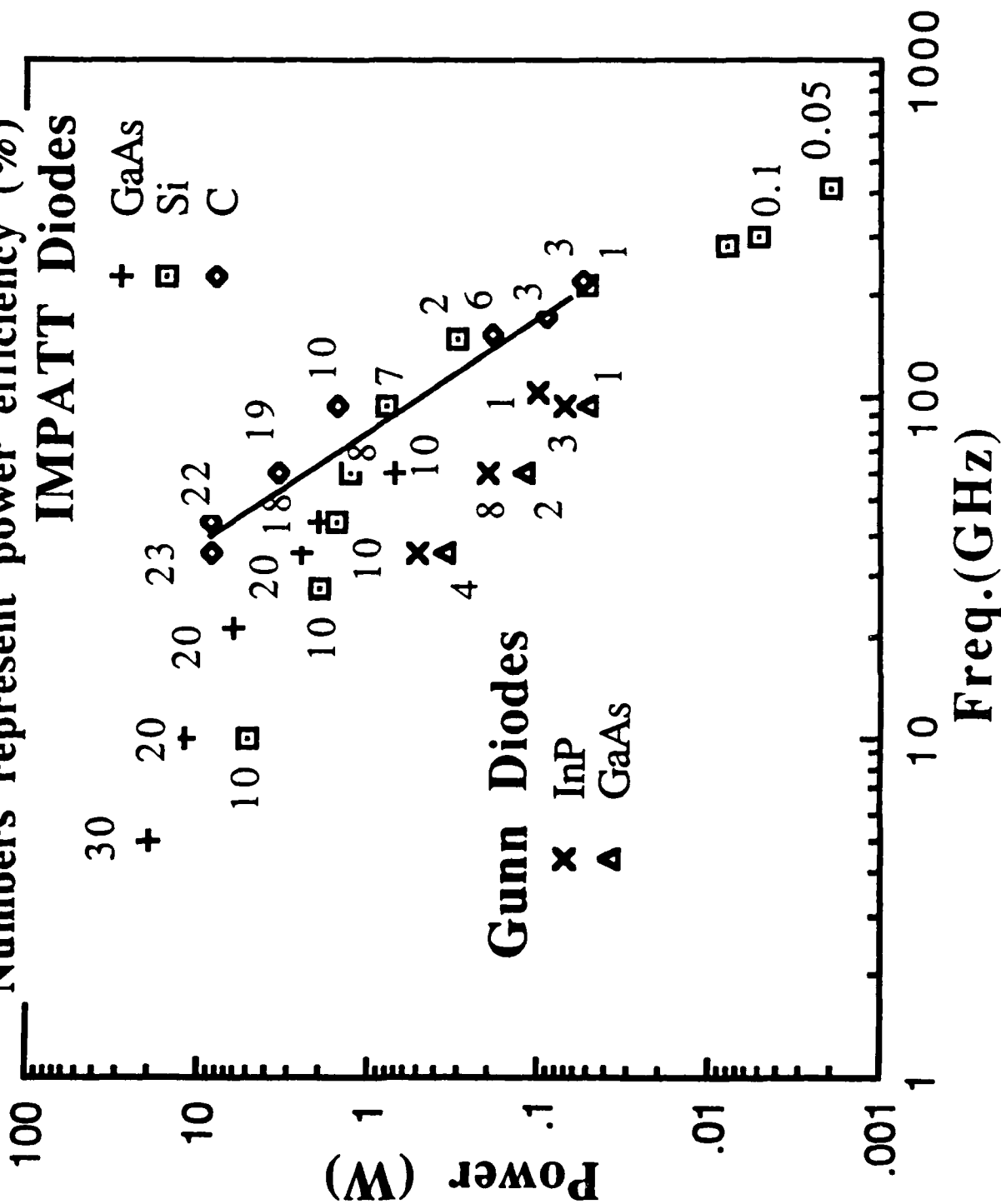IMPATT Diodes

CONCLUSIONS

Diamond IMPATTS show power conversion efficiency similar to that of conventional semiconductors (Si and GaAs) from 35 through 94 GHZ.

Due to the higher breakdown voltages and thermal conductivity, diamond IMPATTs are able to produce greater power than other semiconductors at the same frequency.

Large-signal computer simulations show that diamond IMPATTs can operate at 35 GHZ with 8.26 W, at 60 GHz producing 3.40 W, at 94 GHz producing 1.51 W, and at 220 GHz producing 54 mW of power.

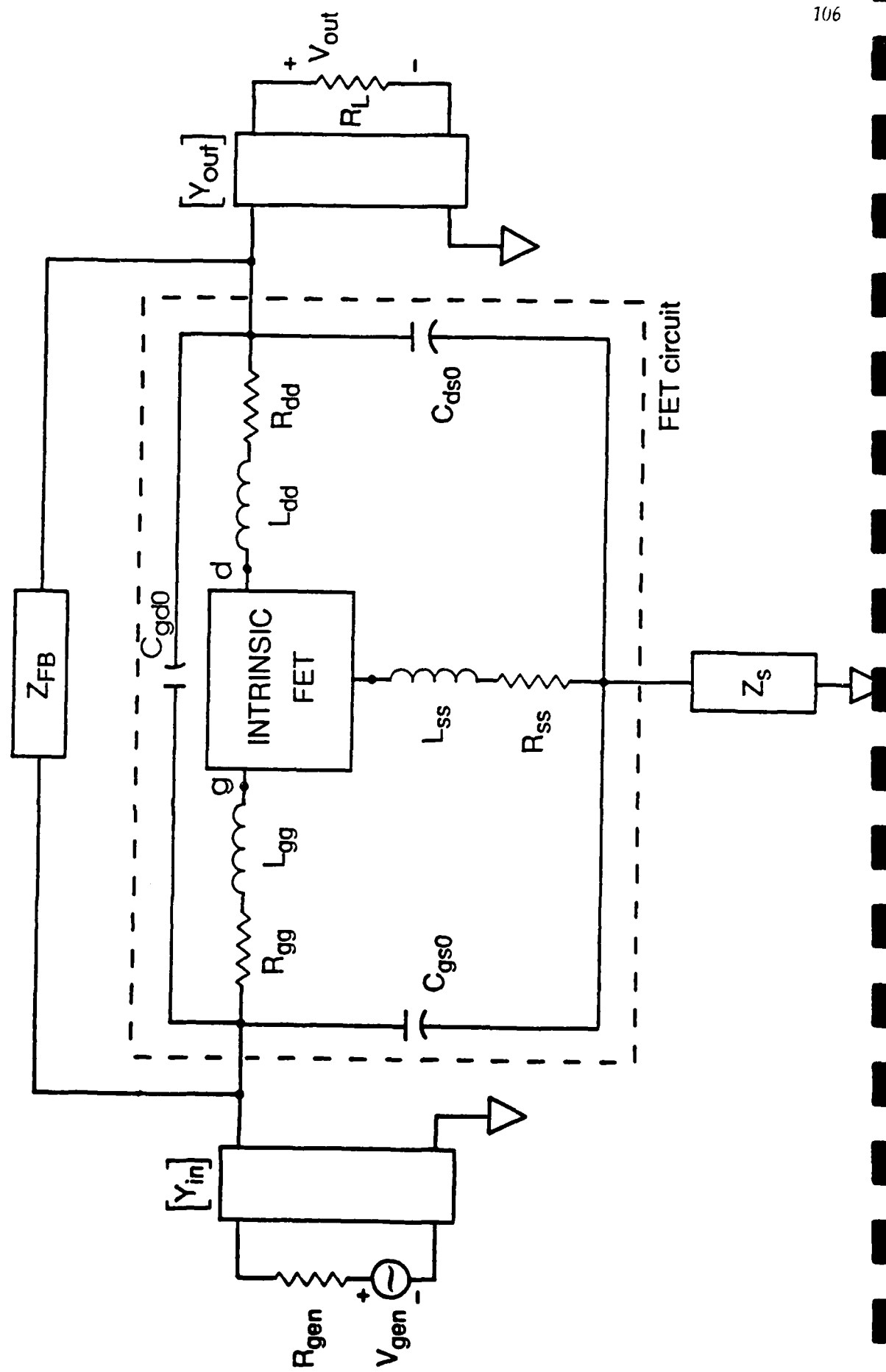**PROBLEM:** To investigate the large-signal RF and thermal performance of diamond power MESFETs.

APROACH: Determine the RF performance of optimized devices at X-band and compare with GaAs devices using the NCSU large signal MESFET simulator.

Features of the New FET Model

- It is physics based and does not require empirical parameters. A device design can be investigated before fabrication.

- It is a true large-signal, non-linear model.

- Deviations from channel space-charge neutrality are included.

- The 2-dimensional velocity vector is included.

- The 'abrupt depletion approximation' is not used.

- Thermal effect is included.

- Various materials are allowed.

- The model is computationally efficient.

MESFET RF Circuit Block Diagram

THERMAL RESISTANCE

Spreading resistance between device and heat sink

Thermal resistance of substrate

Thermal resistance of active layer

$$\Theta_{th} = \frac{2}{\pi \kappa_{hs} d} + R_{pkg} + \frac{4l_1 T_1}{225 \kappa \pi d^2} + \frac{4l_2 T_2}{560 \kappa \pi d^2} \ (°K/W)$$

d = diameter (cm)
κ_{hs} = thermal conductivity of heat sink (W/°K-cm)
κ = thermal conductivity of semiconductor (W/°K-cm)
R_{pkg} = thermal resistance of package and bonding (°K/W)
l_1 = substrate thickness (cm)
T_1 = average temp. of substrate (°K)
l_2 = active layer thickness (cm)
T_2 = average temp. of active layer (°K)

JUNCTION TEMPERATURE

$$T_j = 300 + \Theta_{th}(1-\eta)V_{dc}J_{dc}A \ (°K)$$

J_{dc} = Bias current density (A/cm^2)
A = Channel area (cm^2)
η = RF generation efficiency
V_{dc} = Bias voltage (V)

Basic Information for Thermal Effect

- Current: $I \propto T^{-\alpha}$

- Mobility: $\mu \propto T^{-\alpha}$

- Saturation velocity: $v_s \propto T^{-\alpha}$

Calculation of Temperature:

$$T = T_0 + \triangle T$$

Where

$$\triangle T = \Theta \times P_{dc} \times (1 - \eta)$$

$$P_{dc} = I_d(DC) \times V_{dd}$$

$$\Theta = \text{Thermal resistance } (^{o}K/Watt)$$

$$\eta = \text{Power added efficiency}$$

$$\alpha = \text{Temperature dependence coefficient}$$

Velocity-Field Curve of P-type diamond

$$v = \mu_0 E \left(1 - \tfrac{1}{2}\left(\tfrac{E}{E_c}\right)^{1/2} + \tfrac{1}{16}\tfrac{E}{E_c}\right) \qquad E \leq 4E_c$$

$$v = v_s + \tfrac{v_s}{2}\left(1 - 4\tfrac{E_c}{E}\right)^2 \qquad E \geq 4E_c$$

DIAMOND POWER MESFET

$$L_{ds}$$

$$L_{gs} \qquad L_g$$
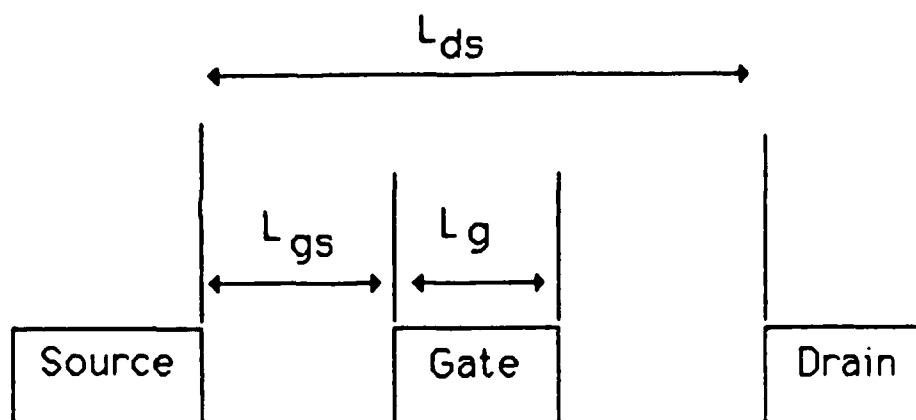
| Source | | Gate | | Drain |

Channel

- -

Substrate

_____

	Value	
Parameter	Diamond	GaAs
L_g	0.5 μm	0.5 μm
L_{ds}	3.5 μm	3.5 μm
L_{gs}	1 μm	1 μm
$N_{d'}$	$4 \times 10^{17} \text{cm}^{-3}$	$2.5 \times 10^{17} \text{cm}^{-3}$
a	0.15 μm	0.23 μm
W	1 mm	1 mm
$\Phi_{bi}(\text{Au})$	1.71 eV	0.6 eV
R_c	$\sim 10^{-4} \Omega\text{-cm}^2$	$\sim 10^{-6} \Omega\text{-cm}^2$

Doping Profile

I-V (with thermal effect) of P-channel diamond MESFET

Large-signal performance (with thermal effect) of p-channel diamond power MESFET at 10 GHz

Large-signal performance (with thermal effect) of p-channel diamond power MESFET at 10 GHz

Large-signal performance (with thermal effect) of p-channel diamond power MESFET at 10 GHz

Comparision of P-channel diamond and N-channel GaAs power MESFET at 10 GHz

Comparision of P-channel diamond and N-channel GaAs power
MESFET at 10 GHz

Comparision of P-channel diamond and N-channel GaAs power MESFET at 10 GHz

P-channel diamond

P-channel diamond

P-channel diamond

Comparision of P- and N-channel diamond power MESFET at 60 GHz

Comparision of P- and N-channel diamond power MESFET at 60 GHz

Comparision of P- and N-channel diamond power MESFET at 60 GHz

CONCLUSIONS

- The optimized design of uniform doped p-channel X-band diamond power MESFET has been investigated.

- A p-channel diamond MESFET offers the potential to produce devices with RF output power greater than 10 W/mm gate width (or 18 W/unit gate width) with greater than 40% power-added efficiency at 10 GHz.

- The high thermal conductivity of diamond allows high RF output power before thermal effects occur.

- The high breakdown voltage of diamond allows large input RF voltages to be applied before saturation occurs.

- The large-signal performance of a p-channel diamond power MESFET has been compared to an n-channel GaAs MESFET at 10 GHz.

- Various designs of p-channel diamond devices have been investigated for a range of frequency 10 GHz - 100 GHz.

- N-channel diamond MESFETs have improved RF performance compared to comparable p-channel MESFETs. A comparison at 60 GHz has been presented.

IX. Collaboration with Other SDIO programs

For the most effective use of SDIO/IST funds cooperation and collaboration of SDIO contractors is very desirable. NCSU has a significant history of past collaboration with other diamond programs and will continue this spirit in the future. For example, past exchanges have included:

Research Triangle Institute

- Professor R. J. Nemanich in the Department of Physics at NCSU has been funded to do Raman spectroscopy for various groups, most notably RTI.

- A student of the Materials Science and Engineering Department at NCSU has spent part of his research time at RTI working on the preparation of substrates.

- NCSU has provided RTI with prepared substrates for diamond growth (including monocrystalline SiC) and with diamond samples to utilize as standards in their analysis system.

- A NCSU student has spent time with an RTI employee teaching him TEM sample preparation techniques for diamond.

- RTI and NCSU have also shared information on the design of substrate heaters and filaments for diamond CVD systems, as well as information on the analysis of diamond and diamond-like films. In this regard, Dan Vithavage and John Posthill have given NCSU personnel much advice and consultation in the areas of surface analysis and TEM, respectively.

- NCSU provided SIMS and TEM analysis of RTI films in the early stages of the diamond program.

Other Groups

- A NCSU graduate student involved in the design and construction of the microwave CVD system spent several days at Penn State University visiting Professor R. Messier's group. Valuable information was gained from the earlier experience in diamond CVD obtained at Penn State.

- Another NCSU graduate student involved in the hot filament CVD system construction received advice from Professor W. Yarborough's group at Penn State.

- Regular contact between NCSU and Dr. M. Geis of Lincoln Labs has been very beneficial for the NCSU program, especially in the area of hot filament growth on diamond substrates.

- One of the NCSU P.I.'s has visited Dr. B. Pate of Stanford to exchange information and provided him with SiC samples for comparison with diamond using the various synchrotron analytical techniques in which Dr. Pate specializes.

- A diamond sample has also been sent to Dr. Ma at Brookhaven National Labs for synchrotron analysis. Professor Swanson and his students have provided NCSU with implantation.

- Along with these specific interactions, numerous informal discussions at a variety of conferences have occurred between NCSU investigators and investigators from other programs. This type of interaction has been enhanced by several of the investigators serving as members on the same conference committees over the past two years.

This type of collaboration will continue and expand in the future during the renewal period. For example, Professors Glass and Messier co-chaired an MRS diamond symposium in the Fall of 1989 and again with Dr. Butler (NRL), a JNDF diamond conference in 1990. Furthermore, Professors Davis and Glass of NCSU are co-editors of a book which will include contributions from several other SDIO/ONR sponsored program leaders. More specifically, future collaborations will include providing diamond samples to Aerodyne's ONR sponsored research into the fluorination of diamond surfaces. A NCSU student will continue to work part time in RTI's laboratory in the area of substrate preparation. It is also proposed that NCSU's electrical engineering phase of the diamond program will provide device parameters obtained from their modeling research (i.e., doping levels, device dimensions, etc.) to other SDIO/ONR programs to allow fabrication of optimum devices. Mask designs for these devices will also be shared. Film property data such as saturated drift velocity will also be available for other programs to utilize. It is also proposed that Penn State and NCSU researchers visit each other's facilities one to two times per year to discuss various aspects of the diamond programs. It is envisioned that each visit would concentrate on a different aspect such as microwave plasma growth, electrical properties, etc. Graduate students conducting research in these programs would be involved in these visits which have already been discussed by Professors Messier and Glass. Professor Nemanich of NCSU will continue to work with RTI and is, in fact, a subcontractor on the new RTI contract and will also continue to receive funding from and work with other NCSU researchers. Professor Bernholc (NCSU) will provide advice on dopant species and unique growth species, which his calculations find promising, for the CVD deposition research. The technical feasibility of a collaboration with K. Spear and M. Frenklach on the TEM of diamond particles is also under investigation.

Available NCSU Facilities

- Materials Analysis (TEM, AES, XPS, etc.)

- Microwave and Hot Filament CVD

- Device Modeling

- Photolithography

Acknowledgements

Appendix
Distribution List—Annual Report
Contract Number N00014-86-K-0666

Address	Number of Copies	Address	Number of Copies
Mr. Max Yoder Office of Naval Research Electronics Program–Code 1114 800 North Quincy Street Arlington, VA 22217	8	**Dr. James Butler** Naval Research Laboratory Code 6174 Washington, DC 20375	1
Office of Naval Research Resident Representative Georgia Institute of Technology 206 O'Keefe Building Atlanta, GA 30332-0490	1	**James Mayer** Materials Science and Engineering 210 Bard Hall Cornell University Ithaca, NY 14853	1
Director Naval Research Laboratory Attention: Code 2627 Washington, DC 20314	6	**Dr. Bradford Pate** Department of Physics Washington State University Pullmany, WA 99164-2184	1
Defense Technical Information Center Building 5 Cameron Station Alexandria, VA 22314	12	**Professor Pankove** Electrical and Computer Engineering University of Colorado Boulder, CO 80309-0455	1
Robert J. Markunas Research Triangle Institute Post Office Box 12194 Research Triangle Park, NC 27709-2194	1	Office of Naval Research Attention: Code 1131M Arlington, VA 22217	1
Michael W. Geis Lincoln Laboratories 244 Wood Street P. O. Box 73 Lexington, MA 02173	1	Naval Research Laboratory Attention: Code 4683 Washington, DC 20375	1
		Naval Research Laboratory Attention: Code 6820 Washington, DC 20375	1
Professor N. Parikh Department of Physics University of North Carolina at Chapel Hill Chapel Hill, NC 27514	1	Naval Research Laboratory Attention: Code 6211 Washington, DC 20375	1
Professor Russell Messier 265 Materials Research Laboratory Pennsylvania State University University Park, PA 16802	1	Naval Research Laboratory Attention: Code 6684 Washington, DC 20375	1

Naval Research Laboratory Attention: Code 4684 Washington, DC 20375	1
Dr. Jim Zeidler Naval Ocean Systems Center Attention: Code 7601 San Diego, CA 92152	1
Naval Ocean Systems Center Attention: Code 911 San Diego, CA 92152	1
Naval Ocean Systems Center Attention: Code 56 San Diego, CA 92152	1
Dwight Duston OSD/SDIO/IST Pentagon Washington, DC 20301-7100	1
DARPA/D.S.O. 1400 Wilson Boulevard Arlington, VA 22209	1
Professor R. F. Davis Materials Science and Engineering Box 7907 North Carolina State University Raleigh, NC 27695-7907	1
Professor K. J. Bachmann Materials Science and Engineering Box 7907 North Carolina State University Raleigh, NC 27695-7907	1
Professor R. J. Nemanich Department of Physics Box 8202 North Carolina State University Raleigh, NC 27695-8202	1
Professor R. J. Trew Electrical and Computer Engineering Box 7911 North Carolina State University Raleigh, NC 27695-7911	1
Dr. Sandor Holly Rocketdyne Division Rockwell International, MS FA03 Canoga Park, CA 91304	1

Professor G. Walrafen Chemistry Department Howard University 5325 Potomac Avenue, NW Washington, DC 20016	1
Professor I. Lindau Synchrotron Radiation Laboratory Stanford, CA 94305	1
A. J. Purde Texas Instruments MS 147 P. O. Box 655936 Dallas, TX 75265	1
W. D. Partlow Westinghouse Research and Development Center 1310 Beulah Road Pittsburgh, PA 15235	1
R. L. Adams 21002 North 19th Avenue Suite 5 Phoenix, AZ 85027	1
Professor John C. Angus Chemical Engineering Case Western Reserve University Cleveland, OH 44106	1
Prof. Thomas R. Anthony General Electric Corporation Research and Development Center Building K-1, Room 1CSO P. O. Box 8 Schnectady, NY 12301	1
Yehuda Arie SRI Sarnoff Center Princeton, NJ 08540	1
P. J. Boudreaux Laboratory for Physical Science 4928 College Avenue College Park, MD 20740	1
Professor R. F. Bunshaw University of California 6532 Buelter Hall Los Angeles, CA 90024	1

Ray Calloway   1
Aerospace Corporation
Post Office Box 92957
Los Angeles, CA 90009

Jerome J. Cuomo   1
T. J. Watson Center
Yorktown Heights, NY 10598

Professor P. H. Fang   1
Department of Physics
Boston College
Chestnut Hill, MA 02167

Wen Hsu   1
Sandia National Laboratories
Division 8347
Box 969
Livermore, CA 94550

Professor W. Lanford   1
Physics Department
S.U.N.Y.
Albany, NY 12222

Professor E. S. Machlin   1
44 Morningstar Drive
Croton-on-Hudson, NY 10520

Michael Pinneo   1
Crystallume
3180 Porter Drive, Suite 2
Palo Alto, CA 94304

Kenneth Russell   1
J. P. L. M. S. 122-123
4800 Oak Grove Drive
Pasadena, CA 91109

Professor T. D. Moustakas   1
Exxon Research
Ammandale, NJ 08801

Professor J. L. Davidson   1
200 Brown Hall
Auburn University
Auburn, AL 36849

B. Meyerson   1
IBM
T. J. Watson Center
Yorktown Heights, NY 10598

Paul Caldwell   1
DASIAS Field Office
2560 Huntington Avenue
Suite 500
Alexandria, VA 22303

Defense Nuclear Agency   1
ATTN: RAEE (CAPT Fore)
Washington, DC 20305-1000

Dr. Ian Brown   1
Lawrence Berkeley Laboratory
Bldg. 53
University of California
Berkeley, CA 94720

Dr. Andrez Badzian   1
271 Materials Research Laboratory
The Pennslyvania State University
University Park, PA 16802

Prof. Jerzy Bernholc   1
Department of Physics
Box 8202
North Carolina State University
Raleigh, NC 27695-8202

Tarasankar *DebRoy*   1
Materials Science and Engineering
Penn State University
212 Steidle Building
University Park, PA 16802

Andrew Freedman   1
    and Charter Stinespring
Aerodyne Research Inc.
45 Manning Road
Billerica, MA 01821

Michael Frenklach   1
Penn State University
202 Academic Projects Building
University Park, PA 16802

Maurice Landstrass   1
Crystallume
125 Constitution Drive
Menlo Park, CA 94025

Keppi Wu   1
OSD/SDIO/IST
Washington, DC 20301-7100

Warren Pickett 1	**Thomas Perry** 1
Code 4692	Physics Department
Naval Research Laboratory	GM Tech Center
Washington, DC 20375-5000	Warren, MI 48090
Ron Rudder 1	**R. Hauge** 1
Research Triangle Institute	Chemistry Department
P. O. Box 12194	Rice University
Research Triangle Park, NC 27709-2194	P. O. Box 1892
	Houston, TX 77251
John B. Posthill 1	
Research Triangle Institute	**Ken Stalder** 1
P. O. Box 12194	SRI International
Research Triangle Park, NC 27709-2194	333 Ravenswood Avenue
	Menlo Park, CA 94025
Howard Schmidt 1	
Schmidt Instruments	**C. Richard Guarnieri** 1
2476 Bolsover, Suite 234	IBM Research Center
Houston, TX 77005	Yorktown Heights, NY 10598
Dr. Skotheim 1	**William Banholzer** 1
Moltech Corporation	K1-CEB G20, P. O. Box 8
Box 572	Schenectady, NY 12301
Woodville Road	
Shoreham, NJ 11786	**Albert Feldman** 1
	NIST
Karl Spear 1	Gaithersburg, MD
Pennsylvania State University	
201 Steidle	**Dario Narducci** 1
University Park, PA 16802	IBM Research Division
	P. O. Box 219
Max Swanson 1	Yorktown Heights, NY 10598
Department of Physics	
University of North Carolina	**Prof. Gar B. Hoflund** 1
Chapel Hill, NC 27514	Chemical Engineering
	227 Chemical Engineering Building
Robert Schwartz 1	Gainsville, FL 32611
NWC Code 38504	
Naval Weapons Center	**Dr. A. T. Collins** 1
China Lake, CA	Wheatstone Physics Laboratory
	King's College London, Strand
T. S. Sudarshan 1	London WC2R 2LS
Materials Modification, Inc.	UNITED KINGDOM
P. O. Box 4817	
Falls Church, VA 22044	**Joe Beeler** 1
	Materials Science and Engineering
Wally Yarbrough 1	Box 7907
Penn State University	North Carolina State University
271 MRL	Raleigh, NC 27695-7907
University Park, PA 16802	